UNIVERSITÀ DEGLI STUDI DI UDINE
hic sunt futura

www.uniud.it

Doctor of Philosophy degree in Environmental and Energy Engineering Science

Cycle XXX

The influence of water in methane oxidation catalysts based on Pd supported on CeO_2 and CeO_2-containing materials

PhD candidate
Alessandra Toso

Supervisor
Prof. Alessandro Trovarelli
Co-supervisor
Dott.ssa Sara Colussi

Year 2018

Acknowledgments

I would like to thank my Supervisor prof. Alessandro Trovarelli for giving me the opportunity to do PhD at the lab of Catalysis for Energy and Environment research group at University of Udine. Also, I would like to thank him for his teachings and advices during the research period.

I would like to make a special thanks to my co-supervisor Doctor Sara Colussi for her teachings, and support during the experimental activities and the writing of the thesis, and also for the time spent together at 25th North-American Meeting in Denver.

I am also grateful to my colleagues for the time spent together during these three years. I would like to thank my colleague Monica Julieth Valencia Botero for her support and the funny moments spent together.

I would like to thank Prof. Jordi Llorca from Energy Technique Institute of the Polytechnic University of Catalonia (Barcelona, Spain) for having kindly performed HR-TEM measurements.

I would like also to thank Ford Motor Company (Dearborn, MI, USA), who has financially supported the University Research Project "Three-Way Catalyst Materials for Compressed Natural Gas Vehicles".

Finally, I would like to thank my mother Loredana, my father Riccardo, my boyfriend Fabio and my two best friends Barbara and Nicoletta for their precious support during the PhD.

Abstract

The purpose of this PhD thesis is the study of catalytic methane oxidation over Pd-based catalysts supported on different CeO_2-based oxides for their application on natural gas fuelled vehicles (NGVs). This research work has been carried out with the financial support from Ford Motor Company (Dearborn, MI, USA) under the University Research Project award "Three-Way Catalyst Materials for Compressed Natural Gas Vehicles".

Pd supported on CeO_2-based oxides are recognized as the most promising catalytic materials for methane oxidation. The objective of the thesis work was to address the study of new catalytic materials supported on different CeO_2-based oxides and prepared by *single-step* solution combustion synthesis (SCS). Particular attention was dedicated to the study of water poisoning, a key issue in designing catalytic materials for NGVs, as water is known to strongly deactivate Pd-based catalysts.

The first part of the work was dedicated to the investigation of the catalytic behavior of $Pd/Ce_xZr_{1-x}O_2$ catalysts for CH_4 oxidation in lean atmosphere: the performance of each sample was evaluated both in temperature programmed and steady-state conditions in the presence and in the absence of steam and compared with analogues compositions prepared by traditional incipient wetness technique (IW). In order to explain the difference in terms of catalytic activity between SCS and IW samples, a relevant part of the work was focused on the study of their redox properties, and in particular to the characterization of PdO-Pd-PdO phase transformation. The results indicate that solution combustion synthesized $Pd/Ce_xZr_{1-x}O_2$ catalysts are not only more active than their IW counterparts, but also display an improved resistance to hydrothermal ageing. The results also highlighted the beneficial use of $Ce_{0.75}Zr_{0.25}O_2$ mixed oxide to reduce the deactivation observed in presence of water vapor. Once the effectiveness of solution combustion synthesis to prepare active and stable Pd-based catalysts was assessed, other supports were investigated. Pd supported on CeO_2-SiO_2 and CeO_2-Al_2O_3 mixed oxides were prepared to study the effect of SiO_2 and Al_2O_3 addition on the redox properties and catalytic activity of Pd/CeO_2. Finally, the most promising materials were tested also in stoichiometric conditions, varying oxygen/methane ratio in the feed, with the aim to evaluate the effect of gas feed composition on their catalytic performance and obtain preliminary results on their catalytic behavior as three-way-catalysts.

Keywords: CH_4 oxidation, Pd/CeO_2-ZrO_2, water poisoning, Pd-PdO transformation, solution combustion synthesis

List of Figures

List of Tables

Contents

Chapter 1

Natural gas fuelled vehicles (NGVs) and related after-treatment technology

1.1. After-treatment technology of NGVs

It is well established that natural gas, with CH_4 being its main compound, is one of the best clean alternatives to traditional fuels. The use of methane in spark ignition engines allows to reduce polycyclic aromatic hydrocarbons (PAH), PM_{10} and CO_2 emissions up to 25% by having the highest H/C ratio. Even though NGVs are considered a good choice in terms of environmental impact, they still present a critical point: unburned methane resulting from the incomplete combustion reaction is in fact a powerful greenhouse gas, with a *Global Warming Potential* (GWP) of about 20 times that of CO_2 [1]. In order to reduce methane emissions in atmosphere, an exhaust gas after treatment technology must be applied. Catalytic abatement of noxious compounds in exhaust stream represents a powerful tool to reduce pollutant emissions and it is already employed successfully in gasoline and diesel powered engines. The composition of exhaust gases is closely related to the air/fuel ratio (A/F), varying between lean-burn and stoichiometric engines. In lean-burn engines, an excess of air is employed during the combustion process with an A/F value close to 23.5 [2]. The high O_2 available in the combustion chamber guarantees a low emission of CO and HC but high NO_x emissions. In lean burn engines, a properly optimized oxidation catalysts (OC) is able to significantly reduce engine-out emissions of HC, while deNO_x system as Selective Catalytic Reduction (SCR) by ammonia/urea or NO_x trap are added for the NO_x abatement [3]. The stringent NO_x emission standards from Euro V to VI have determined the prevalence of stoichiometric technology [4]. Stoichiometric engines operating with A/F ratio close to 17.2 allow to reduce NO_x emissions but with an increase of CO due to less O_2 available. Stoichiometric powered vehicles equipped with water cooled exhaust gas recirculation (EGR) and three-way catalytic converter (TWC) are able to meet stringent emission regulations [5, 6, 7]. The three-way catalytic system is able to realize simultaneously the reduction of Non Methane Hydrocarbons (NMHC) and NO_x emissions up to 95% [6, 8].

Although the after treatment of exhaust gases is well established for diesel and gasoline

engines, this technology has to be optimized for natural gas mobile applications. The exhaust gas stream from NGVs contains low amount of CH_4 (500-1000 ppm), large amount of steam and CO_2 (10-15%) and traces of SO_x and NO_x compounds with output temperature less than 550°C [9].

Among other hydrocarbons, the oxidation of methane requires more energy (450 kJ/mol) due to the high stability of CH_4 molecule [10, 11]. Figure 1.1 illustrates the light-off curve of NMHC and CH_4 where the conversion is plotted against temperature. Within the operating window of NGVs the conversion of NMHC has already reached 100 %, whereas the abatement of CH_4 requires higher temperatures.

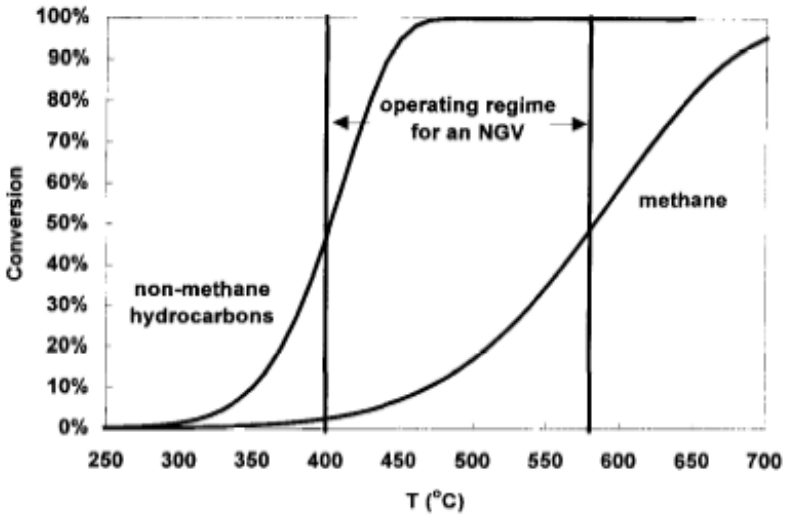

Figure 1.1: light off curves for methane and NMHC in comparison with NGV exhaust gas temperatures [11]

In order to abate the residual methane at the tailpipe, an oxidation catalyst with high activity at low temperatures is required, also due to the large amount of methane produced during cold-start [12].

Two families of catalysts for complete methane oxidation have been studied: noble metals (Pd, Pt, Rh) and transition metal oxides such as Cu and Co. Transition metal oxides, although cheaper than noble metals, are less active at low temperatures and require much higher metal loading (15-30 wt.%).

1.2. Palladium based catalysts

Palladium-based catalysts are renowned to be the most active for CH_4 combustion with low light-off temperature [13]. The performance of Pd catalysts is strongly related to the oxidation state of noble metal during the reaction: several experimental [14, 15, 16] and theoretical studies [17, 18, 19, 20] have been dedicated to the investigation of the active sites and reaction mechanism during CH_4 oxidation, even though this topic is still much debated. It is generally accepted that methane oxidation over Pd-based catalysts follows a *Mars and van Krevelen*

redox mechanism where the dehydrogenation of CH_4 is considered the rate-limiting step. The difficulty in defining the reaction mechanism is related to the different PdO species that can be generated at varying synthesis method, oxygen partial pressure, temperature and thermal treatment [15, 21, 22, 23, 24]. In the earliest papers, most of the authors indicated palladium oxide (PdO) as the active phase for methane oxidation at low temperature, while Pd was considered less active or the inactive form [24, 25]. Demoulin *et al.* suggested that the lattice oxygen of PdO crystallites is consumed by CH_4; this process creates oxygen vacancies in PdO crystallite that could be re-oxidized from O_2 of the gas phase or from the bulk, regenerating palladium oxide. They also emphasized the importance of temperature and oxygen partial pressure in the reaction pathway [25].

Some authors proposed that PdO_x (an intermediate phase between metal and stoichiometric oxide) or sites consisting of oxygen atoms (surface PdO) and oxygen vacancies (surface Pd) play a key role in methane activation. Iglesia's research group proposed a complex reaction mechanism where oxygen from the gas phase adsorbed on oxygen vacancy, dissociating in O atoms; the dissociative adsorption of CH_4 occurs over *coordinatively unsaturated Pd* site (cus-Pd) on PdO crystallites, then H-atom is removed from CH_4 by the neighbor Pd-O site with the formation of Pd-OH. The oxygen vacancies on PdO surface are regenerated at the end of reaction through a recombination of hydroxyl groups [26, 27]. Hellmann's research group by DFT calculations coupled with *in situ* surface X-ray diffraction (SXRD) measurements calculated lower activation energies for methane dissociation when CH_4 adsorbed over cus-Pd sites, where Pd is coordinated to only three oxygen atoms, or on metallic Pd, concluding the importance of these two sites to activate efficiently methane molecule [17]. Kinnunen *et al.* by experimental [15] and DFT studies [20] concluded that the simultaneous presence of Pd and PdO_x are able to lowered light-off of methane. Again, by *operando* Raman spectroscopy and *in situ* CO-DRIFT experiments, Xu *et al*. argued that both Pd and PdO_x phases are needed to gain high catalytic activity in lean-burn conditions: at temperature below 673 K CH_4 oxidation mainly proceeds over metallic Pd sites; as the temperature increases the reaction takes place over PdO_x, generated from the progressive oxidation of Pd [28]. The reaction mechanism during CH_4 oxidation is not straightforward to establish because of a continuous change in the oxidation state of Pd throughout the reaction, where different variables affect the oxidation state of Pd. This aspect is still matter of debate, but there are some points that seem to be clear in the literature.

Figure 1.2 (left) shows a typical light-off curve on Pd supported catalyst, where CH_4 conversion is plotted against temperature.

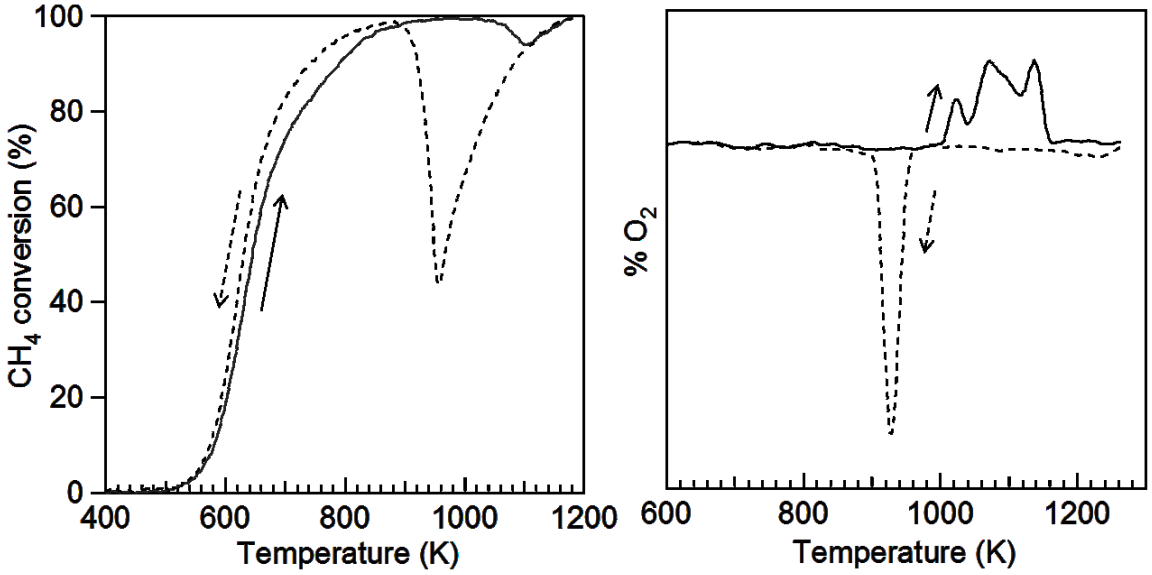

Figure 1.2: light-off curve (left) and oxygen release/uptake profile (2 vol.% O_2) (right) for Pd-based catalysts; solid line: heating; dotted line: cooling.

During the heating ramp a sharp increase of the conversion is observed in the low-medium temperatures when the reaction starts and it is in kinetically controlled regime. After a further increase in temperature, a stable conversion is observed where the catalytic reaction is controlled by mass transfer. At 1050 K (Figure 1.2 (left)) a drop in catalytic activity is detected due to the phase transition of PdO to metallic Pd, less active in methane oxidation [9]; in the cooling part of the cycle (Figure 1.2 dotted line) a sharp reduction in activity is observed due to the presence of metallic Pd, reaching a minimum in CH_4 conversion at 956 K. Only below this temperature a progressive increase of catalytic activity is observed due to Pd re-oxidation, reaching a maximum value, to decrease again upon cooling [29]. PdO-Pd phase transition is a reversible process but occurs with a large hysteresis gap (~ 100 K) causing a severe deactivation of catalytic performance in this temperature window. The dynamic of PdO ↔ Pd transformation is commonly investigated by Temperature Programmed Oxidation (TPO) experiments where the catalyst is subjected to a flow of O_2/N_2 gas mixture. Figure 1.2 (right) shows a typical TPO profile of 1% Pd-supported catalyst in 2 vol.% O_2/N_2 where oxygen concentration is continuously monitored during the heating/cooling ramp. In the heating branch, a large O_2 release peak (positive peak) is observed due to PdO decomposition to metallic Pd; while an O_2 uptake peak (negative peak) due to the regeneration of PdO is observed during the cooling step reaching a minimum at 926 K. From TPO experiments it is evident that PdO-Pd transition occurs with a thermal hysteresis of about 100 K. In this temperature window PdO is not re-formed, remaining in metallic state.

Many papers have investigated PdO decomposition and its re-formation through Thermal Gravimetric Analysis (TGA) [30, 31, 32] and Temperature Programmed experiments [33, 34, 35],

depicting a complex redox behavior of Pd catalysts. McCarty *et al.* observed during the heating ramp a two-step oxygen release peak consistent with two different kinds of PdO species: the peak at lower temperature was attributed to the decomposition of bulk PdO, whereas the second one to complexes near the surface [35]. The multistage PdO decomposition was also observed by Groppi and co-workers on Pd catalysts supported on La_2O_3 stabilized alumina: they found three separate steps associated to different thermal stability of PdO whose distribution was dependent on oxygen partial pressure [34]. They ascribed the peak at higher temperature to PdO species in strong interaction with the support. Some authors observed that the qualitative profile of PdO reduction was strongly related to the thermal history of the catalyst [33, 35]. Colussi *et al.*, in fact, observed that the O_2 release/uptake profile during TPO changed with the conditions of previous PdO re-oxidation, with the formation of intermediate PdO_x [35], already detected by Farrauto *et al.* [30]. In a recent publication, Chen and co-workers from the results collected by TG and structural investigation have proposed a core-shell mechanism [32]. They suggest that the reduction of PdO is initiated at the surface, according to the previous results reported by Datye *et. al.* [29]. The thin shell formed by metallic Pd might stabilize the PdO core, shifting the decomposition of residual PdO to higher temperature [32].

The re-oxidation of Pd to PdO is a quite complex process and several mechanisms have been proposed to explain the hysteresis behavior. Mc.Carty *et al.* [35] suggested that metallic Pd is not fully oxidized during the cooling step likely due to the formation of chemisorbed oxygen layer. This passive layer pushes PdO re-formation to lower temperatures and hinders the nucleation and growth of stoichiometric PdO crystallites [35].

Datye *et al.* proposed the random formation of polycrystalline PdO species in contact with metallic Pd particles as the most predominant mechanism during PdO re-formation [29]. Groppi *et al.* from in-situ XRD experiments got to similar results with a possible involvement of a shrinking core mechanism. A deep study on the dynamic of PdO-Pd transformation has been carried out by Colussi *et al.*: they found the presence of intermediate PdO_x throughout TPO experiments as a precursor for PdO formation, and suggested that Pd re-oxidation is a kinetically limited process [35].

The dynamic PdO-Pd transition is strongly affected by the nature of the support: the addition of rare earth oxides (REO) into common alumina-supported catalysts is able to enhance PdO stability in the high temperature region compared to bare alumina-supported materials [37] [35, 38]. Among REO group, cerium oxide certainly plays a key role in the automotive pollutants abatement. CeO_2 behaves in fact like an oxygen buffer, releasing O_2 in rich reaction conditions and storing O_2 in lean atmosphere through the dynamic transition $Ce^{4+} \leftrightarrow Ce^{3+}$. In

addition, it is able to promote metal dispersion and increase the thermal stability of the alumina support [39]. The effect of CeO_2 as support on the thermal decomposition of PdO was described at first by Farrauto *et al.* [31]. They found that the use of CeO_2 promoted PdO re-formation at higher temperatures, therefore reducing the hysteresis gap. Groppi *et al.* got to the same conclusions observing that the threshold of Pd re-oxidation was strongly dependent on the support with a shift of Pd re-formation to high temperature for CeO_2-doped material [40]. A faster Pd re-oxidation on Ce-doped catalyst was observed by Colussi *et al.*: during TPO experiments on Pd/ceria-alumina Pd re-oxidation occurred in two separate steps with the larger peak at higher temperature associated to the re-oxidation of Pd particles in contact with CeO_2 and the second at lower temperature associated to Pd particles in contact with alumina [35]. Ceria, in fact, is able to provide lattice oxygen for PdO regeneration through the redox couple Ce^{4+}/Ce^{3+} [35, 41, 37], with a positive effect on the activity loss during the light off [40, 42]. For these reasons its use has been proven to be beneficial for Pd-based methane combustion catalysts.

1.2.1. Water poisoning of Pd catalysts

Despite their high performance, Pd catalyst are known for their high susceptibility to water vapor and sulfur-containing compounds: the presence of steam and SO_x dramatically deactivates the catalytic material with a severe reduction of its performances [9, 13, 43, 44]. In natural gas fuelled vehicles sulphur poisoning can be considered negligible compared to that caused by steam due to the low concentration of SO_x (< 1 ppm), while water vapor is present up to 15 vol %.

The water effect on Pd based catalysts depends on several factors such as temperature, catalyst composition and metal-support interaction. Water has an inhibition/deactivation effect on Pd catalysts and the level of inhibition/deactivation is temperature-dependent. A strong inhibition effect is detected in the low-T region (< 500°C): some authors attributed the catalyst deactivation to the formation of inactive $Pd(OH)_2$ due to the reaction of PdO with water molecules [45]. Other researchers proposed an alternative explanation: the shift of methane activation to higher temperatures in presence of water is attributed to the competitive adsorption between CH_4 and H_2O [46, 47, 48]. These authors suggested that at low-medium temperatures the desorption of H_2O produced during reaction is the rate limiting step; the presence of H_2O into the gas feed would make this step even slower with a decrease of catalytic performance [46]. Above 500°C the sintering of metal particles and/or collapse of the support with encapsulation of Pd might occur resulting in a reduction of Pd dispersion, and this seems to be the main reason for the deactivation at high temperature, with or without the presence of water [10, 49, 50].

Several papers have investigated the behavior of standard Pd/Al_2O_3, which exhibits a strong deactivation in wet atmosphere due to the high coverage of hydroxyls groups on Al_2O_3 and growth of particle size during reaction [51, 52, 53, 54].

One method to increase the resistance to H_2O-poisoning is the use of bimetallic Pd-Pt catalysts. The introduction of Pt improves the stability of the monometallic Pd/Al_2O_3, strongly dependent on the molar ratio Pd:Pt, but at the expenses of a lower catalytic activity [55]. Another approach to reduce the deactivation consists in the use of reducible and/or with high oxygen mobility supports. Schwartz and co-workers in fact ascribed the inhibition effect to a reduction of oxygen exchange between metal and support due to the build-up of hydroxyls groups on the catalytic surface [48, 56]. Some authors report that ceria-zirconia mixed oxides or zirconia can prevent the strong deactivation observed on alumina-supported catalysts [56, 57].

Ceria-zirconia solid solutions ($Ce_xZr_{1-x}O_2$) are widely exploited in TWC due to the enhancement of oxygen storage capacity (OSC) compared to pure ceria. The incorporation of Zr^{4+} into CeO_2 improves the redox properties of CeO_2 through the promotion of $Ce^{4+} \leftrightarrow Ce^{3+}$ transition. Furthermore, the presence of zirconia increases the thermal stability of CeO_2 in the high temperature region [39, 58].

An interesting suggestion on possible strategies for the improvement of stability comes from studies on the inclusion of noble-metal into a reducible carrier, where metal and support are in intimate contact. Metal-support interaction is a very important issue for the catalytic behavior of Pd catalysts. It has been observed that M-O-Ce sites improve the catalytic activity for NO reduction and HC oxidation [49, 59, 60]. In particular, in the field of methane oxidation, it has been found that the formation of M-O-Ce active sites increases the catalytic performance [61] by stabilizing highly dispersed Pd-O centers, preventing the sintering of noble metal particles after exposure to severe thermal treatment [49, 62, 63]. Moreover, the presence in this structure of highly undercoordinated oxygen species improves the overall reactivity towards methane activation. Other works have shown that an enhanced Pd-ceria interaction boosts the catalytic activity for methane combustion [64, 65]. All the aspects discussed above enlighten the complexity of the catalytic behaviour of Pd-based materials.

The goal of this PhD thesis was to address the issues still open for the improvement of both activity and stability of Pd-based catalysts by preparing new materials on different metal oxides as supports (CeO_2, $Ce_{0.75}Zr_{0.25}O_2$, ZrO_2, Ce-Si and Ce-Al) prepared via solution combustion synthesis. Their performances have been investigated for CH_4 oxidation with particular attention to the effect of water on the catalytic performance under steady-state and non-steady state conditions. Moreover, a deep structural and redox characterization has been

carried out in order to try to find a correlation between the observed behaviour and the physic-chemical characteristics of the materials.

References

[1] T. Lipman and M. Delucchi, *Climatic Change,* vol. 53, p. 477–516, 2002.

[2] M. Khan, T. Yasmin and A. Shakoor, *Renawable and Suistanable Enery Reviews,* vol. 51, pp. 785-797, 2015.

[3] R. Hecke, *Applied Catalysis A: General,* vol. 221, pp. 443-457, 2001.

[4] «https://www.dieselnet.com/standards/eu/hd.php,».

[5] G. Karavalakis, M. Hajbabaei, Y. Jiang, J. Yang, K. Johnson and D. Cocke, *Fuel,* vol. 175, pp. 146-156, 2016.

[6] H. Cho and B. He, *Energy Conversion and Management,* vol. 48, pp. 608-618, 2007.

[7] I. Saanum and M. Bysveen, "Lean Burn Versus Stoichiometric Operation with EGR and 3-Way Catalyst of an Engine Fueled with Natural Gas and Hydrogen Enriched Natural Gas," Journal of Engines, 2007.

[8] R. Carwford, J. Lyons and J. Heiken, SierraResearch, 2010.

[9] P. Gelin and M. Primet, *Applied Catalysis B: Environmental,* vol. 39, p. 1–37, 2002.

[10] R. Gholami, M. Alyani and K. Smith, *Catalysts,* vol. 5, pp. 561-594, 2015.

[11] J. Lampert, M. Kazi and R. Farrauto, *Applied Catalysis B: Environmental (,* vol. 14, pp. 211-223, 1997.

[12] M. Lin, X. Wu, J. Wan, S. Liu, R. Ran and D. Weng, *Catalysis Today,* vol. 242, pp. 322-328, 2015.

[13] P. Gelin, L. Urfels, M. Primet and E. Tenab, *Catalysis Today,* vol. 83, pp. 45-57, 2003.

[14] R. Burch and M. Hayes, *Journal of Molecular Catalysis A: Chemical,* vol. 100, pp. 13-33, 1995.

[15] M. Kinnunen, J. Hirvi, T. Vanakainen, M. Suvanto and T. Pakkanen, *Applied Catlysis A: General,* vol. 397, pp. 54-61, 2011.

[16] F. Niu, S. Li, Y. Zong and Q. Yao, *J. Phys . Chem C,* vol. 118, pp. 19165-19171, 2014.

[17] A. Hellmann, A. Resta, N. Martin, J. Gustafson, A. Trinchero and P. Carlsson, *J. Phys. Chem. Lett.,* vol. 3, p. 678–682, 2012.

[18] A. Dianat, N. Seriani, L. Chiacchi, M. Bobeth and G. Cuniberti, *Chemical Physics,* vol. 443, pp. 53-60, 2014.

[19] T. A., A. Hellmann and H. Gronbeck, *Phys. Status Solidi,* vol. 8, pp. 605-609, 2014.

[20] N. M. Kinnunen, J. Hirvi, T. Vanaleinen, M. Suvano and T. Pakkanen, *Applied Catalysis A,* vol. 397, pp. 54-61, 2011.

[21] D. Ciuparu, F. Verduraz and L. Pfefferle, *J. Phys. Chem. B,* vol. 106, pp. 3434-3442, 2002.

[22] A. Saatsuma, K. Osakia, M. Yanagiharaa, J. Ohyamaa and K. Shimizub, *Catalysis Today,* vol. 258, pp. 83-89, 2015.

[23] S. Colussi, A. Gayen, M. Boaro, J. Llorca and A. Trovarelli, *ChemCatChem,* vol. 7, p. 2222–2229, 2015.

[24] R. Burch and . F. Urbano, *Applied Catalysis A: General,* vol. 124, pp. 121-139, 1995.

[25] O. Demoulin, M. Navez and P. Ruiz, *Applied Catlysis A: General,* vol. 295, pp. 59-70, 2005.

[26] K. Fujjimoto , F. Ribeiro, M. Borja and E. Iglesia, *Journal of Catalysis,* vol. 179, pp. 431-442, 1998.

[27] J. Au-Yeung, K. Chen, A. T. Bell and E. Iglesia, *Journal of Catalysis,* vol. 188, p. 132–139, 1999.

[28] J. Xu , L. Ouyang, W. Mao , X.-J. Yang, X.-C. Xu, S. Jun-Jie, T.-Z. Zhuang, H. Li and Y.-F. Han, *ACS Catalysis,* vol. 2, pp. 261-269, 2012.

[29] A. Datye, J. Bravo, T. Nelson, P. Atsanova, M. Lyubovsky and L. Pfefferle, *Applied Catalysis A: General,* vol. 198, no. Issues 1–2, p. 179–196, 2000.

[30] R. Farrauto, M. Hobson, T. Kennelly and E. Watermann, *Applied Catalysis A:General,* vol. 81, pp. 227-237, 1992.

[31] R. Farrauto, J. Lampert, M. Holbson and E. Watermann, *Applied Catalysis B: Environmental,* vol. 6, pp. 263-270, 1995.

[32] X. Chen, J. Schwank, G. Fisher, Y. Cheng, m. Jagner, R. McCabe, M. B. Katz, G. Graham and X. Pan, *Applied Catalysis A: General,* vol. 475, p. 420–426, 2014.

[33] G. Groppi, C. Artioli, C. Cristiani, L. Lietti and P. Forzatti, *Studies in Surface Science and Catalysis,* pp. 345-350, 2001.

[34] G. Groppi, C. Cristiani, L. Lietti and P. Forzatti, *Studies in Surface Science and Catalysis,* vol. 130, pp. 3801-3806, 2000.

[35] S. Colussi, A. Trovarelli, E. Vesselli, A. Baraldi, G. Comelli, G. Groppi and J. Lorca, *Applied Catalysis A: General,* vol. 390, pp. 1-10, 2010.

[36] McCarty J.G, *Catalysis Today,* vol. 26, pp. 283-293, 1995.

[37] S. Colussi, A. Trovarelli, G. Groppi and J. Llorca, *Catalysis Communications,* vol. 8, pp. 1263-1266, 2007.

[38] K. Persson, A. Ersson, S. Colussi, A. Trovarelli and S. Jaras, *Apllied Catalysis B:Environmental,* vol. 66, pp. 175-185, 2006.

[39] J. Kaspar, P. Fornasiero and N. Hickey, *Catalysis Today,* vol. 77, p. 419–449, 2003.

[40] G. Groppi, C. Cristaini, L. Lietti, C. Ramella, M. Valentin and P. Forzatti, *Catalysis Today,* vol. 50, pp. 399-412, 1999.

[41] Q. Wang, *Journal of Molecular Catalysis A,* vol. 339, 2011.

[42] S. Colussi, A. Trovarelli, CristainiC., L. Lietti and G. Groppi, *Catalysis Today,* vol. 180, pp. 124-130, 2012.

[43] L. Hu and S. Williams, SAE International, 2007.

[44] S. Colussi, F. Arosio, T. Monatanari, G. Busca , G. Groppi and A. Trovarelli, *Catalysis Today,* vol. 155, pp. 59-65, 2010.

[45] R. Burch, F. Urbano and P. Loader , *Applied Catalysis A: General,* vol. 123, pp. 173-184, 1995.

[46] D. Ciuparu and P. L., *Applied Catalysis A:General,* vol. 209, pp. 415-428, 2001.

[47] F. Zhang, C. Hakanoglu, J. J. Hiojosa and J. Weaver, *Surface Science,* vol. 617, pp. 249-255, 2013.

[48] W. Schwartz, D. Ciuparu and L. Pfefferle, *J. Phys. Chem. C,* vol. 116, pp. 8587-8593, 2012.

[49] Y. Cao, R. Ran, X. Wu, B. Zhao , J. Wan and D. Weng, *Applied Catalysis A: General,* vol. 457, pp. 52-61, 2013.

[50] Q. Xu, K. Kharas, B. Croley and A. Datye, *ChemCatChem,* vol. 3, pp. 1004-1014, 2011.

[51] R. Kikuchi, S. Maeda, K. Sasaki, S. Wennerstrom and K. Eguchi, *Applied Catalysis A: General,* vol. 232, pp. 23-28, 2002.

[52] P. Hurtado, S. Ordonez, H. Sastre and F. Diez, *Applied Catalysis B: Envriromental,* vol. 47, pp. 85-93, 2004.

[53] J. Park, J. Cho, Y. Kim, E. Kim, H. Han and C. Shin, *Applied Catalysis B: Environemental,* Vols. 160-161, pp. 135-143, 2014.

[54] J. Park, J. Ahn, H. Sim, G. Seo, H.-S. Han and C. Shin, *Catalysis Communications,* vol. 56, pp. 157-163, 2014.

[55] K. Persson, P. L.D, W. Schwartz, A. Ersson and S. Jars, *Applied Catalyssi B: Environmental,* vol. 74, pp. 242-250, 2007.

[56] D. Ciuparu, E. Perkins and Pfefferle L., *Applied Catalysis A: General,* vol. 263, pp. 145-153, 2004.

[57] D. Ciuparu and P. L., *Catalysis Today,* vol. 77, pp. 167-179, 2002.

[58] S. Bedrane, C. Descorme and D. Duprez, *Catalysis Today,* vol. 73, p. 233–238, 2002.

[59] P. Bera, K. Patil, V. Jayaram, G. Subbanna e M. Hegde, *Journal of Catalysis,* vol. 196, pp. 293-301, 2000.

[60] K. Priolkar, B. P., P. Sarode, M. Hegde, S. Emura, R. Kumashiro and N. Lalla, *Chem. Mater,* vol. 14, pp. 2120-128, 2002.

[61] S. Colussi, A. Gayen, M. Camellone, M. Boaro, J. Llorca and A. Trovarelli, *Angew. Chem. Int.,* vol. 48, pp. 8481-8484, 2009.

[62] M. Monai, M. T., C. Chen, E. Fonda, G. R.J and F. P., *ChemCatChem,* vol. 0000, pp. 1-14, 2014.

[63] Y. Cao, R. Ran, X. Wu, X. Wu, J. Wan and D. Weng, *Catalysis Today,* vol. 281, pp. 490-499, 2017.

[64] M. Cargnello, J. Jeaen, J. Garrido, K. Bakhmutsky, T. Montini and J. Gamez, *Science,* vol. 337, pp. 713-717, 2012.

[65] P. Dong, L. Wen Zhi, Q. Zhao, Q. F. Haung, H. Qing Hu and S. Chun Yu, *Energy Technology,* vol. 4, p. 943–949, 2016.

Chapter 2

Materials and experimental methods

Palladium-based catalysts supported over different oxides ($Ce_xZr_{1-x}O_2$ with x = 0, 0.75 and 1, CeO_2-SiO_2 with different amount of silica and CeO_2-Al_2O_3 mixed oxide) were prepared by incipient wetness impregnation and solution combustion synthesis.

All catalysts were characterized in terms of structural and morphological properties by means of BET surface area and X-ray powder diffraction.

On the most promising materials also HR-TEM analysis and DRIFT analysis were carried out.

The performance of samples in methane combustion was evaluated by catalytic tests in lean (CH_4:O_2= 1:4) and stoichiometric reaction conditions (CH_4:O_2= 1:2). To check the resistance to water poisoning catalytic measurements were carried out also in the presence of water added to the feed.

In order to simulate the long-time exposure to the exhaust gas, time-on-stream tests were performed to investigate the catalysts deactivation with and without water vapor in the feed.

Consistent part of the work was dedicated also to the study of redox behavior in PdO ↔ Pd transformation both in oxidizing and reducing atmosphere by means of Temperature Programmed Oxidation (TPO) and Temperature Programmed Reduction (TPR) experiments, respectively.

2.1 Catalysts preparation

2.1.1 Incipient wetness impregnation

The catalysts prepared by incipient wetness technique (IW) have been used as reference samples. $Ce_xZr_{1-x}O_2$ supports with different Ce:Zr molar ratios (x = 0, 0.75 and 1) were synthesized by precipitation/co-precipitation, following the procedure proposed by Trovarelli and co-workers [1]. For the preparation of the mixed oxide cerium nitrate exahydrate ($Ce(NO_3)_36H_2O$) (Treibacher Ind.) was dissolved in proper amount of distilled water to obtain a 0.2 M solution; this solution was then mixed with the proper amount of zirconyl nitrate solution ($ZrO(NO_3)_2$,) (Treibacher Ind.). Hydrogen peroxide (H_2O_2, Aldrich, 35%) was poured into the solution to obtain a molar H_2O_2/(Ce+Zr) ratio of 3. Precipitation was obtained by adding ammonia solution (NH_4OH, Sigma Aldrich, 30 %) until the pH reached 10.5. The slurry was maintained under stirring for 4 hours and then it was filtered, washed with distilled water and dried overnight at 373 K. The pure ceria and zirconia oxides were prepared following the same procedure. CeO_2, ZrO_2 and $Ce_{0.75}Zr_{0.25}O_2$ so obtained were calcined at 1173 K for 3 h.
The supports were then impregnated with $Pd(NO_3)_2$ solution (Sigma Aldrich) in order to obtain 1 wt.% of Pd. Once the supports were impregnated, they were dried overnight at 373 K and calcined in air for 3 hours at 1173 K.

Figure 2.1: impregnation of $Ce_{0.75}Zr_{0.25}O_2$ mixed oxide

2.1.2 Solution combustion synthesis

Solution combustion synthesis (SCS) has been widely employed to prepare materials for energy storage, semi-conductors, thin-films, nano-ceramics and heterogeneous catalysts for hydrocarbon reforming/oxidation and automotive exhaust emissions treatments [2]. SCS technique represents in fact a valid route to prepare nanopowder catalysts [3, 4, 5, 6]. SCS involves a self-sustaining redox reaction between salts precursors (nitrates, carbonates or chlorides) as oxidizing agents and a fuel (urea, glycine, oxalyl dihydrazide and others) as the reducing agent [7, 8, 9]. The steps of SCS are illustrated in Figure 2.2.

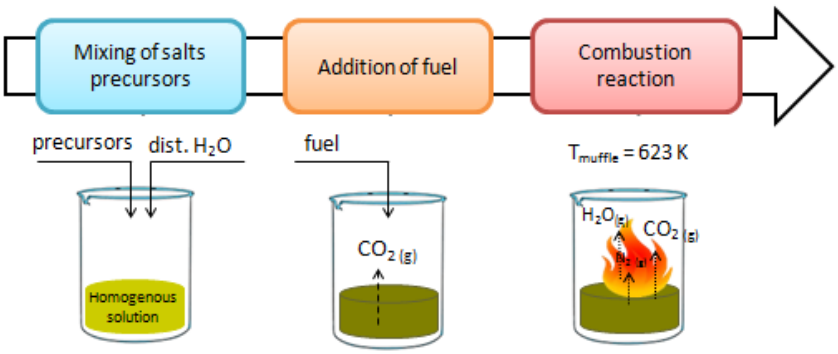

$$M(NO_3)_2 + C_2H_6N_4O_{2(aq)} \rightarrow MO_{(s)} + H_2O_{(g)} + CO_{2(g)} + N_2(g)$$

Figure 2.2: schematic representation of SCS procedure

A homogenous solution and the high reaction temperature reached in the combustion chamber allow to obtain the binary/ternary compound in one step with short reaction time. The starting precursors, the ratio between fuel and air, and the water amount in solution influence the reaction enthalpy and the adiabatic flame temperature, which are closely related to the final morphological properties of the powder, such as crystal structure and surface area. The main advantages of SCS route are the low cost and the short time to prepare the final catalyst: no further thermal treatments are required due to the high temperatures (> 1273 K) reached during the reaction with the possibility to prepare the catalytic material in one-step.

- *Pd supported on ceria-zirconia mixed oxides*

Catalysts with 1 wt.% of Pd supported on CeO_2, $Ce_{0.75}Zr_{0.25}O_2$ and ZrO_2 were prepared by solution combustion synthesis (SCS), following and adapting the procedure adopted by Colussi *et al.* [10, 11].

$Pd(NO_3)_2$ powder (Johnson Matthey) was dissolved in a little amount of deionized water to which a suitable amount of cerium and/or zirconium was added in the form of ceric ammonium nitrate $(NH_4)_2Ce(NO_3)_6$ (CAN, Treibacher Ind.) and zirconyl nitrate $ZrO(NO_3)_2$ (Treibacher Ind.). The liquid mixture was stirred for a few minutes until a clear solution was obtained. A stoichiometric amount of oxalyl dihydrazide ($C_2H_6N_4O_2$) was used as organic fuel and added into the aqueous solution. The obtained liquid mixture was then transferred in a furnace heated up to 623 K where the combustion took place with complete evaporation of water, leaving the final powder catalyst. After cooling, the sample was taken out from the furnace and no further treatment was carried out. The amount of fuel used during the synthesis was calculated based on the total oxidizing valence of precursors, not considering the contribution of nitrogen [8]. The overall redox reactions between salts precursors and fuel for CeO_2-ZrO_2 catalytic materials are reported in Table 2.1.

Table 2.1: overall theoretical redox reaction during SCS synthesis for Pd-supported on ceria, ceria-zirconia mixed oxide and zirconia

Catalyst	Redox reaction
1% Pd/CeO_2 SCS	$0.016Pd(NO_3)_2 + 0.984\ CAN + 2.38\ ODH \rightarrow 0.016\ PdO + 0.98\ CeO_2 + 11.076\ H_2O + 8.712\ N_2 + 4.76\ CO_2$
1% $Pd/Ce_{0.75}Zr_{0.25}O_2$ SCS	$0.015Pd(NO_3)_2 + 0.74\ CAN + 2.171\ ODH + 0.245\ Zr(NO_3)_2 \rightarrow 0.015\ PdO + 0.74\ CeO_2 + 0.245\ ZrO_2 + 9.473H_2O + 7.562N_2 + 4.342\ CO_2$
1 % Pd/ZrO_2 SCS	$0.011Pd(NO_3)_2 + 0.998\ ODH + 0.987\ Zr(NO_3)_2 \rightarrow 0.011\ PdO + 0.987ZrO_2 + 2.994H_2O + 2.994N_2 + 1.996\ CO_2$

- *Pd supported on Si- and Al-doped CeO_2 mixed oxides*

Pd/ceria-silica catalysts were also prepared by solution combustion synthesis with different amount of SiO_2 (2%, 5 wt%, 13 wt% and 20 wt%) and 1 wt% Pd. $Pd(NO_3)_2$ salt (Johnson Matthey) was dissolved in a little amount of distilled water to which a suitable amount of cerium and silicon has been added in the form of ceric ammonium nitrate (CAN, $(NH_4)_2Ce(NO_3)_6$) (Treibacher Industrie) and silicon tetraacetate $Si(OCOCH_3)_4$ (Sigma Aldrich). The aqueous solution was then introduced in the furnace heated up to 623 K, temperature at which the ignition process starts. Pd supported on alumina-doped ceria with 13 wt.% of Al_2O_3 was synthesized starting from $Pd(NO_3)_2$ powder (Johnson Matthey), (CAN, $(NH_4)_2Ce(NO_3)_6$) (Treibacher Industrie) and $Al(NO_3)_3{\cdot}9H_2O$ (Sigma Aldrich), following the same procedure used for Pd/ceria-silica materials. The overall redox reactions between salts and fuel for Si and Al-doped ceria materials are reported in Table 2.2.

Table 2.2: overall theoretical redox reactions during SCS synthesis for Pd-supported on Si-and Al-CeO_2 mixed oxides

Catalyst	Redox reaction
1 % Pd/CeO_2-2% SiO_2	$0.014\ Pd(NO_3)_2 + 0.817CAN + 1.974\ ODH + 0.0477\ Si(OCOCH_3)_4 \rightarrow 0.014\ PdO + 0.817\ CeO_2 + 0.0477\ SiO_2 + 6.26H_2O + 7.23\ N_2 + 4.329\ CO_2$
1 % Pd/CeO_2-5% SiO_2	$0.014\ Pd(NO_3)_2 + 0.857CAN + 2.07\ ODH + 0.129\ Si(OCOCH_3)_4 \rightarrow 0.014\ PdO + 0.857\ CeO_2 + 0.129\ SiO_2 + 10.412\ H_2O + 7.582N_2 + 5.086\ CO_2$
1 % Pd/CeO_2-13 % SiO_2	$0.013Pd(NO_3)_2 + 0.8695\ CAN + 1.681\ ODH + 0.292\ Si(OCOCH_3)_4 \rightarrow 0.013\ PdO + 0.695\ CeO_2 + 0.292\ SiO_2 + 9.575\ H_2O + 6.155N_2 + 5.698\ CO_2$
1 % Pd/CeO_2-20% SiO_2	$0.012\ Pd(NO_3)_2 + 0.576\ CAN + 1.394\ ODH + 0.413\ Si(OCOCH_3)_4 \rightarrow 0.012\ PdO + 0.576\ CeO_2 + 0.413SiO_2 + 8.964\ H_2O + 5.104\ N_2 + 6.092\ CO_2$
1 % Pd/CeO_2-13% Al_2O_3	$0.015\ Pd(NO_3)_2 + 0.787\ CAN + 2.199\ ODH + 0.1975\ Al(NO_3)_3 \cdot 9H_2O \rightarrow 0.015\ PdO + 0.787\ CeO_2 + 0.1975Al_2O_3 + 11.52\ H_2O + 7.857\ N_2 + 4.398\ CO_2$

2.2 Catalysts characterization

2.2.1 BET surface area and X-ray powder Diffraction (XRD)

The surface area measurements were carried out following Brunauer-Emmet-Teller theory in a Micromeritics Tristar porosimeter. Prior to adsorption measurements, the catalysts were degassed in vacuum for 2 hours at 423 K.

X-ray diffraction is a standard analysis method to identify and characterize the crystalline structure of solid powders. XRD technique is based on the scattering phenomena that occurs between atoms into crystal lattice and X-ray waves, leading to the diffusion of light beam in all directions. XRD spectra have been collected in a Philips X'Pert diffractometer equipped with an X'Celerator detector, using Ni-filtered Cu Kα radiation (λ = 1.542 Å) and operating at 40 kV and 40 mA, with a step size of 0.02° and 40 counts per step. Average crystal sizes of the samples were calculated by Scherrer's equation:

$$D_{particle} = \frac{0.9 \times \lambda}{B \times \cos\theta}$$

with $B = \sqrt{B_{obs}^2 - B_{inst}^2}$ being the line broadening at half the maximum intensity (FWHM) in radians, λ the wavelength and θ the Bragg angle in radians.

2.2.2 *TEM analysis*

High Resolution Transmission Electron Microscopy images were collected on a JEOL 2010F instrument equipped with a field emission gun and at an accelerator voltage of 200 kV. The HR-TEM measurements were carried out by prof. Jordi Llorca at the Universitat Politecnica de Catalunya following the procedure reported in the literature [12].
Microstructural characterization of a few samples was carried out by a Zeiss LIBRA 200FE transmission electron microscopy (TEM), equipped with a 200 kV FEG source, in column second-generation omega filter for Energy Selective Spectroscopy (EELS) and Imaging (ESI), High Angular Annular Dark Field Scanning Electron Microscopy (HAADF-STEM) facility and Energy-dispersive X-ray (EDX) probe for chemical analysis. Prior to introduction in the instrument, the samples were ultrasonically dispersed in isopropyl alcohol and a drop of the suspension was deposited onto a lacey carbon copper grid (300 mesh).

2.2.3 *FTIR analysis*

FTIR analysis using mid-infrared Fourier transform spectrometers has become a common technique to obtain information on the adsorbed species on catalysts surface. The DRIFT measurements were collected by a Nicolet™ iS™ 50 FT-IR Spectrometer equipped with Pike Technologies Diffuse IR^{TM} cell (Figure 2.3) using a DTGS detector. A FTIR spectrum recorded over a mirror was used as background, and prior to measurement the cell was purged in nitrogen to eliminate the contribution of CO_2 and H_2O of the atmosphere. The catalyst powder was placed into the sample holder inside the reaction cell; the IR spectra were collected at room temperature (*ex-situ* measurements) in the range 400-4000 cm^{-1} recording 32 scans with a resolution of 4 cm^{-1} at an optical velocity of 0.1581 cm^{-1}. Each IR spectrum was analyzed using OMNIC software.

Figure 2.3: FT-IR spectrometer and IR cell

2.2.4 Temperature Programmed Oxidation

Temperature Programmed Oxidation (TPO) experiments are the state-of-the-art tests for the investigation of PdO-Pd-PdO decomposition/re-oxidation cycles. TPO analysis was performed in the apparatus illustrated in Figure 2.4, using a 2 vol.% O_2 in N_2 mixture with a total flow rate of 60 $mlmin^{-1}$. The catalyst powder (150 mg) was loaded on a quartz wool bed in a quartz micro-reactor. The sample was heated up to 1273 K at a heating rate of 10 $Kmin^{-1}$, then cooled down to 573 K at 10 $Kmin^{-1}$ before a new cycle started. To evaluate the effect of the presence of water on PdO-Pd-PdO transition, TPO experiments were performed also in wet conditions (10 vol.% H_2O (v)), carrying out two cycles (heating/cooling) up to 1273 K at 10 K/min and performing other a subsequent one without water. Oxygen release and consumption were monitored continuously with an ABB paramagnetic Magnos 106 oxygen analyzer.

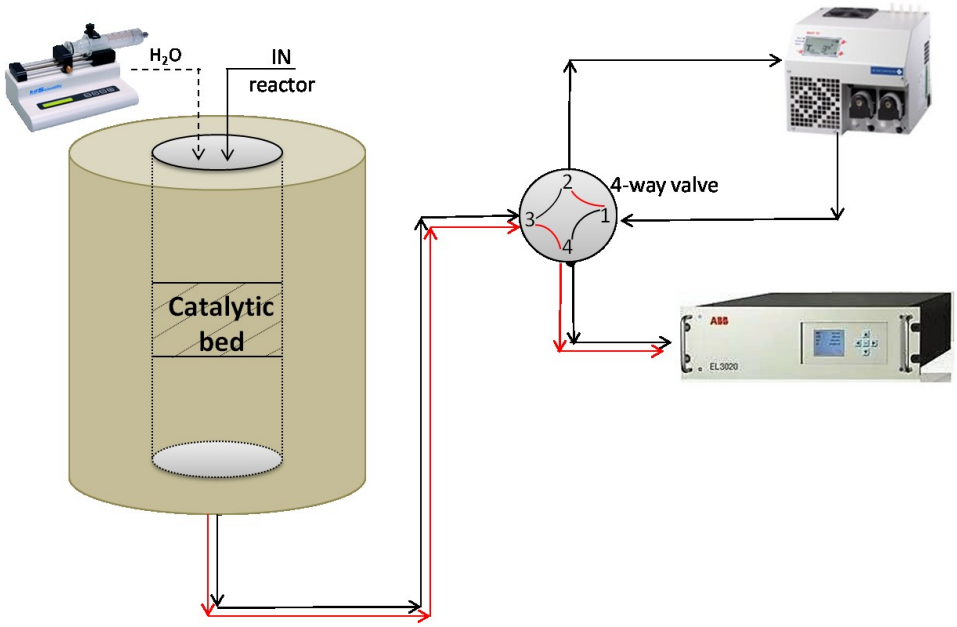

Figure 2.4: scheme of the system used for TPO experiment (red line) and catalytic tests (black line)

2.2.5 H_2-TPR

Along with TPO, Temperature Programmed Reduction (TPR) experiments are the state-of-the-art tests for the investigation of palladium redox behavior. TPR experiments were carried out in a Micromeritics Autochem analyzer: approximately 50 mg of catalyst were placed in a U-shaped quartz reactor and pre-treated in flowing air at 623 K for 1 h to eliminate moisture and adsorbed species. After pre-treatment, the sample was cooled down to 193 K using liquid nitrogen and then it was reduced in a flow of 4.5 vol% H_2/N_2 (35 $mlmin^{-1}$), while increasing the temperature from 193 K up to 1263 K at 10 $Kmin^{-1}$. The amount of H_2 consumption during H_2-TPR was measured by a thermal conductivity detector (TCD).

2.2.6 Catalytic tests in lean conditions

Different catalytic tests have been carried out in order to investigate the activity of the samples for the oxidation of methane. Temperature programmed combustion (TPC) experiments were carried out in a quartz micro-reactor (i.d = 6mm and l = 420 mm). The scheme of the system is shown in Figure 2.4.

In lean experiments, a reaction mixture consisting of 0.5 vol% CH_4, 2 vol% O_2 in He was fed to the reactor with a total flow rate of 180 $mlmin^{-1}$ and with a Gas Hourly Space Velocity (GHSV) of ~180000 h^{-1}. Prior to the test, the samples were pelletized and crushed to obtain particles with a diameter comprised between 100 μm and 200 μm in order to avoid pressure drops. The catalyst (120 mg) was then loaded in the reactor on a quartz-wool bed. For each sample two combustion cycles have been performed heating up to 1173 K at 10 K/min and then cooling down with the same temperature ramp.

To investigate the deactivation induced by the presence of water on the activity of Pd-based catalysts, catalytic tests were carried out in wet atmosphere by adding 10 vol.% $H_2O(v)$ and keeping the same reaction conditions (i.e. flowrate, O_2/CH_4 ratio and temperature cycles) used for the experiments without water. Water was fed into the reactor through a syringe (Kd scientific). In each experiment the sample was heated up to 1173 K with a heating ramp of 10 K/min, then cooled down to room temperature at 10 K/min. After the two heating/cooling cycles in wet conditions, a subsequent heating/cooling ramp was performed without water in order to check the recovery of catalytic activity after exposure to wet atmosphere. In all catalytic tests, combustion products concentration was monitored by ABB AO2020 IR gas analyzer, placed after a gas cooler to condense water and avoid moisture in the IR cell.

To compare quantitatively the catalytic performance of the samples, reaction rate measurements were carried out. Kinetic measurements were performed by recirculating a certain amount of effluent gas through a TTS D10K Micropump in order to operate in

differential conditions as shown in Figure 2.5. The chosen recycle ratio (R/F) was 25 and the flow rate on the recycle branch (R) was measured with a Bronkhorst EL-Flow flow meter. The use of the recycle ensures the operation in differential conditions, which allow in turn a correct kinetic analysis. In this way, in fact, the concentration of reactants and products is nearly uniform throughout the catalytic bed, thanks to the very high space velocity per pass, and therefore also the reaction rate can be considered constant within the catalytic bed.

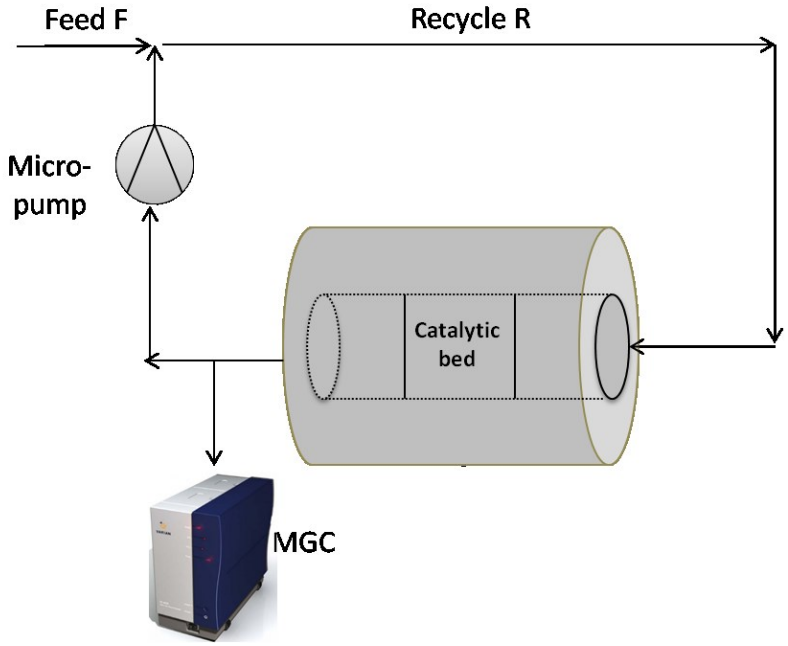

Figure 2.5: scheme of apparatus for kinetic measures.

The reaction rate (r_{CH_4}), is defined as the numbers of moles of methane reacting per unit time and per unit mass of catalyst (mol/s*g_{cat}), and it is calculated as reported in the equation below:

$$r_{CH4} = \frac{F_0^{CH4} \times X_{CH4}}{W_{cat}} [\frac{mol}{s * g_{cat}}]$$

where $F_O^{CH_4}$ (mol/s) is the initial molar flow of methane, $X_{CH_4}$is the methane conversion and W_{cat} (g) is the weight of catalyst. When a precious metal is used as the active phase, it is convenient to express the reaction rate as a function of the weight of the noble metal. In this work the reaction rate will then be expressed as mol/s*g_{Pd}.

Kinetic measurements were carried out after a first heating/cooling cycle up to 1173 K in the reaction gas mixture (0.5 % CH_4, 2 % O_2 in He). The sample (50 mg) was loaded in a quartz micro-reactor on a quartz wool bed and it was exposed to the reaction mixture with a total flow rate of 60 mlmin-1. The concentration of methane and reaction products was monitored by a Micro Gas Chromatograph (MGC) Varian Agilent CP 4900.

In order to simulate a long-term exposure of catalysts to exhaust gases and investigate the deactivation behavior, time-on-stream tests (TOS) were performed. TOS experiments were carried out at 723 K both in dry and wet atmosphere, according to the literature, which indicates that the water poisoning is more severe at temperatures lower than 773 K [13]. Prior to the stability test, each catalyst was exposed to a methane oxidation cycle up to 1173 K at 10 $Kmin^{-1}$ as a pre-treatment in lean conditions, then the temperature was raised up and held at 723 K for 24 hours while monitoring continuously the effluent gases. Methane combustion products concentration was monitored by a Micro Gas Chromatograph (MGC) Varian Agilent CP 4900. In the experiments with steam, water was fed through a Waters 515 HPLC pump.

The ability of the catalysts to regenerate their activity was measured by activity recovery tests. The tests were carried out at 723 K changing periodically from wet-lean (0.5 % CH_4, 2 % O_2, 10 vol.% H_2O (v) in He) to dry-lean mixture (0.5 % CH_4, 2 % O_2 in He), continuously monitoring the change in methane concentration. As performed for time-on stream tests, each catalyst was exposed to a methane oxidation cycle up to 1173 K at 10 $Kmin^{-1}$ as a pre-treatment in wet atmosphere, then the temperature was raised up and held constant at 723 K, while reactants and products concentration was monitored by ABB AO2020 IR analyzer. The steps of activity recovery tests are listed below and illustrated in Figure 2.6.

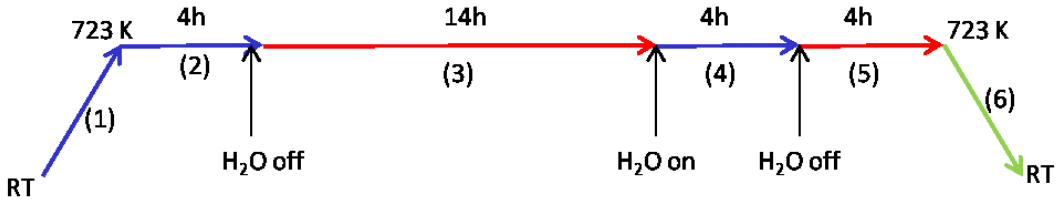

Figure 2.6: steps of activity recovery test

(1) Increasing temperature up to 723 K in 10 vol.% of H_2O (v) at 10 $Kmin^{-1}$;

(2) Isotherm at 723 K for 4 hours in 10 vol% of H_2O (v);

(3) Isotherm at 723 K overnight without water vapour;

(4) Isotherm at 723 K for 4 hours in 10 vol% of H_2O (v);

(5) Isotherm at 723 K for 4 hours without water vapor;

(6) Cooling to room temperature into dry-lean mixture.

2.2.7 Catalytic tests in stoichiometric conditions

For the best samples, the catalytic performance was evaluated also in stoichiometric conditions (CH_4:O_2= 1:2). Stoichiometric mixture (0.5 vol% CH_4, 1.0 vol% O_2, He as balance gas) was fed at total flow rate of 90 $mlmin^{-1}$ with an average GHSV of 180000 h^{-1}. 60 mg of powder catalyst was loaded in a quartz microreactor on a quartz-wool bed and put in a tubular furnace. Two

subsequent methane oxidation cycles were performed on each sample up to 1173 K at a heating ramp of 10 $Kmin^{-1}$ and then cooled down to room temperature.

To assess the resistance to water poisoning, catalytic tests were carried out in the presence of water vapour (10 vol.% H_2O (v)), setting the same reaction conditions used for the experiments without water and following the same experimental procedure used in wet-lean reaction conditions.

References

[1] M. Moser, G. Vilè, S. Colussi, F. Krumeich, D. Teschner, L. Szentmiklòsi, A. Trovarelli and J. Ramiréz, *Journal of Catalysis*, vol. 331, pp. 128-137, 2015.

[2] W. Wen e J.-M. Wu, *RSC Advances*, vol. 4, pp. 58090-58100, 2014.

[3] P. Bera, K. Patil, V. Jayaram, G. Subbanna and M. Hegde, *Journal of Catalysis*, vol. 196, pp. 293-301, 2000.

[4] K. Priolkar, P. Bera, P. Sarode, M. Hegde, S. Emura , R. Kumashiro and N. Lalla, *Chem. Mater*, vol. 14, pp. 2120-128, 2002.

[5] S. Specchia, E. Finocchio, G. Busca, P. Palmisano and V. Specchia, *Journal of Catalysis*, vol. 263, pp. 134-145, 2009.

[6] A. Gayen, M. Boaro , C. De Leitenburg, J. Llorca and A. Trovarelli , *Journal of Catalysis*, vol. 270, pp. 285-298, 2010.

[7] S.L. Gonzales-Cortes and F. E. Imbert, *Applied Catalysis A: General*, vol. 452, pp. 117-131, 2013.

[8] S. Specchia, C. Galletti and V. Specchia, *Studies in Surface Science and Catalysis*, vol. 175, pp. 59-67, 2010.

[9] A. Varma, A.S. Mukasyan, A.S. Rogachev and K.V. Manukyan, *Chem. Rev.*, vol. 116, p. 14493–14586, 2016.

[10] S. Colussi, A. Gayen, M. Boaro, J. Llorca and A. Trovarelli, *ChemCatChem*, vol. 7, p. 2222–2229, 2015.

[11] S. Colussi, A. Gayen, J. Llorca, C. De Leitenburg, G. Dolcetti and A. Trovarelli, *Ind. Eng. Chem. Res.*, vol. 51, p. 7510–7517, 2012.

[12] S. Maiti, J. Llorca, M. Dominguez, S. Colussi, A. Trovarelli, K. R. Priolkar, G. Aquilanti and A. Gayen, *Journal of Power Sources*, vol. 304, pp. 319-331, 2016.

[13] R. Gholami, M. Alyani e K. Smith, *Catalysts*, vol. 5, pp. 561-594, 2015.

[14] K.R. Priolkar, P. Bera , P. Sarode, M. Hegde, S. Emura, R. Kumashiro e N. Lalla, *Chem. Matter.*, vol. 14, pp. 2120-2128, 2002.

Chapter 3

Structural characterization and redox behavior of $Pd/Ce_xZr_{1-x}O_2$ catalysts

This chapter is focused on the characterization of the physico-chemical properties of Pd-based catalysts supported on CeO_2, $Ce_{0.75}Zr_{0.25}O_2$ and ZrO_2 prepared by solution combustion synthesis. BET surface area measurements, X-ray Powder Diffraction, High Resolution Transmission Electron Microscopy (HR-TEM) analysis were employed to characterize the series of Pd-supported catalysts on different metal oxides by a structural and morphological point of view. Temperature Programmed techniques (i.e Temperature-Programmed Oxidation (TPO) and Temperature Programmed Reduction (H_2-TPR)) were performed to investigate the redox behavior of the samples under oxidizing and reducing atmosphere. The structural and redox properties of combustion synthesized samples will be compared to those of corresponding catalysts prepared by traditional IW technique.

3.1. Structural and textural properties

3.1.1 Surface area and X-ray diffraction analysis

Table 3.1 summarizes the noble metal loading of catalysts as measured by ICP and BET surface area of all samples. The measured Pd amount on each catalyst is quite close to 1 wt.% while the Pd content for 1PdZr SCS is slightly higher with respect to the nominal loading. All catalysts have a low surface area due to the high temperatures reached during the synthesis: during combustion in fact the temperature in the furnace can quickly exceed 1273 K due to the exothermic nature of the reaction [1]. Despite a higher temperature is locally reached during the combustion synthesis [1], SCS samples show a larger surface area with respect to their corresponding IW ones.

Table 3.1: noble metal loading and surface area of 1%Pd/$Ce_xZr_{1-x}O_2$ catalysts.

Catalyst	**preparation method**	**Sample name**	**Pd [wt. %][a]**	**S_{BET} (m^2g^{-1})**
1%Pd/CeO_2 IW	impregnation method	1PdCe IW	0.97	3.8
1%Pd/$Ce_{0.75}Zr_{0.25}O_2$ IW	impregnation method	1PdCZ75 IW	0.99	13.5
1%Pd/ZrO_2 IW	impregnation method	1PdZr IW	0.98	11.4
1%Pd/CeO_2 SCS	solution combustion synthesis	1PdCe SCS	1.09	6.6
1%Pd/$Ce_{0.75}Zr_{0.25}O_2$ SCS	solution combustion synthesis	1PdCZ75 SCS	0.97	18.4
1%Pd/ZrO_2 SCS	solution combustion synthesis	1PdZr SCS	1.29	15.9

[a] measured by ICP elemental analysis

Irrespective of the preparation method, the introduction of 25 mol% of ZrO_2 into the ceria lattice stabilizes the surface area, as expected from previous literature studies [3]. The XRD patterns of IW and SCS catalysts are shown in Figure 3.1 and 3.2, respectively. The exposure to high temperatures during the preparation is reflected in the XRD profiles, where all samples present quite sharp and intense diffraction peaks. Looking at XRD patterns of 1PdCe IW and

1PdCe SCS, the characteristic peaks relative to cerium oxide in cubic fluorite-like structure are clearly observed.

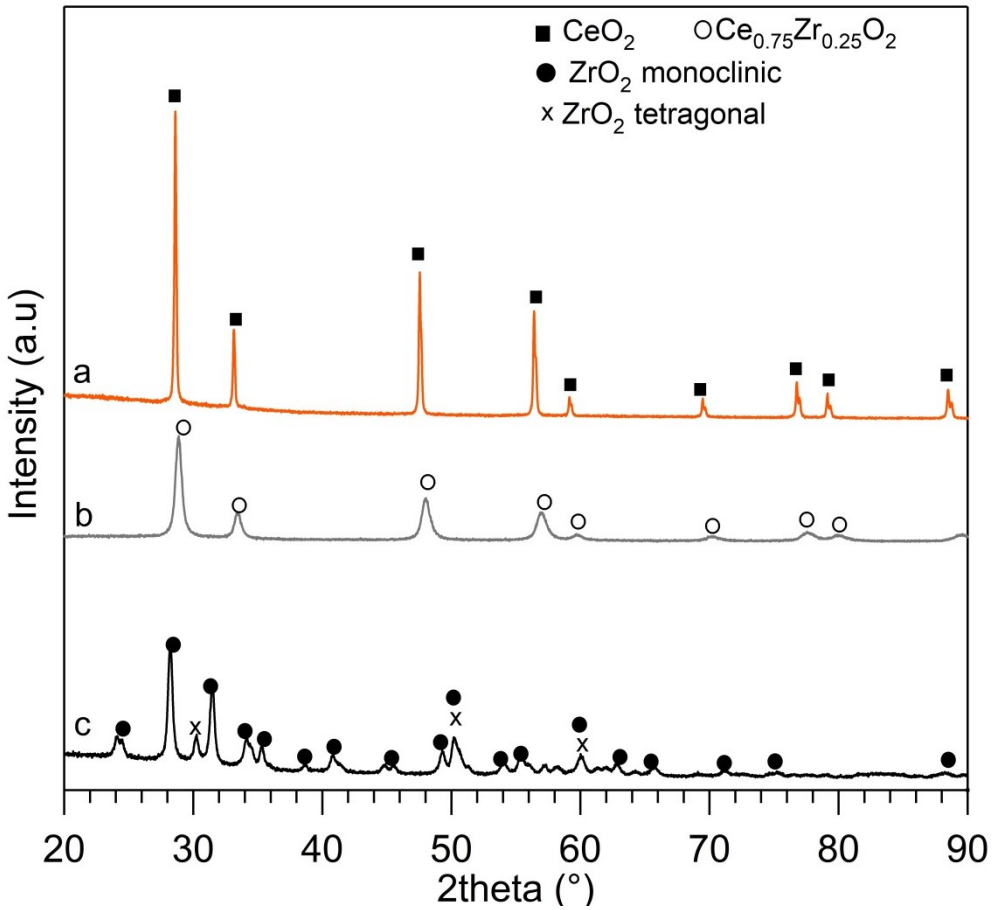

Figure 3.1: XRD patterns of IW catalysts: (a) 1PdCe IW, (b) 1PdCZ75 IW, (c) 1PdZr IW

The reflections of 1PdCZ75 IW catalysts are shifted towards higher diffraction angles according to the formation of a solid solution with Ce:Zr = 0.75:0.25 molar composition [2, 4]. The formation of a homogenous ceria-zirconia mixed oxide is confirmed by the symmetric diffraction peaks observable on 1PdCZ75 IW [2]. On the contrary, structural heterogeneity is observed on 1PdCZ75 SCS where the diffraction peaks are asymmetric indicating a non-homogeneous phase enriched in CeO_2 due to the segregation of zirconia [2]. On ceria-containing samples, independently of the preparation method, no peaks belonging to PdO or Pd are detected. This can be due to the low noble metal loading and/or to the fine dispersion of Pd/PdO particles.

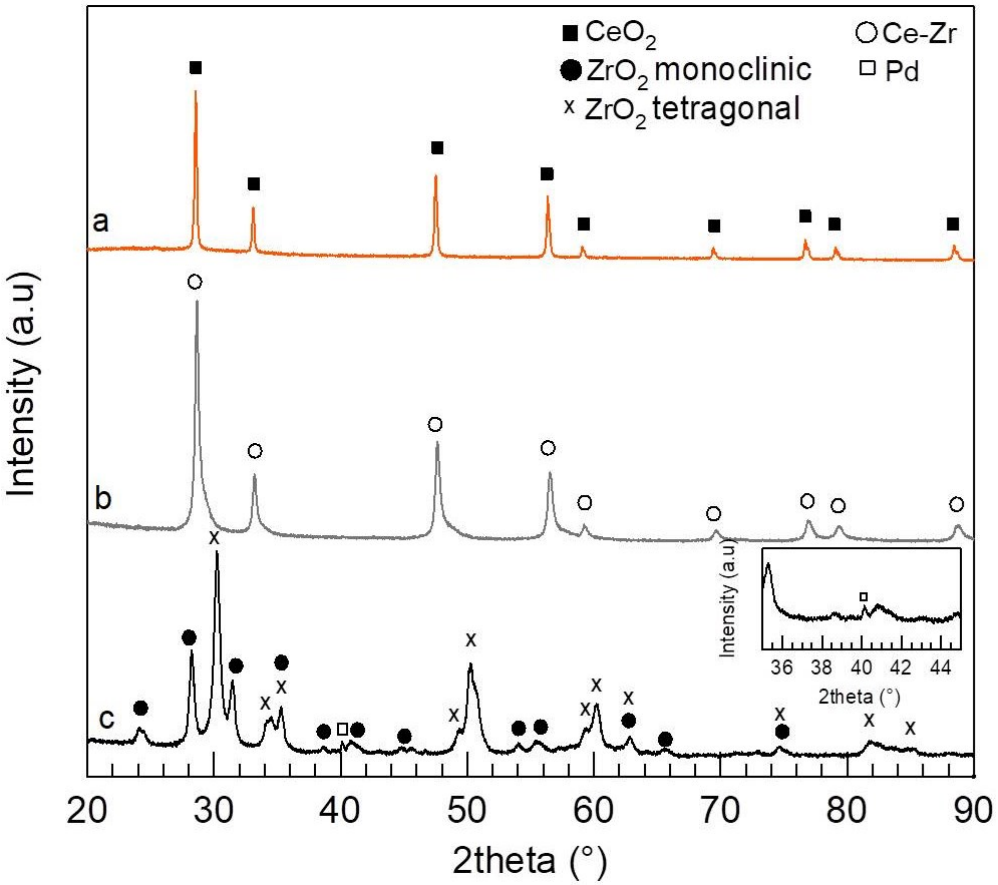

Figure 3.2: XRD patterns of SCS catalysts: (a) 1PdCe SCS, (b) 1PdCZ75 SCS, (c) 1PdZr SCS

Regarding zirconia-supported samples, the support exhibits the characteristic peaks of monoclinic (ZrO_2-m) and tetragonal phase (ZrO_2-t), according to the phase transition from monoclinic to tetragonal induced by severe thermal treatment [5]. The monoclinic form is prevalent on 1PdZr IW. On 1PdZr SCS a weak diffraction peak of metallic Pd(111) is detected at $2\theta = 40.2°$ (clearly visible in the inset of Figure 3.2). The presence of metallic Pd on combustion synthesized samples is in line with the redox reaction that can take place during the preparation [6].

The mean particle size of catalysts has been calculated by Scherrer's equation on the basis of XRD patterns. For ceria-doped catalysts the particle size has been calculated on the basis of main diffraction peak of CeO_2 at $2\theta = 28.2°$ and for zirconia-based samples with respect to the main diffraction peak of ZrO_2 located at 30.2° (for 1PdZr SCS) and 28.2° (for 1PdZr IW). The particle size of SCS samples increases in the order 1PdZr SCS < 1PdCZ75 SCS < 1PdCe SCS, being equal to 20 nm, 24 nm and 46 nm, respectively. The fine particle size of SCS catalysis is associated to the production of large amount of gases during combustion synthesis [7]. The mean particle size of the catalysts prepared by impregnation method has been estimated with the same procedure and equal to 21 nm, 15 nm and 68 nm for 1PdZr IW, 1PdCZ75 IW and 1PdCe IW, respectively.

3.1.2 HR-TEM analysis

High-resolution transmission electron microscopy images collected for 1PdCe SCS and 1PdCe IW catalysts as-prepared are illustrated in Figure 3.4 and 3.5, respectively.

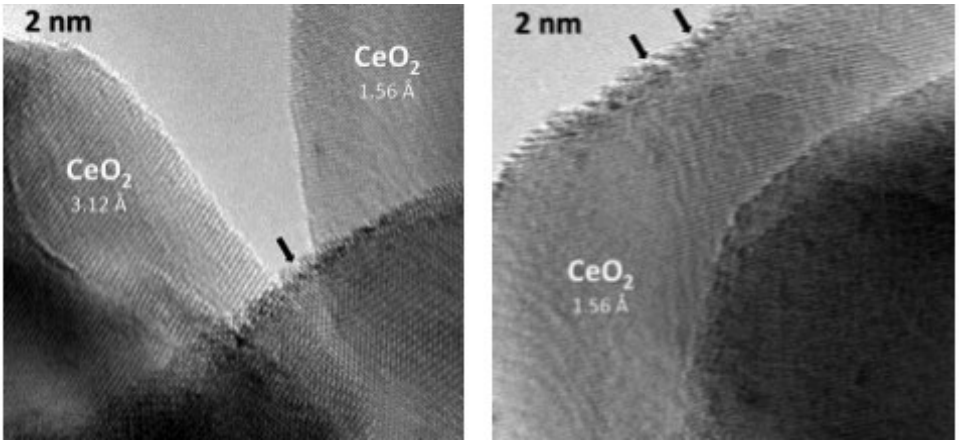

Figure 3.3: HR-TEM images of fresh 1PdCe SCS catalyst

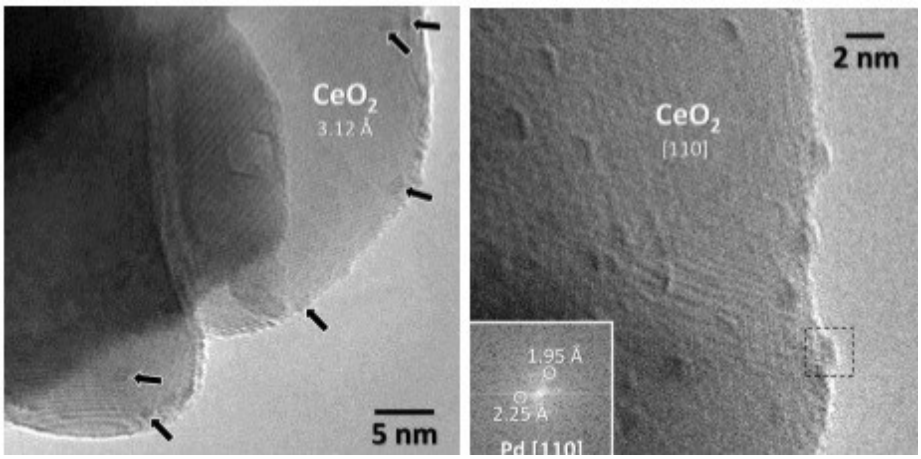

Figure 3.4: HR-TEM images of fresh 1PdCe IW catalyst

On SCS catalyst, ceria particles have a broad size distribution, ranging from about 30 nm up to 200 nm, which is likely a direct consequence of the SCS route. No well-defined Pd nanoparticles are observed; a surface roughness is evident in some of the profile view of images reported in Figure 3.3: lattice fringes at 3.12 and 1.56 Å correspond to the (111) and (222) crystallographic planes of ceria, respectively. This surface roughness is likely attributed to the Pd-O-Ce superstructure, as already observed in previous works from our and other groups [6] [7, 8, 9]. The formation of M-O-Ce bond is promoted by the interaction of CeO_2 with noble metal at high temperatures and oxygen containing atmosphere [5]. In some cases this solid solution can appear as an ordered structure in which a Pd ion substitutes one out of four cerium atoms, giving rise to a reconstruction of CeO_2 surface with the formation of an equivalent number of oxygen vacancies [9].

On 1PdCeIW sample (Figure 3.4), palladium is present in the form of very small nanoparticles of about 1-2 nm, well-dispersed over the ceria support. The analysis of the FT image (Figure 3. 4

(right)) corresponding to one of the Pd nanoparticles shows spots at 2.25 and 1.95 Å, which are ascribed to the (111) and (200) crystallographic planes of Pd, respectively. In Figure 3.5 an HR-TEM image of 1PdCZ75 SCS is shown.

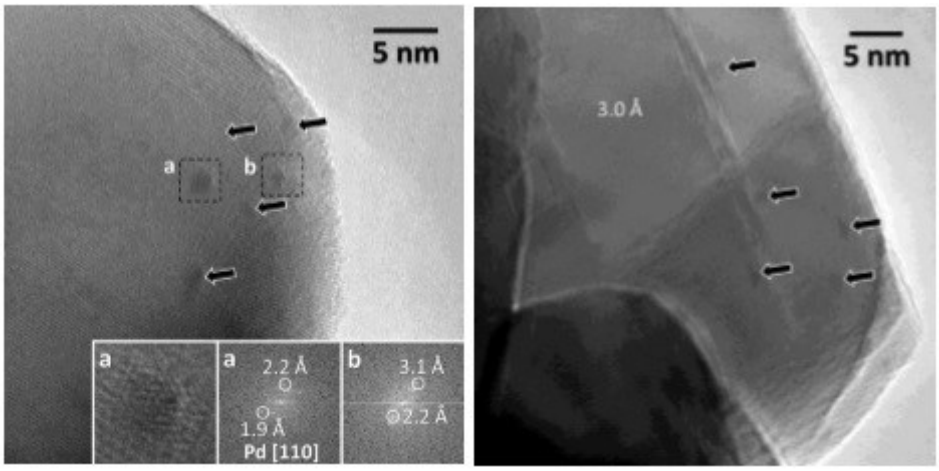

Figure 3.5: HR-TEM images of fresh 1PdCZ75 SCS catalyst

Some of the Pd particles are indicated by arrows. The FT images of the particles labeled "a" and "b" show spots at 2.2 and 1.9 Å corresponding to the (111) and (200) crystallographic planes of Pd, respectively. Spots at 3.1 Å correspond to the (111) crystallographic planes of the CeO_2-ZrO_2 support. Several Pd nanoparticles with ~2 nm diameter are well distributed over the CZ support. It appears that the incorporation of zirconium oxide into the ceria lattice prevents the formation of an ordered surface Pd-O-Ce structure and very small Pd particles segregate on the surface of the $Ce_{0.75}Zr_{0.25}O_2$ support.

3.2. Redox properties under oxidizing and reducing atmosphere

3.2.1 TPO experiments

Temperature programmed oxidation experiments were carried out to study the PdO-Pd transformation during heating/cooling cycles. The study of redox properties is a key point to evaluate the modifications of the active phase occurring on Pd catalysts. The main objective of these TPO experiments was to study the influence of preparation method on the dynamic of PdO–Pd-PdO phase transformation. For each sample three heating/cooling cycles were performed up to 1273 K. The qualitative oxygen profile collected during the three TPO cycles for 1PdCe SCS and 1PdCe IW are reported in Figure 3.6 and 3.7, respectively.

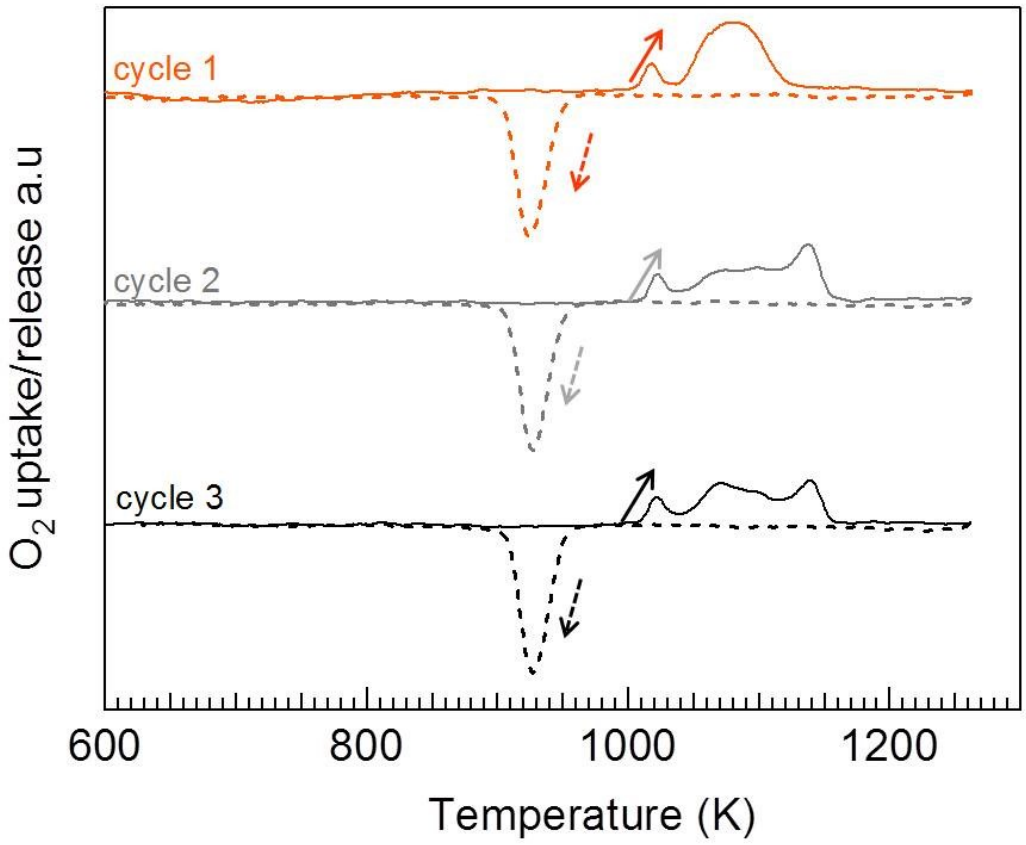

Figure 3.6: O_2 profile of 1PdCe SCS catalysts; solid line: heating, dotted line: cooling

Looking at TPO profile of 1PdCe SCS (Figure 3.6) two O_2 release peaks are observed during the first cycle and are related to PdO decomposition ($\mathbf{PdO \rightarrow Pd + \frac{1}{2} O_2}$): the first one, smaller, takes place at about 1014 K and a second larger peak at about 1080 K. Before PdO decomposition, a slight O_2 uptake is present in the range 620-760 K likely due to the oxidation of some metallic Pd particles. Focusing on the cooling part of the cycle, a single O_2 peak at 929 K is observed due to Pd re-oxidation. This re-oxidation takes place with a thermal hysteresis of about 100 K with respect to the decomposition process, as already widely reported in the literature [10, 11, 12 13]. If we observe the O_2 profile collected for 1PdCe IW (Figure 3.7) during the first cycle, a different picture appears: PdO decomposition starts at higher temperature (about 1075 K) with a broader O_2 release peak, and the low temperature feature is more pronounced with respect to the SCS counterpart, whereas the high temperature peak is much smaller.

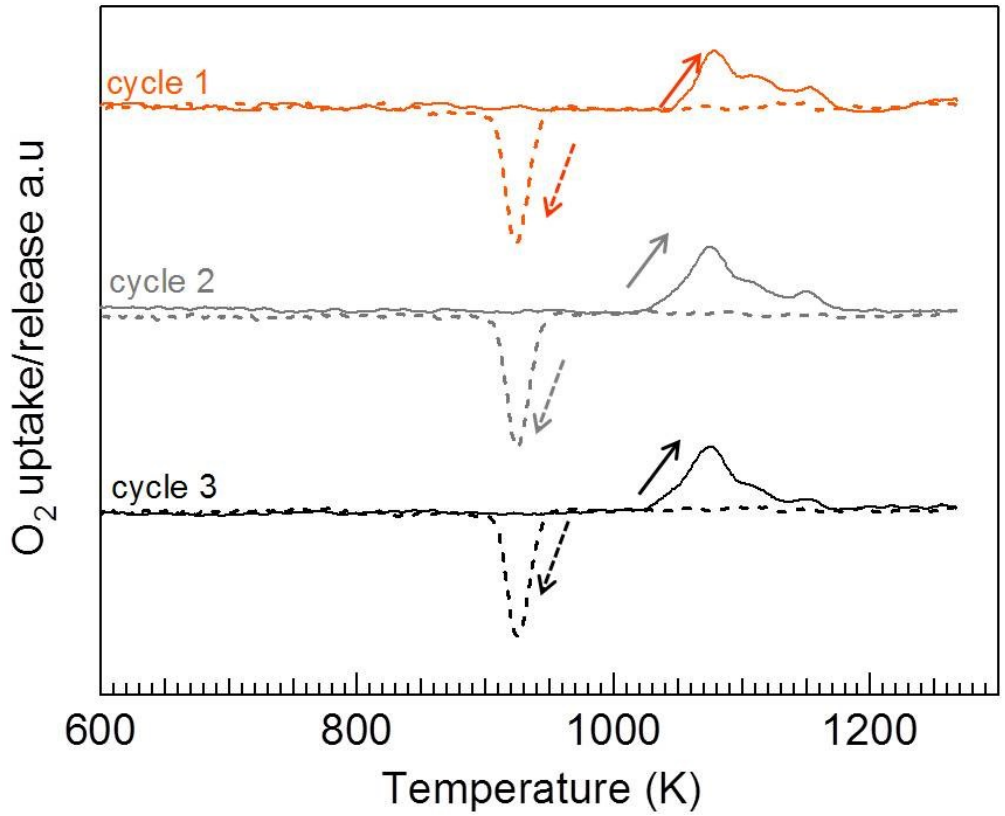

Figure 3.7: O_2 profile of 1PdCe IW catalysts; solid line: heating, dotted line: cooling

By observing the O_2 profile collected during cycles 2 and 3, the heating part appears quite different with respect to the first one, in particular for SCS sample: this behavior can be attributed to the different thermal treatment of Pd particles in air during the synthesis and in lower O_2 partial pressure during TPO measurements [14]. In the second and third runs on 1PdCe SCS, PdO → Pd transformation takes place in three well distinct steps with maxima at 1022 K, 1072 K and 1138 K, respectively. On impregnated sample, the qualitative oxygen profile during the heating ramp exhibits a slight variation during the second and third cycle. Looking at the cooling part during the 2nd and 3rd TPO run a single oxygen uptake peak is observable belonging to Pd re-oxidation ($\mathbf{Pd + \frac{1}{2}\, O_2 \rightarrow PdO}$) which takes place at 929 K for both samples. Since from the second redox cycle onward the qualitative oxygen profile of catalysts does not show significant variations, the third cycle has been chosen as the reference one to compare TPO profile of SCS samples with their corresponding impregnated ones. Figure 3.8, 3.9 and 3.10 show the comparison of the third TPO cycle for CeO_2, CZ75 and ZrO_2-supported catalysts, respectively, and Table 3.2 summarizes the temperatures of oxygen release/uptake maxima for each sample.

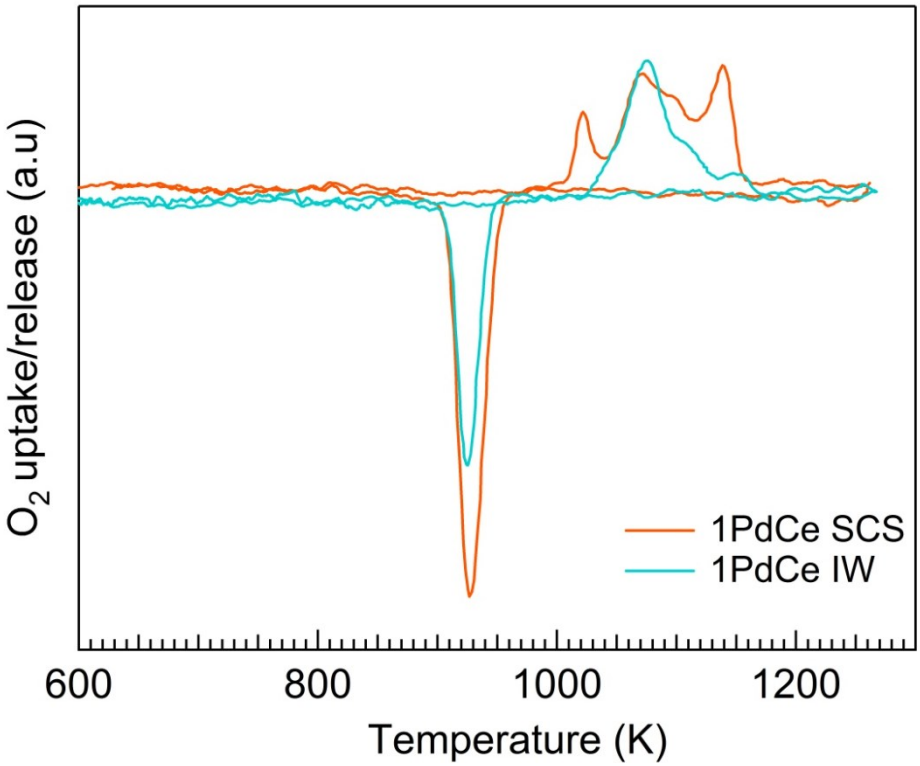

Figure 3.8: comparison of the third TPO cycle of 1PdCe SCS and 1PdCe IW (2 vol.% O_2/N_2).

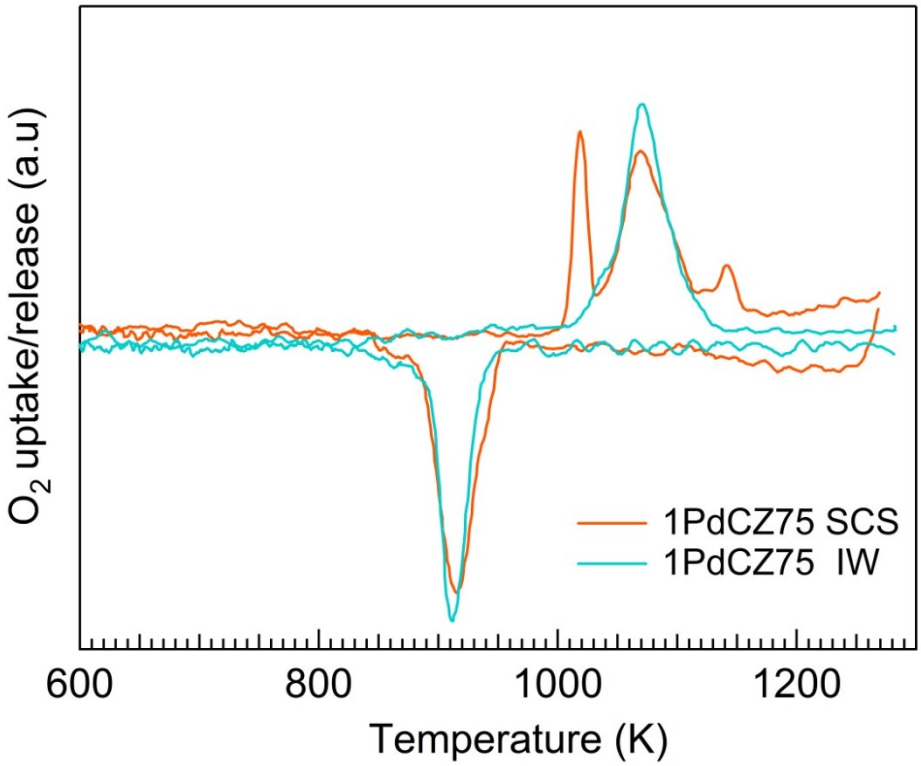

Figure 3.9: comparison of the third TPO cycle of 1PdCZ75 SCS and 1PdCZ75 IW (2 vol.% O_2/N_2)

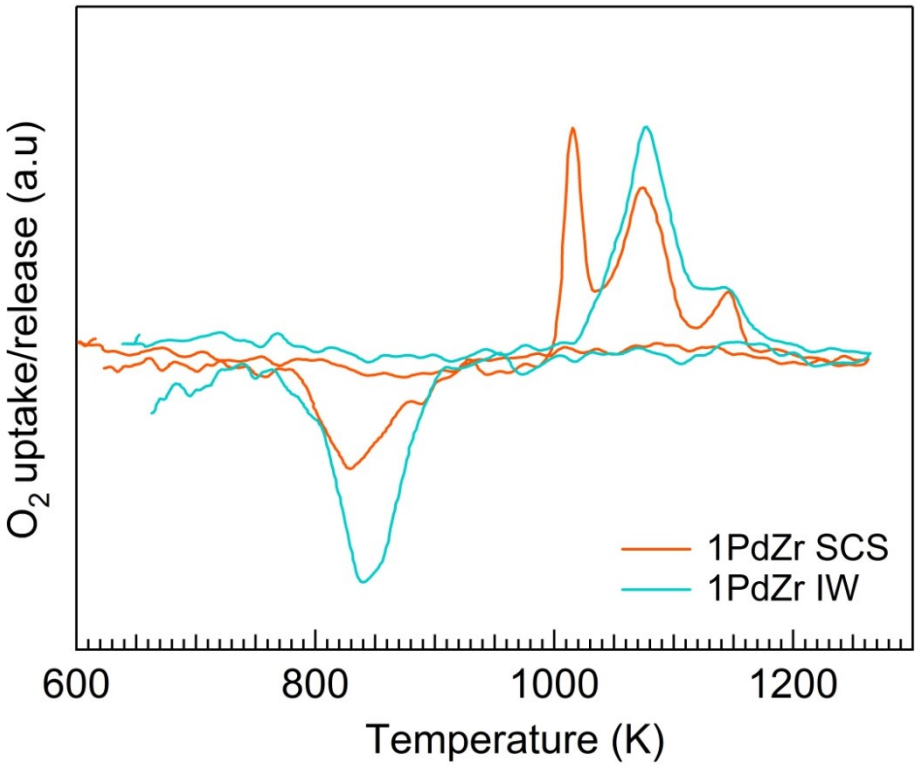

Figure 3.10: comparison of the third TPO cycle of 1PdZr SCS and 1PdZr IW (2 vol.% O_2/N_2)

Table 3.2: characteristic temperatures of PdO-Pd-PdO transformation during the 3rd TPO cycle

Catalyst	T_{max} of first oxygen release peak (K)	T_{max} of re-oxidation peak (K)	ΔT_{D-R} (K)[a]
1PdCe IW	1075	929	146
1PdCZ75 IW	1074	911	163
1PdZr IW	1075	846	229
1PdCe SCS	1022	929	93
1PdCZ75 SCS	1018	917	101
1PdZr SCS	1013	833	180

[a] calculated as the temperature difference between T_{max} of first oxygen release peak and T_{min} of re-oxidation peak

Looking at Figure 3.8 and focusing on the heating part of the cycle, PdO decomposition starts 53 K lower on 1PdCe SCS (Table 3.2), compared to 1PdCe IW and it is completed at about 1150 K for both samples.

On 1PdCZ75 SCS (Figure 3.9) PdO decomposition occurs with a sharp O_2 release peak at 1018 K, while the second and the third ones are located at 1070 K and 1141 K, respectively with PdO decomposition completed at 1163 K. On its correspondent IW, instead, PdO-Pd transition takes place in a single step at 1074 K and it is concluded at ~ 1140 K. By comparing the qualitative profile during the heating ramp of ZrO_2-supported catalysts (Figure 3.10), a similar picture can be observed where the reduction of PdO to metallic Pd is anticipated on 1PdZr SCS of 62 K

compared to 1PdZr IW. Irrespective of the oxide carrier, PdO decomposition over SCS samples involves a well-defined multi-step redox process.

This behavior was already detected in the previous studies where two or three oxygen release peaks were identified. During the second heating/cooling cycle in TGA experiment Farrauto *et al.* detected two decomposition stages: the first weight loss was attributed to the reduction of surface PdO_x formed upon Pd re-dispersion during cooling, while the second weight loss to bulk PdO [10]. McCarty also observed two decomposition steps on 5 wt.% Pd/γ-Al_2O_3 during TPD experiments where the step located at higher temperature was assigned to interfacial PdO near the support oxide [15]. The peak located at higher temperature was ascribed to the reduction of PdO species in strong interaction with the support by Colussi *et al.* [13]. Recently Chen *et al.* [16] proposed a core-shell redox mechanism to explain the nature of the two-step PdO decomposition: they suggested that PdO decomposition initiates at the surface of PdO particles, as already described previously by Datye *et al.* [17] with the formation of metallic Pd shell around PdO core [16]. Along with the results reported in the literature, therefore, it is reasonable to attribute the complex oxygen evolution of SCS samples to the presence of different PdO species: the first O_2 peak can be associated with the reduction of surface PdO_x species, the second peak to bulk PdO and the peak located at high temperatures to PdO in strong interaction with the support [13] or to the core of PdO particles [16]. On impregnated samples, instead, the PdO decomposition features are not well defined and the oxygen release takes place with a broader peak in which the contribution of the low temperature feature is absent for 1PdCe IW and 1PdZr IW, and only slightly observable on 1PdCZ75 IW. The temperature at which PdO starts to reduce on IW samples seems well in agreement with the temperature at which bulk PdO decomposes [16].

Focusing on the cooling part of the cycle, on all catalysts Pd re-oxidation takes place with a large thermal hysteresis with respect to the decomposition process with a single oxygen uptake peak relative to PdO re-formation. Pd→PdO transformation was suggested to be ruled by the kinetics of PdO formation at elevated temperatures due the presence of chemisorbed oxygen on the metallic Pd particles. The chemisorbed oxygen acts as a passive layer for the growth of PdO particles, slowing the complete oxidation of Pd^0 and causing the well-known thermal hysteresis [15, 18].

On CeO_2- and CZ75-supported catalysts, PdO re-oxidation occurs at 929 K and at around 910 K, respectively. For samples supported on pure zirconia a larger thermal gap is observed on which the re-oxidation of Pd to PdO takes place at around 840 K (Table 3.2). The presence of cerium oxide into the support significantly reduces the hysteresis during PdO-Pd-PdO transformation, likely due to the contribution of lattice oxygen coming from the redox couple Ce^{4+}-Ce^{3+} that facilitates Pd re-oxidation [12, 19]. Irrespective of the type of support, a narrower

hysteresis gap is observed for combustion synthesized catalysts (Table 3.2) likely due to a stronger metal-support interaction and/or to the presence of smaller Pd clusters. Figure 3.11 illustrates the comparison of the third TPO cycle of all SCS samples.

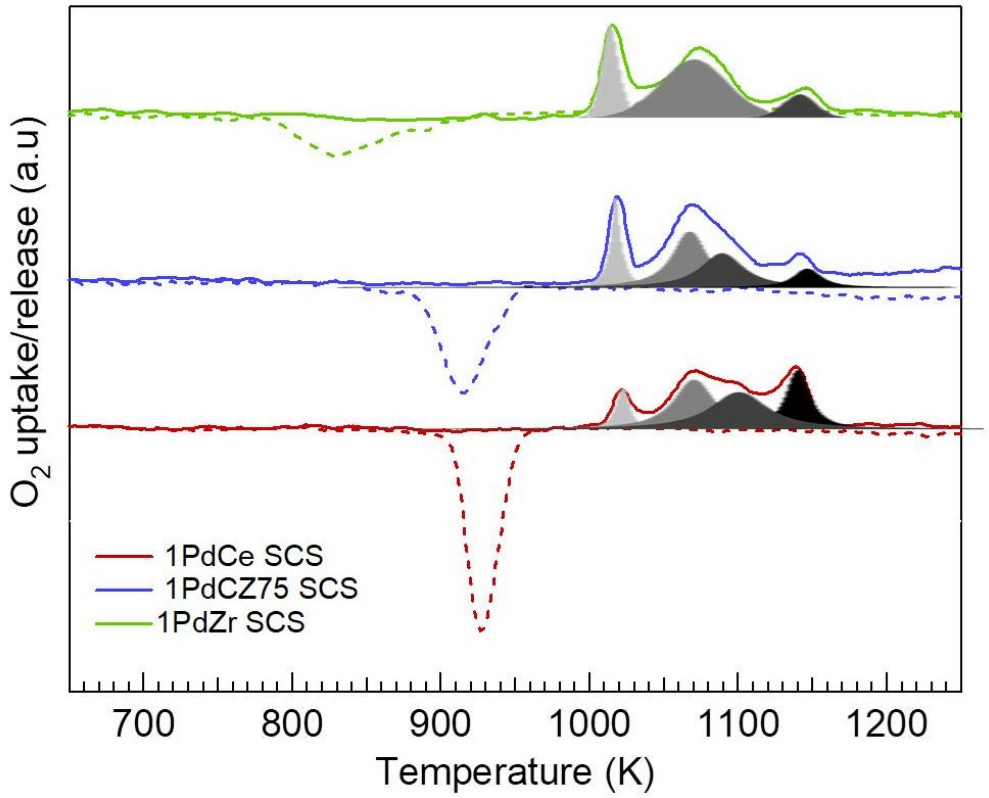

Figure 3.11: TPO profile during the third cycle of 1PdCe SCS, 1PdCZ75 SCS and 1PdZr SCS catalysts

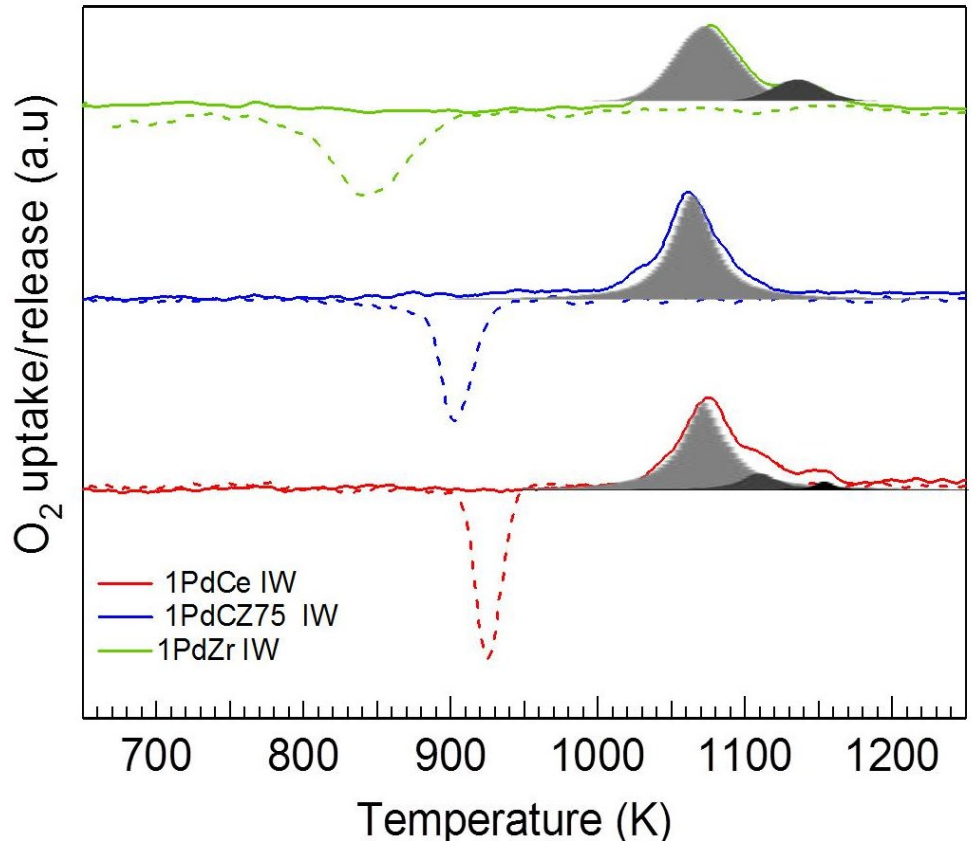

Figure 3.12: TPO profile during the third cycle of 1PdCe IW, 1PdCZ75 IW and 1PdZr IW catalysts

It can be observed that there are no significant differences in the decomposition threshold during the heating ramp, but only in the distribution of different PdO species. The contribution of each decomposition step was estimated by Lorentzian fitting. The best fitting for SCS samples was obtained with four peaks: the contribution of the first peak increases in the order 1PdCe SCS < 1PdCZ75 SCS < 1PdZr SCS, in line with previous observations where for ceria-free sample the first decomposition peak was predominant with respect to ceria-doped catalyst [13].

If we compare the fitting obtained for SCS and IW catalysts, we can observe that the major contribution on SCS catalysts arises from the two high-temperature stages, whereas on IW samples the contribution of bulk PdO species is the predominant one. On solution combustion synthesized catalysts, when CeO_2 is present into the support, the amount of PdO decomposed at a higher temperature represents approximately 50% of the entire PdO, according to the stabilizing effect of ceria on palladium oxide.

Regardless of the synthesis procedure, the nature of the support affects strongly the Pd re-oxidation threshold: the presence of ceria yields a faster PdO re-formation, reducing the thermal gap during decomposition/re-oxidation. On the contrary, the amplitude of the hysteresis becomes larger when ZrO_2 is used as support: the oxygen uptake starts at 940 K and is completed only at 780 K with a temperature gap of 180 K and 225 K for 1PdZr SCS and 1PdZr IW, respectively.

3.2.2 H_2-TPR

Temperature-Programmed Reduction experiments were performed in order to gain further insights into the redox properties of different Pd-based catalysts.

The qualitative reduction profile for combustion synthesized catalysts is compared to that of the corresponding impregnated ones and the results are illustrated in Figure 3.13.

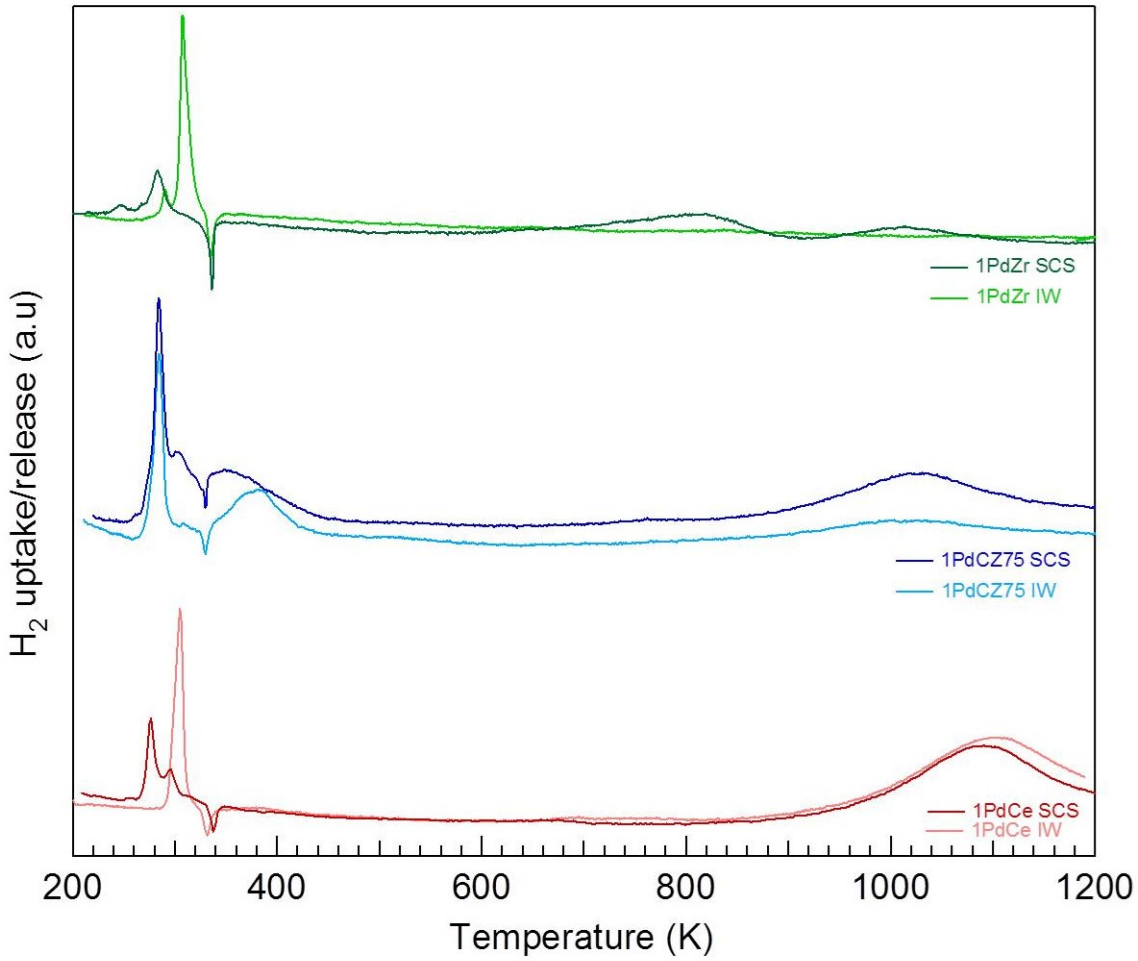

Figure 3.13: H_2-TPR profiles of CeO_2-supported catalysts (4.5% H_2/N_2)

The hydrogen uptake in the low-temperature region (LT) between 200 K and 450 K is observed on all samples and it involves the reduction of PdO to metallic Pd. Some differences can be highlighted between SCS and IW samples in the LT region. Considering CeO_2- and CZ75-supported catalysts, two peaks in the LT region can be distinguished, whereas on impregnated samples generally a single hydrogen consumption peak is observed. The assignment of each hydrogen peak is not straightforward. Luo *et al.* after redox treatment on $Pd/Ce_{0.5}Zr_{0.5}O_2$ catalyst observed two hydrogen uptake peaks in the LT region ascribed to the heterogeneous size distribution of PdO and/or to the diffusion of PdO into $Ce_{0.5}Zr_{0.5}O_2$ lattice [20]. The high temperatures locally reached during combustion synthesis combined with short reaction time could promote a heterogeneous distribution of PdO particles and/or the presence of PdO_x with different stoichiometry [6]. According to these considerations, the presence of PdO_x species or a non-uniform size distribution of PdO particles can explain the complex reduction profile of SCS samples.

On 1PdCe SCS the reduction of PdO takes place about 30 K lower than on 1PdCe IW. For ceria-zirconia based samples, instead, the reduction of palladium oxide to metallic Pd occurs at the

same temperature (284 K). The hydrogen consumption was estimated by the integration of the peak area from 200 K to 500 K (Table 3.3).

Table 3.3: quantitative analysis of TPR experiments

Sample	**H_2 uptake (ml) 200-500 K**	**μmolH_2/g_{cat} 200-500 K**
1PdCe IW	0.127	103
1PdCZ75 IW	0.364	294
1PdZr IW	0.14	111
1PdCe SCS	0.137	111
1PdCZ75 SCS	0.503	393
1PdZr SCS	0.067	53

The amount of hydrogen consumed exceeds the stoichiometric value required for PdO reduction (~ 87 μmol H_2/g_{cat}) in the case of ceria-containing samples, due to hydrogen spillover on the support. The phenomenon has been widely described in the literature: the presence of noble metals promotes ceria reducibility at lower temperatures [21, 22]. The large hydrogen consumption at approximately 1110 K is attributed to the reduction of bulk ceria crystallites [21]. A strong modification of the TPR profile is observed for $Ce_{0.75}Zr_{0.25}O_2$-supported samples: irrespective of the preparation procedure the H_2 consumption in the LT region significantly exceeds the stoichiometric amount for PdO reduction being even higher than that observed for ceria-based samples. The introduction of Zr^{4+} into the ceria lattice strongly promotes the reduction of surface ceria: this behavior was attributed to the enhanced oxygen mobility of Ce-Zr mixed oxides with respect to pure ceria [22]. Regarding pure zirconia-supported catalysts, both samples show two H_2 consumption peaks in the LT region, where the first one is barely present and it is located 30 K lower for 1PdZr SCS with respect to 1PdZr IW. At temperature above 600 K 1PdZr SCS presents two H_2 uptake peaks. Fujimoto *et al.* hypothesized a strong interaction between PdO_x and ZrO_2 where the treatment in H_2 atmosphere reduced the crystallites of stable PdO_x-ZrO_2 only at temperature above 773 K [23]. In line with this result, Franchini and co-workers obtained a similar TPR profile over $Pd/Zr/Al_2O_3$ where the second peak was attributed to the reduction of PdO particles interacting with ZrO_2 [24].

The negative peak at 320-340 K, present on all samples, is attributed to the release of hydrogen from the decomposition of palladium hydride (PdH_2), resulting from the absorption of H_2 by metallic Pd [25, 26]. This peak becomes very sharp for 1PdZr SCS likely due to the presence of large Pd particles [27].

The results obtained from TPO and TPR measurements reveal a complex redox behavior of SCS catalysts compared to IW samples, regardless of the nature of the support. This behavior can be linked to the presence of different PdO_x species and/or non-uniform particle size distribution, which in turn can be ascribed to the short reaction time and high temperatures locally reached during SCS.

References

[1] S. Specchia, C. Galletti and V. Specchia, *Studies in surface science and catalysis,* vol. 175, pp. 59-67, 2010.

[2] M. Moser, G. Vilè, S. Colussi, F. Krumeich, D. Teschner, L. Szentmiklòsi, A. Trovarelli and J. Ramiréz, *Journal of Catalysis,* vol. 331, pp. 128-137, 2015.

[3] E. Aneggi, C. De Leitenburg and A. Trovarelli, *Catalysis Today,* vol. 181, pp. 108-115, 2012.

[4] S. Specchia, E. Finocchio, G. Busca, P. Palmisano and V. Specchia, *Journal of Catalysis,* vol. 263, pp. 134-145, 2009.

[5] A. Trovarelli and P. Fornasiero, Catalysis by Ceria and Related Materials, Imperial Collage Press, 2013.

[6] S. Colussi, A. Gayen, M. Boaro, J. Llorca and A. Trovarelli, *ChemCatChem,* vol. 7, p. 2222–2229, 2015.

[7] P. Bera, A. Gayen, M. Hegde, N. Lalla, L. Spadaro, F. Frusteri and F. Arena, *J. Phys. Chem B,* vol. 107, pp. 6122-6130, 2003.

[8] K. R. Priolkar, P. Bera, P. Sarode, M. Hegde, S. Emura, R. Kumashiro and N. Lalla, *Chem. Matter.,* vol. 14, pp. 2120-2128, 2002.

[9] S. Colussi, A. Gayen, M. Cammellone, M. Boaro, J. Llorca, S. Fabris and A. Trovarelli, *Angew. Chem. Int.,* vol. 48, pp. 8481-8484, 2009.

[10] R.J. Farrauto, M. Hobson, T. Kennelly and E. Watermann, *Applied Catalysis A: General,* vol. 81, pp. 227-237, 1992.

[11] G. Groppi, C. Cristiani, L. Lietti and P. Forzatti, *Studies in Surface Science and Catalysis,* vol. 130, pp. 3801-3806, 2000.

[12] S. Colussi, A. Trovarelli and J. Llorca, *Catalysis Communications,* vol. 8, pp. 1263-1266, 2007.

[13] S. Colussi, A. Trovarelli, E. Vesselli, A. Baraldi, G. Comelli, G. Groppi and J. Llorca, *Applied Catalysis A: General,* vol. 390, pp. 1-10, 2010.

[14] H. Gabasch, W. Unterberger, K. Hayek, B. Klotzer, E. Kleimenov, D. Teschner, S. Zefeiratos, M. Havecker, A. Knop-Gericke, R. Schlogl, J. Han, F. Ribeiro, B. Aszalos-Kiss, T. Curtin and D. Zemlyanov, *Surface Science,* vol. 600, pp. 2980-2989, 2006.

[15] J.G. McCarty, *Catalysis Today*, vol. 26, pp. 283-293, 1995.

[16] X. Chen, J. Schwank, G. Fisher, Y. Cheng, M. Jagner and R. McCabe, *Applied Catalysis A: General,* vol. 475, p. 420–426, 2014.

[17] A.K. Datye, J. Bravo, T. Nelson, P. Atasanova, M. Lyubovsky and L. Pfefferle, *Applied Catalysis A: General,* vol. 198, no. Issues 1–2, p. 179–196, 2000.

[18] P. Forzatti, *Catalysis Today,* vol. 83, pp. 3-18, 2003.

[19] L. Simplicio, S. Brandao, D. Domingos, F. Bozon-Verduraz and E. Sales, *Applied Catalysis A: General,* vol. 360, pp. 2-7, 2009.

[20] M.-F. Luo and X.-M. Zheng, *Applied Catalysis A: General,* vol. 189, p. 15–21, 1999.

[21] A. Trovarelli, *Catalysis Reviews Science and Engineering,* vol. 38, no. 4, pp. 439 - 520, 1996.

[22] P. Fornasiero, R. Di Monte, G. Ranga Rao, J. Kaspar, S. Meriani, A. Trovarelli and M. Graziani, *Journal of Catalysis,* vol. 151, pp. 168-177, 1995.

[23] K. Fujimoto, F. Ribeiro, M. Borja and E. Iglesia, *Journal of Catalysis,* vol. 179, pp. 431-442, 1998.

[24] C. A. Franchini, D. V. Cesar and M. Schmal, *Catalysis Letters*, vol. 137, p. 45–54, 2010.

[25] T. Chang, J. Chen and C. Yeh, *Journal of Catalysis*, vol. 96, pp. 51-57, 1985.

[26] A. Baylet, P. Marecot, D. Duprez, P. Castellazzi, G. Groppi and P. Forzatti, *Phys. Chem. Chem. Phys*, vol. 13, p. 4607–4613, 2011.

[27] Y. Cao, R. Ran, X. Wu, B. Zjao, J. Wan and D. Weng, *Applied Catalysis A: General*, vol. 457, pp. 52-61, 2013.

Chapter 4

Catalytic activity of $Pd/Ce_xZr_{1-x}O_2$ catalysts for lean and stoichiometric methane oxidation

This chapter presents the study of the catalytic activity of the series 1% $Pd/Ce_xZr_{1-x}O_2$ prepared by SCS and compared with those of the corresponding IW ones. The catalytic properties of the various samples have been tested during cyclic temperature programmed combustion experiments under lean conditions and in a wide range of temperatures (400-1173 K). The durability of Pd-based catalysts under long-time exposure to reaction mixture was simulated by time-on-stream tests carried out at 723 K for 24 hours. In the second part of the chapter, the preliminary results on the performance of the best SCS samples in stoichiometric reaction conditions are discussed.

4.1. Catalytic performance in lean conditions

4.1.1. Light-off experiments

The catalytic performance of each sample in methane oxidation was investigated by temperature programmed combustion under lean reaction conditions ($O_2/CH_4 = 4$) during two heating/cooling cycles.

The results are reported in terms of the light-off profile, where methane conversion is plotted against temperature. The conversion is calculated according to the following equation:

$$CH_4 conversion(\%) = \frac{CH_4^{in} - CH_4^{out}}{CH_4^{in}} \times 100$$

In Figure 4.1 the light-off profile of 1PdCe SCS is reported.

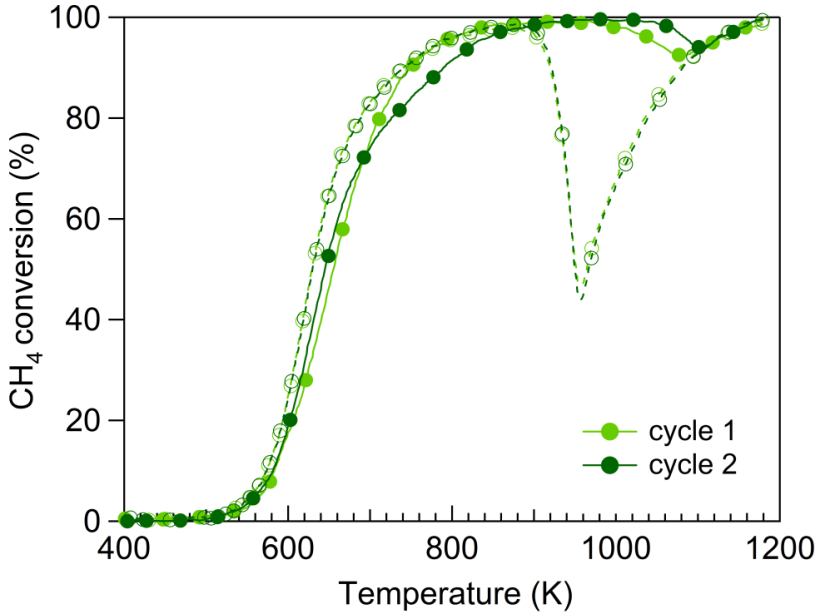

Figure 4.1: light-off behavior of 1PdCe SCS in lean-methane oxidation; solid line, filled symbols: heating; dotted line, open symbols: cooling.

1PdCe SCS shows a good oxidation activity, with the ignition of CH_4 taking place at about 540 K during both cycles, and reaching 100% conversion at ~ 820 K. During the heating branch, above 980 K the activity gradually decreases reaching a minimum of 90% at 1080 K due to the decomposition of PdO to metallic Pd, recognized to be less active towards methane oxidation [1, 2, 3]. In the cooling step, a transient deactivation is clearly observed where methane conversion sharply drops, reaching a minimum of 42% at 940 K; below this temperature the catalytic performance is completely restored due to the progressive PdO re-formation [1, 2, 3]. The drop in activity during the cooling segment is more pronounced than during the heating ramp because the re-oxidation of Pd to PdO is a kinetically limited process [4, 5], as mentioned in section 3.2.1, and during cooling there is no contribution of the homogeneous combustion. When a second cycle is carried out, it exhibits the same behaviour with a slight reduction of

T_{50} (temperature at which 50% of CH_4 conversion is achieved) from 657 K to 644 K. Figure 4.2 illustrates the catalytic activity of 1PdCZ75 SCS during the two heating/cooling ramps.

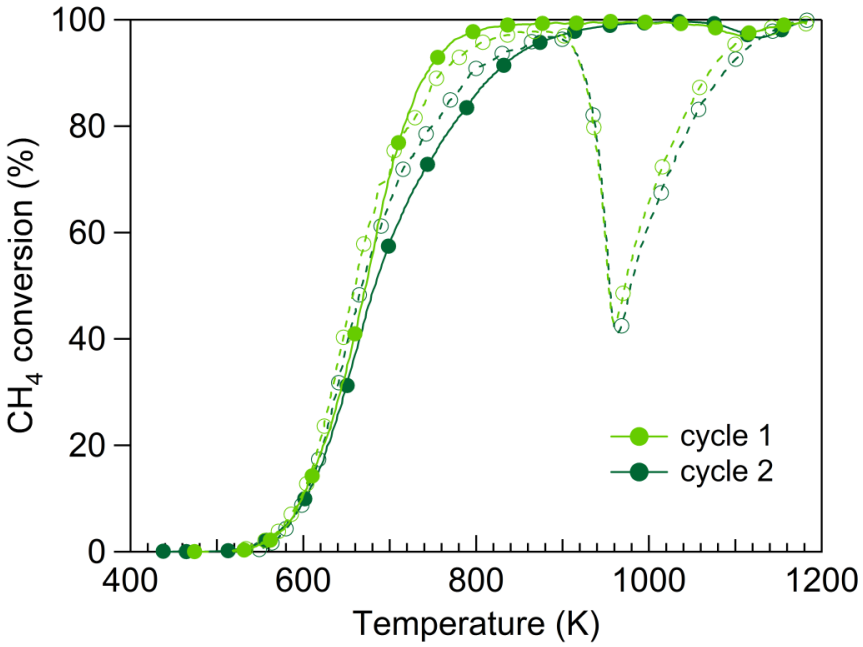

Figure 4.2: light-off behavior of 1PdCZ75 SCS in lean-methane oxidation; solid line, filled symbols: heating; dotted line, open symbols: cooling.

In the first heating-up 10% and 50% of CH_4 conversion are achieved at 598 K and 675 K, respectively, and complete conversion is reached around 820 K. In the following cycle, 10% of CH_4 conversion is reached at a similar temperature, whereas T_{50} is slightly shifted to higher temperatures (684 K). By observing the cooling branch, the methane conversion reaches a minimum of 41 %. The temperature and the size of activity loss is similar during the two oxidation cycles.

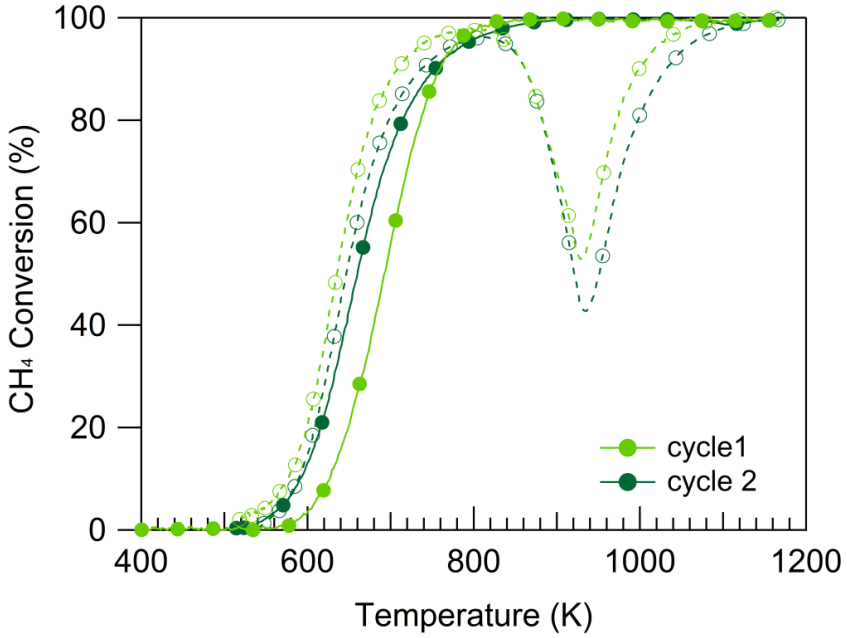

Figure 4.3: light-off behavior on 1PdZr SCS in lean-methane oxidation; solid line, filled symbols: heating; dotted line, filled symbols: cooling.

The light-off profiles over 1PdZr SCS are presented in Figure 4.3. During the first run, methane conversion reaches 10% and 50% at 628 K and 693 K, respectively. After the first cycle, the catalytic performance is strongly enhanced in terms of light-off temperatures. Focusing on the cooling part of cycle 2 the catalytic activity drops to 42 % at 934 K, increasing again after Pd re-oxidation.

The results presented above confirm the existence of the well-known thermal hysteresis associated to the occurrence of the reversible PdO-Pd phase transformation. The hysteresis during cyclic methane oxidation was assigned to a stable chemisorbed oxygen on metallic Pd particles which hinders the complete oxidation of bulk PdO [6, 7]. A strong activity drop during the cooling step is observed in the temperature range where Pd is still at the metallic state, indicating that the presence of PdO is necessary to gain high CH_4 conversions. It is worth to observe that for all samples the cooling branch is slightly more active than the heat-up below ~ 840 K. It is generally agreed that methane oxidation on Pd is "structure-sensitive" [5, 8, 9]. It was suggested that PdO particles undergo a reconstruction when exposed to the reaction atmosphere [5, 8]. After exposure to high temperatures, Pd can re-disperse in O_2-containing atmosphere during cooling and this process has been suggested to enhance the catalytic activity [6]. However, no clear and definitive explanation has been found yet due to the several parameters which influence the PdO-Pd-PdO transformation, such as space velocity, reaction atmosphere, particle size, type of support, metal-support interaction and cooling rate.

The catalysts prepared by IW procedure were investigated through two successive oxidation cycles, whose characteristic temperatures are reported in Table 4.1.

Table 4.1: T_{10} and T_{50} of 1 $Pd/Ce_xZr_{1-x}O_2$ IW during the heating ramps of two subsequent methane oxidation cycles

	cycle 1		cycle 2	
Sample	**T_{10} (K)**	**T_{50} (K)**	**T_{10} (K)**	**T_{50} (K)**
1PdCe IW	609	773	619	718
1PdCZ75 IW	598	716	614	718
1PdZr IW	591	708	601	676
1PdCe SCS	581	657	581	644
1PdCZ75 SCS	598	675	602	684
1PdZr SCS	628	693	594	661

Looking at Table 4.1, the T_{10} increases slightly between the first and the second heating ramp; the T_{50} values decrease on 1PdCe IW and 1PdZr IW of 55 K and 32 K, respectively, compared to the first cycle, whereas on 1PdCZ75 IW T_{50} remains almost unchanged. Since it is generally agreed that after a first light-off cycle the catalytic activity reaches a sort of steady state, in order to evaluate the influence of preparation method on the activity the second cycle was

chosen as the most representative one. Figure 4.4 shows the comparison of methane oxidation profiles over 1PdCe SCS and 1PdCe IW.

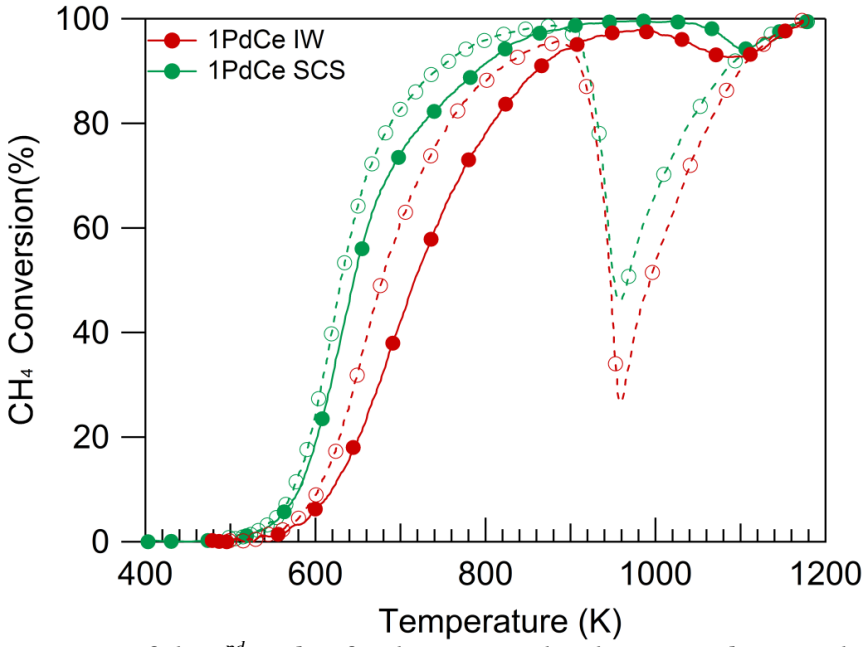

Figure 4.4: comparison of the 2nd cycle of 1PdCe SCS and 1PdCe IW in lean-methane oxidation; solid line-filled symbols: heating, dotted line-open symbols: cooling

Looking at Figure 4.4 and focusing on the heating branch, 1PdCe SCS shows a superior activity with respect to 1PdCe IW, reaching 50 % of methane conversion already at 644 K, 74 K lower than that of IW one. In the cooling step, between 880 and 1200 K a severe deactivation is observed for 1PdCe IW with a decrease in CH_4 conversion down to 26 %. The re-oxidation of Pd to PdO, accompanied by a progressive recovery of catalytic activity, occurs at the same temperature (957 K) but the activity loss is definitely much severe with respect to 1PdCe SCS.

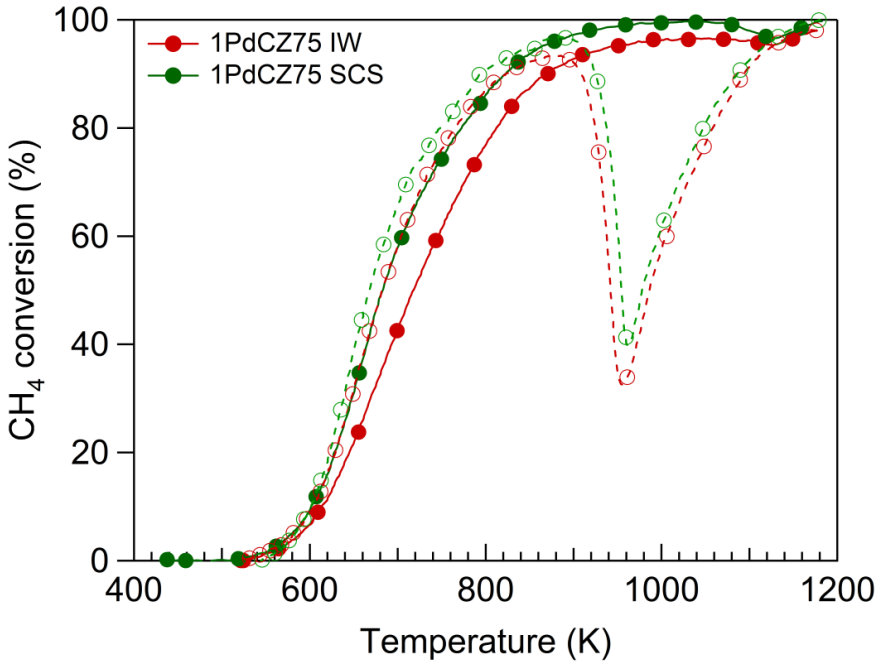

Figure 4.5: comparison of the 2nd cycle of 1PdCZ75 SCS and 1PdCZ75 IW in lean-methane oxidation; solid line-filled symbols: heating, dotted line-open symbols: cooling

For ceria-zirconia mixed oxide (Figure 4.5) similar considerations can be drawn: 1PdCZ75 made by combustion synthesis shows a superior activity compared to 1PdCZ75 IW, with a T_{10} and T_{50} set at 602 K and 684 K, respectively. On the contrary, 1PdCZ75 IW exhibits lower activity towards methane reaching 10% and 50% at 614 K and 718 K, respectively. During the cooling stage, no difference is observed in the temperature at which Pd is re-oxidized to PdO ($T_{ox} \cong$ 956 K) but the activity decay due to PdO-Pd transformation is slightly more pronounced for the impregnated sample.

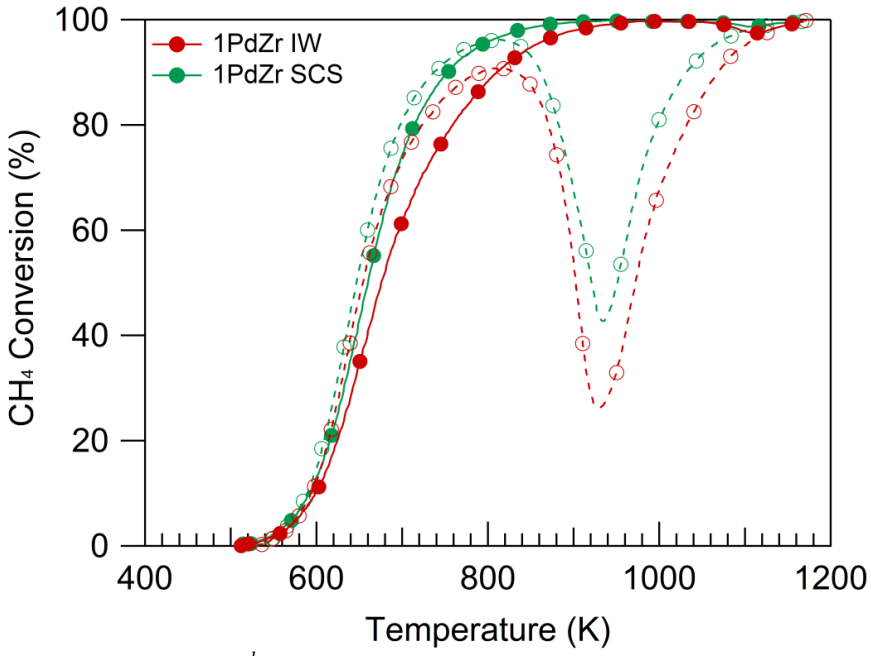

Figure 4.6: comparison of the 2nd cycle of 1PdZr SCS and 1PdZr IW in lean-methane oxidation; solid line-filled symbols: heating, dotted line-open symbols: cooling

By comparing the results collected for ZrO_2-supported catalysts (Figure 4.6), the light off curves for IW and SCS are very similar, showing a close T_{10} value. Above 640 K though, 1PdZr SCS shows clearly a superior activity with respect to 1PdZr IW. On the latter sample complete methane oxidation is reached only above 940 K, against 820 K over 1PdZr SCS. When the samples are cooled down a sharp drop in catalytic activity is detected over 1PdZr IW, where CH_4 conversion falls to 28% and it is not fully recovered after Pd re-oxidation.

Summarizing briefly the results obtained by comparing the two preparation methods, SCS allows to obtain more active catalysts throughout the whole methane oxidation cycle, especially on ceria-based supports. Additionally, the activity decay at high temperature is less severe for CeO_2-containing catalysts made by SCS and this is line with data obtained during TPO measurements where PdO regeneration is facilitated on 1PdCe SCS and 1PdCZ75 SCS; this behavior is linked to the intimate contact of Pd with CeO_2, resulting in a lower activity loss. Ceria-containing oxides are able to supply structural oxygen through Ce^{4+}/Ce^{3+} transformation, acting as stabilizers of PdO phase [11, 12].

Figure 4.7 illustrates the comparison of the oxidation profile of all SCS samples during the second cycle.

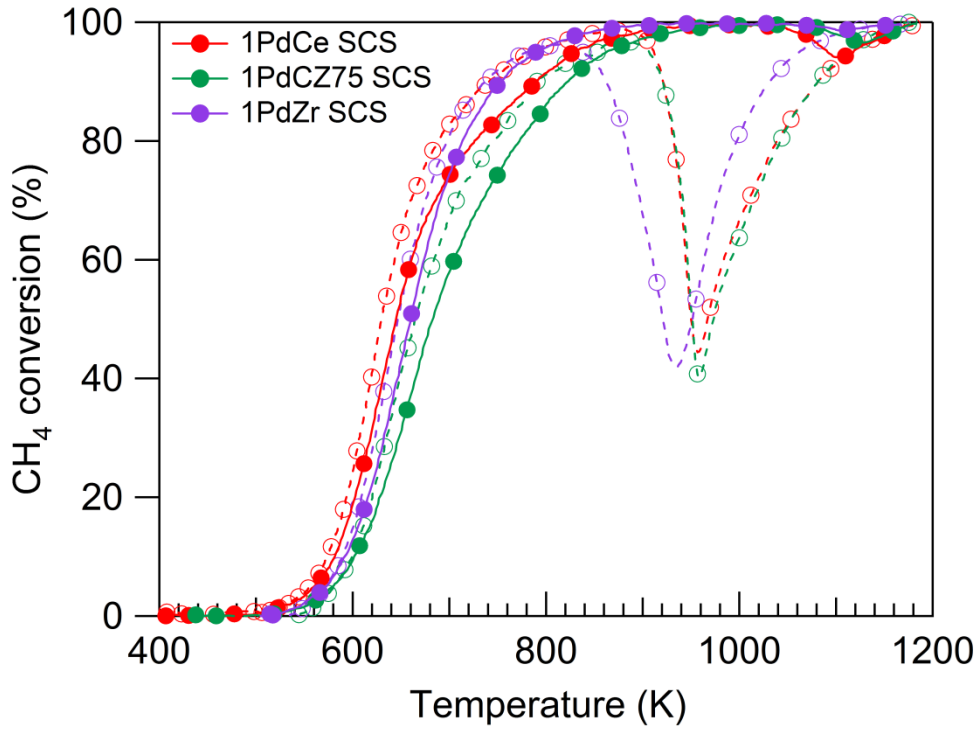

Figure 4.7: catalytic activity during the second heating/cooling ramp in lean methane oxidation for 1%Pd/$Ce_xZr_{1-x}O_2$ SCS samples. Solid line-filled symbols: heating; dotted line- open symbols: cooling

Looking at the heating part of the run, the best performance in the kinetically controlled regime is recorded for 1PdCe SCS, followed by 1PdZr SCS and 1PdCZ75 SCS; only above 680 K 1PdZr SCS exceeds the performance of 1PdCe SCS.

In the cooling part of the cycle, the effect of the support is observable: Pd re-oxidation takes place at higher temperatures on ceria-containing samples following the order 1PdCe SCS (957 K), 1PdCZ75 (957 K) < 1PdZr SCS (934 K). The trend of Pd re-oxidation is well in accordance with the onset of oxygen uptake for Pd re-oxidation detected during TPO experiments (Chapter 3, Figure 3.11). The shape as well as the extent of activity loss, instead, is almost similar for all SCS catalysts, reaching a minimum of about 40%. When ceria is present into the support it has a positive effect on the transient deactivation as reported by Colussi *et al.* and Groppi *et al.*: they observed a markedly lower deactivation in the cooling segment on Ce-doped catalyst with a shift of the position of the minimum to higher temperatures [7, 12]. This behavior is linked to the stabilization effect of ceria on PdO: as stated previously ceria is able to provide oxygen through Ce^{4+}/Ce^{3+} transformation, improving the stability window of PdO [11, 12]. The comparison of the second oxidation cycle of impregnated catalysts is shown in Figure 4.8.

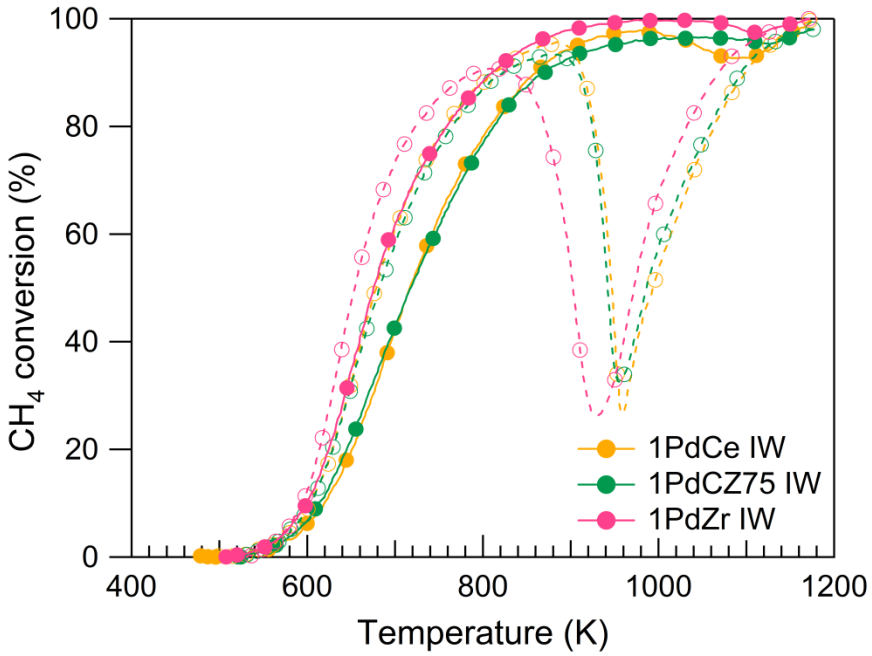

Figure 4.8: catalytic activity during the second heating/cooling ramp in lean methane oxidation on 1%Pd/$Ce_xZr_{1-x}O_2$ IW samples. Solid line, filled symbols: heating; dotted line, open symbols: cooling

In the case of IW samples, the best performance is recorded for 1PdZr IW, whereas 1PdCe IW and 1PdCZ75 IW exhibit a similar light-off behavior with close T_{10} and T_{50} values, as inferred from Table 4.1. The major difference arises during the cooling part of the cycle: the presence of ceria into the support yields Pd re-oxidation at higher temperatures (~ 957 K), although a severe deactivation is observed with a decrease in CH_4 conversion to 26-33 %. For 1PdZr IW, Pd-PdO transition is delayed and occurs at 929 K with an activity loss down to 25% of methane conversion.

To compare quantitatively the catalytic behaviour of various catalysts and to better understand the differences between SCS and IW samples in CH_4 oxidation, kinetic measurements were carried out at 623 K in a recycle-reactor described in section 2.2.6. During kinetic measurements, the recycle ratio was maintained at high value (R=25), with the purpose to ensure the occurrence of differential conditions and, thus, performing a correct kinetic analysis. The reaction rate is calculated in terms of CH_4 moles reacted per gram of noble metal and the values obtained are reported in Table 4.2.

Table 4.2: reaction rates measured at 623 K on 1%Pd/$Ce_xZr_{1-x}O_2$ made by SCS and IW for lean methane oxidation

Catalysts	**rate (μmolCH_4/g_{Pd}*s)**
1PdCe IW	32.9
1PdCZ75 IW	58.9
1PdZr IW	79.8
1PdCe SCS	111.4
1PdCZ75SCS	91.9
1PdZr SCS	78.4

The data obtained by kinetic measurements confirm the higher activity of 1PdCe SCS and 1PdCZ75 SCS when compared to their correspondent IW samples; in particular 1PdCZ75 SCS and 1PdCe SCS exhibit a reaction rate twice and three times higher than that measured on IW counterparts, respectively. Regarding ZrO_2-supported materials, similar reaction rates are measured. The results of kinetic measurements indicate also that decreasing the ceria content into the support the effect of preparation procedure in kinetically regime becomes less pronounced, as detected qualitatively during catalytic tests.

The superior performance of Pd/CeO_2 prepared by SCS has been assessed by other authors and has been attributed to the stabilization of Pd^{2+} into ceria lattice resulting in a strong Pd-CeO_2 interaction in the form of $Ce_{1-x}Pd_xO_{2-\delta}$ solid solution [13, 14, 15, 16]. On 1PdCe SCS a surface roughness caused by a reconstruction of CeO_2 has been detected by HR-TEM and, although not well defined, has been assigned to the formation of Pd-O-Ce superstructure (Figure 3.3). The dissolution of Pd^{2+} into CeO_2 structure leads to the formation of an equivalent number of oxygen vacancies, indicated as new oxygen exchange sites: the formation of ordered (or random) oxygen vacancies has been indicated to play a key role in the improvement of the overall reactivity towards methane activation [15, 17]. It is plausible to hypothesize a similar scenario for CZ75-based samples, although 1PdCZ75 SCS does not shown the evidence of the formation of a Pd-O-Ce superstructure due to the insertion of Zr^{4+} (Figure 3.5). Therefore, the lower light-off temperature measured on 1PdCZ75 SCS can be related to the stronger Pd/Ce-Zr interaction with the formation of random Pd-O-Ce sites, effective sites for catalytic reaction. The formation of Pd-O-Ce linkages through strong Pd-Ce interaction is promoted by high temperatures and redox conditions achieved during solution combustion synthesis. This kind of structure obtained by SCS is known to enhance the catalytic activity towards CO/CH_4 oxidation and NO reduction [16, 17, 18, 19, 20]. Therefore, the higher catalytic activity of CeO_2-based catalysts prepared by combustion procedure can be attributed to the presence of stable

PdO in the form of Pd-O-Ce linkages [15]. For ZrO_2-supported samples, the preparation procedure does not affect significantly the catalytic activity towards methane oxidation.

4.1.2. Time-on-stream tests

In order to evaluate the durability of different samples during long time exposure to exhaust gas, time-on-stream activity tests were performed at 723 K up to 24 hours in lean conditions by monitoring CH_4 conversion as a function of time. This temperature was chosen based on the results of the literature, where it is indicated that the deactivation is more severe up to 773 K, and consistently with the operating window of NGV (673-873 K). The comparison of the results obtained for each sample is reported in Figure 4.9 in terms of normalized CH_4 conversion calculated as:

$$normalized\ CH_4\ conversion = \frac{X_{CH4}(t)}{X_{CH4}(0)}$$

where $X_{CH4}(0)$ is the conversion at the beginning of the experiment (t = 0), i.e. when the reactor reaches 723 K. Figure 4.9 shows the comparison of the time-on-stream tests for all catalysts.

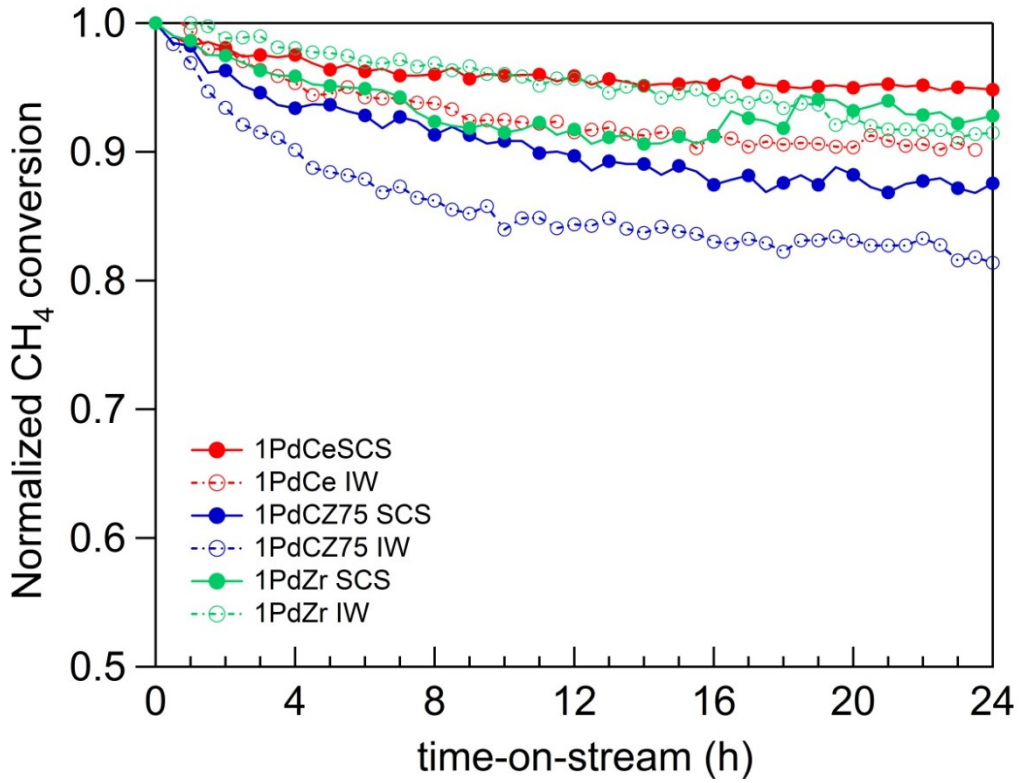

Figure 4.9: time-on-stream behavior of 1Pd/$Ce_xZr_{1-x}O_2$ made by SCS and IW at 723 K during lean-methane oxidation; filled symbols: SCS, open symbols: IW

1PdCe SCS shows a good stability throughout the test with a loss in activity of only 4% with respect to the initial conversion, reaching a stable value after 7 hours. Conversely, 1PdCe IW presents a more severe deactivation with a final conversion about 16 % lower of its initial value.

Looking at the stability curves of the Ce-Zr-based samples, on 1PdCZ75 SCS the normalized conversion is progressively reduced from 1 to 0.92 in 8 hours; instead 1PdCZ75 IW presents a higher deactivation rate with a drop of normalized conversion from 1.0 to 0.85 in the same time-period with a final loss in conversion of 20% (against 13 % measured over SCS sample). A different situation appears for zirconia-based catalysts: 1PdZr IW reveals a very small decrease in CH_4 conversion, similar to that measured on 1PdCe SCS, but after 16 hours the conversion further decreases. In contrast, 1PdZr SCS shows a less stable behavior during the first 8 hours, deactivating more severely; however, at the end of the test a similar activity loss (~ 8%) is measured on both samples. All catalysts, during the first hours, undergo a faster deactivation, generally reaching after several hours a stable value. This behavior might be ascribed to the accumulation of small amount of water generated during oxidation which remain adsorbed on the catalytic surface hindering the accessibility of CH_4 molecules to the active sites [21].
Kinetic data in the literature report the reaction order with respect to CH_4, H_2O, CO_2 over PdO being 1, -1 and 0, respectively. The first-reaction order with respect to CH_4 indicate that C-H dissociation is the rate limiting step and the negative-order dependency of oxidation rate on H_2O (where water is produced during the reaction or added into the gas feed) suggests its strong inhibiting role on the reaction. The inhibition effect of CO_2 has been found negligible on methane oxidation [8, 22, 23]. Ciuparu *et al.* suggested that hydroxyl groups generated from methane dissociation remain adsorbed on the catalytic surface longer than CO_2 due to their slower desorption rate and their effect is important up to 723 K [24]. The improved long-term stability of SCS catalysts prepared on CeO_2 and CZ75 with respect to IW counterparts can be associated to the presence of stable Pd-O-Ce sites. Regarding the zirconia-supported catalysts the results obtained are well in agreement with those of the previous works, which indicated the good resistance to lean-ageing treatment when zirconia is employed as support or promoter [25, 26, 27]. The similar performances of 1PdZr IW and 1PdZr SCS might indicate that on this support the preparation method has little or no effect on the time-on-stream stability, somehow reinforcing the hypothesis of a beneficial effect of the stronger Pd-ceria interaction obtained by SCS on ceria-containing samples.

4.2. Catalytic performance in stoichiometric conditions

As reported in Chapter 1, natural gas vehicles can be equipped with both lean burn or stoichiometric engine. In the latter, continuous oscillations of the air-to-fuel ratio from lean to rich value can occur and for this reason the catalytic performance of the best SCS catalysts has been evaluated under stoichiometric reaction mixture ($O_2/CH_4 = 2$).

For each sample two successive heating/cooling ramps were performed up to 1173 K; the characteristic temperatures for methane conversion during the two oxidation cycles are summarized in Table 4.3.

Table 4.3: T_{10} and T_{50} measured over 1PdCe SCS and 1PdCZ75 SCS during the heating ramps of two oxidation cycles (O_2/CH_4 = 2)

	cycle 1		cycle 2	
Sample	**T_{10} (K)**	**T_{50} (K)**	**T_{10} (K)**	**T_{50} (K)**
1PdCe SCS	595	681	588	663
1PdCZ75 SCS	605	691	578	650

Looking at Table 4.3, for 1PdCe SCS T_{10} remains almost unchanged between two oxidation cycles, while T_{50} decreases of 22 K. For 1PdCZ75 SCS in the kinetically-controlled regime the performance is improved after one cycle and this improvement is further increased for T_{50} which decreases of 46 K during cycle 2.

The effect of varying oxygen concentration in the feed on the light-off performance is shown on the basis of the second oxidation cycle and the results are reported in Figures 4.10 and 4.11 for 1PdCe SCS and 1 PdCZ75 SCS, respectively.

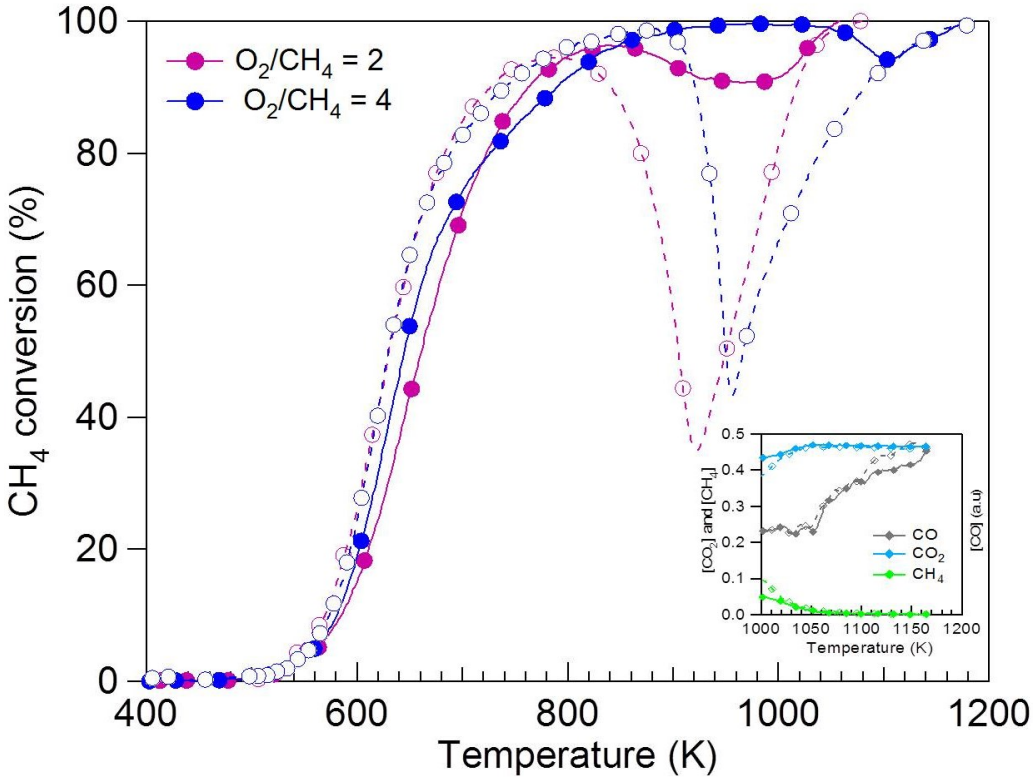

Figure 4.10: comparison of the 2nd oxidation cycle on 1PdCe SCS in O_2/CH_4= 2 and O_2/CH_4= 4 reaction mixture; Solid line, closed symbols: heating; dotted line, open symbols: cooling.

When 1PdCe SCS is exposed to a stoichiometric feed (Figure 4.10), no appreciable differences are detected below 800 K with respect fuel lean atmosphere. In the high temperature window,

instead, PdO decomposition takes place at 159 K lower compared to lean mixture due to the lack of oxygen. During the cooling part of the cycle, in fuel lean feed Pd re-oxidation is promoted and takes place at higher temperatures (957 K) compared to stoichiometric mixture (926 K) with a more stable behavior. However, after Pd re-oxidation, the light-off curve in stoichiometric conditions again overlaps the cooling branch of the lean curve.

Figure 4.11 shows the light-off curves as a function of temperature at varying of oxygen-methane ratio for1PdCZ75 SCS.

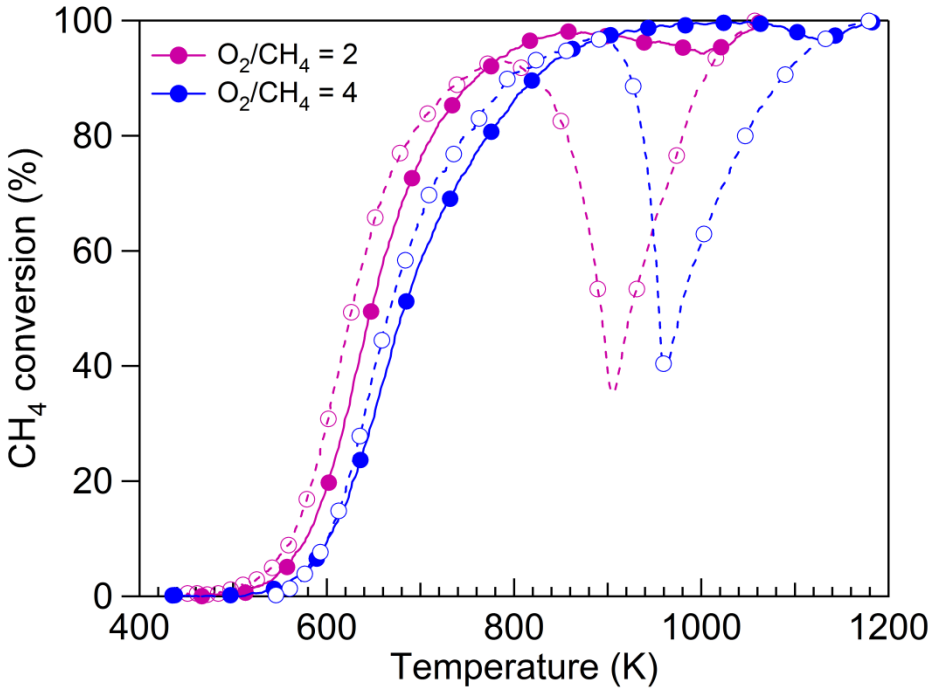

Figure 4.11: comparison of the 2nd oxidation cycle of 1PdCZ75 SCS in O_2/CH_4= 2 and O_2/CH_4= 4 reaction mixture; Solid line, closed symbols: heating; dotted line, filled symbols: cooling.

A significant decrease of T_{10} and T_{50} of 23 K and 35 K, respectively, is detected during stoichiometric operation. When oxygen has been almost totally consumed for CH_4 oxidation, high-temperature deactivation due to PdO reduction is clearly observable, accompanied by a drop in methane conversion. Upon cooling, the catalytic performance drops to 36% and Pd re-oxidation occurs at 56 K lower than in fuel-lean atmosphere, while the size of activity loss remains almost similar.

For both catalysts, PdO decomposition process and its re-formation in oxygen-deficient mixture are shifted to lower temperature. The dynamics of PdO-Pd-PdO phase transformation is remarkably influenced by oxygen partial pressure and this topic have been extensively investigated by our and other research groups [2, 4, 28]. The oxygen partial pressure affects the onset of decomposition temperature: by increasing the oxygen content from 0.5% to 21% the stabilization window of PdO as well as the temperature at which Pd is re-oxidized to PdO move towards higher temperature [4]. Monai *et al.* got the same conclusions, observing that the activity loss as well as the minimum in CH_4 conversion during the cooling part of the light-

off were closely related to the oxygen partial pressure: at increasing oxygen concentration the re-formation of palladium oxide was shifted to higher temperature accompanied by a smaller transient deactivation due to PdO-Pd phase transformation [28].

Noteworthy, for 1PdCe SCS above 1050 K (see inset in Figure 4.11) some traces of carbon monoxide were detected at high temperature, indicating the occurrence of other reaction beside the total methane oxidation. Interestingly, for 1PdCZ75 SCS no CO was observed throughout the cycle and this could be related to the higher oxygen mobility of CZ75 mixed oxide [29], which can contribute to complete the oxidation of CO to CO_2 in lack of oxygen. Depending on the oxygen/methane ratio, secondary reactions have been reported in the literature to take place during CH_4 oxidation, such as reforming of methane, partial oxidation and water-gas shift [30, 31, 32]. Demoulin *et al.* proposed different pathways for methane oxidation depending on O_2 content and temperature: high temperatures and low O_2 partial pressure can promote the formation of CO and H_2 [33]. In the kinetic regime, Lyubovsky *et al.* detected only CO_2 as carbon-containing reaction product; at further increasing temperature they observed the production of CO and H_2 as soon as oxygen was almost totally consumed [30]. In line with these results, Geng *et al.* identified two regions: in the first one, below 873 K, the reaction was mainly CH_4 oxidation with CO_2 as main carbon-containing product, while in the second one at higher temperature H_2 and CO were produced by reforming of methane [32]. However, it is important to underline that the works mentioned above investigate methane in fuel-rich mixtures: in this case the evidence of side reactions and the presence of partial oxidation products are easier to establish with respect to our stoichiometric conditions. In our case, since CO_2 concentration slightly decreases and CH_4 is further consumed, methane removal might occur via dry reforming ($CH_4 + CO_2 \rightarrow 2CO + 2H_2$). The reforming reactions are strongly endothermic and, thus, they are promoted at high temperature. It cannot be excluded the occurrence of partial oxidation of CH_4 and reverse water gas shift (RWGS) since oxygen becomes the rate-limiting reactant at high temperature. These first results obtained in stoichiometric feed suggest that catalytic activity of Pd catalysts and the reaction mechanism strongly depend on the O_2/CH_4 ratio: methane oxidation in oxygen-deficient conditions involves a complex process with the occurrence of exothermic and endothermic reactions depending on temperature, reactant concentration and nature of the support.

Conclusions

The series of $Pd/Ce_xZr_{1-x}O_2$ prepared by one-step SCS procedure was investigated in lean-methane oxidation and compared to the corresponding samples prepared by conventional IW method. When ceria is present in the support, SCS catalysts have a higher catalytic activity: 1PdCZ75 SCS and 1PdCe SCS exhibit a reaction rate of 91.9 $\mu molCH_4/g_{Pd}s$ and 111.4 $\mu molCH_4/g_{Pd}s$, respectively, against 58.9 $\mu molCH_4/g_{Pd}s$ of 1PdCZ75 IW and 32.9 $\mu molCH_4/g_{Pd}s$ of 1PdCe IW. Considering their TPO and TPR profiles (Chapter 3, Figure 3.11, 3.12, 3.13), SCS samples exhibit a complex redox behavior with the occurrence of separate decomposition/reduction steps and ascribed to the presence of various kind of PdO species, whereas mainly bulk PdO is present on their IW counterparts. In the case of ZrO_2-supported catalysts, similar reaction rates have been measured for IW and SCS sample, even though 1PdZr SCS shows multi-step decomposition and reduction peaks under oxidizing and reducing conditions, respectively. This indicate that the presence of different PdO species does not elucidate completely the better activity of solution combustion synthesized samples.

The higher catalytic activity of 1PdCe SCS and 1PdCZ75 SCS towards methane oxidation can be attributed to a strong Pd/ceria and Pd/ceria-zirconia interaction with the formation of ordered or random Pd-O-Ce linkages constituting active sites for methane dissociation [14, 15, 16]. This strong metal-support interaction is promoted by a synergistic interplay of reducible oxide, high temperature and strong redox conditions achieved during solution combustion synthesis. Among combustion synthesized catalysts, the use of intrinsically active oxides like ceria and ceria-zirconia and the presence of Pd-O-Ce bonds lead to the formation of active sites facilitating methane oxidation and improving the overall reaction rate [14, 15, 16]. The beneficial presence of CeO_2 is also observed in the cooling part of the cycle: when ceria is present into the support, Pd re-oxidation takes place at higher temperature due to the ability to change its oxidation state, providing lattice oxygen available for PdO re-oxidation. The better catalytic behavior of 1PdCe SCS and 1PdCZ75 SCS with respect their corresponding IW is also clear during time-on-stream tests: ceria and ceria-zirconia-supported catalysts prepared by SCS present a more stable behavior during lean-aging experiments, maintaining a good performance throughout the test. Again, when pure zirconia is used as support the deactivation degree during time-on-stream is almost similar between SCS and IW samples.

The single-step approach, thus, reveals to be an intriguing method to obtain efficient and stable ceria-based catalysts with better activity and stability in methane oxidation compared to the catalysts with the same composition prepared by standard IW procedure.

Concerning the experiments carried out in stoichiometric mixture, Pd catalysts supported on ceria and ceria-zirconia made by SCS still present high activity towards methane oxidation; in

particular, at temperatures below 800 K 1PdCZ75 SCS exhibits a better performance in lower oxygen partial pressure, probably due to the higher oxygen mobility of ceria-zirconia mixed oxide. The performance of Pd catalysts towards CH_4 oxidation changes markedly in the high temperature window: in lower oxygen partial pressure PdO decomposition is anticipated and its regeneration is shifted to lower temperature due to the lack of oxygen. The results suggest that the reaction pathway could be different from fuel lean conditions depending on temperature and support. In stoichiometric conditions in fact reforming, partial oxidation and RWGS at high temperatures can occur and compete or contribute to methane removal.

References

[1] P. Gelin and M. Primet, *Applied Catalysis B: Environmental,* vol. 39, pp. 1-37, 2002.

[2] G. Groppi, C. Cristiani, L. Lietti and P. Forzatti, *Studies in Surface Science and Catalysis,* vol. 130, pp. 3801-3806, 2000.

[3] P. Forzatti, *Catalysis Today,* vol. 83, pp. 3-18, 2003.

[4] S. Colussi, A. Trovarelli, E. Vesselli, A. Baraldi, G. Comelli, G. Groppi and J. Llorca, *Applied Catalysis A: General,* vol. 390, pp. 1-10, 2010.

[5] A.K. Datye, J. Bravo, T. Nelson, P. Atasanova, M. Lyubovsky and L. Pfefferle, *Applied Catalysis A: General,* vol. 198, no. Issues 1–2, p. 179–196, 2000.

[6] J.G McCarty, *Catalysis Today,* vol. 26, pp. 283-293, 1995.

[7] G. Groppi, C. Cristiani, L. Lietti, C. Ramella, M. Valentin and P. Forzatti, *Catalysis Today,* vol. 50, pp. 399-412, 1999.

[8] K. Fujimoto, F. Ribeiro, M. Borja and E. Iglesia, *Journal of Catalysis,* vol. 179, pp. 431-442, 1998.

[9] D. Ciuparu, M. Lyubovski, E. Altman, L.D. Pfefferle and A. Datye, *Catalysis Reviews,* vol. 44, pp. 593-649, 2002.

[10] X. Chen, Y. Cheng, C. Yup Seo, J.W. Schwank and R. W. McCabe, *Applied Catalysis B: Environmental,* vol. 163, pp. 499-509, 2015.

[11] S. Colussi, C. De Leitenburg, G. Dolcetti and A. Trovarelli, *Journal of Alloys and Compounds,* vol. 374, pp. 387-392, 2004.

[12] S. Colussi, A. Trovarelli, C. Cristiani and G. Groppi, *Catalysis Today,* vol. 180, pp. 124-130, 2012.

[13] P. Bera, A. Gayen, M. Hegde, N. Lalla, L. Spadaro, F. Frusteri and F. Arena, *J. Phys. Chem B,* vol. 107, pp. 6122-6130, 2003.

[14] K. R. Priolkar, P. Bera, P. Sarode, M. Hegde, S. Emura, R. Kumashiro and N. Lalla, *Chem. Matter.,* vol. 14, pp. 2120-2128, 2002.

[15] S. Colussi, A. Gayen, M. Cammellone, M. Boaro, J. Llorca, S. Fabris and A. Trovarelli, *Angew. Chem. Int.,* vol. 48, pp. 8481-8484, 2009.

[16] P. Bera, K. Patil, V. Jayaram, G. Subbanna and M. Hegde, *Journal of Catalysis,* vol. 196, pp. 293-301, 2000.

[17] S. Colussi, A. Gayen, M. Boaro, J. Llorca and A. Trovarelli, *ChemCatChem,* vol. 7, p. 2222–2229, 2015.

[18] Y. Cao, R. Ran, X. Wu, B. Zjao, J. Wan and D. Weng, *Applied Catalysis A: General,* vol. 457, pp. 52-61, 2013.

[19] S. Hinokuma, H. Fujii, M. Okamoto, K. Ikeue and M. Machida, *Chem. Mater.,* vol. 22, pp. 6183-6190, 2010.

[20] S. Colussi, A. Gayen, J. Llorca, C. de Leitenburg, G. Dolcetti and A. Trovarelli, *Ind. Eng. Chem. Res.,* vol. 51, p. 7510–7517, 2012.

[21] D. Pi, Z. Weng, L. Zhao, Q. Huang, H. Hu and C. Shao, *Energy Technology,* vol. 4, p. 943–949, 2016.

[22] F.H. Ribeiro, M. Chow and R. Dalla Betta, *Journal of Catalysis,* vol. 146, pp. 537-544, 1994.

[23] R. Burch, F. Urbano and P. Loader, *Applied Catalysis A: General,* vol. 123, pp. 173-184, 1995.

[24] D. Ciuparu, N. Katsikis and L.D. Pfefferle, *Applied Catalysis A: General,* vol. 216, pp. 209-215, 2001.

[25] L. Escandon, S. Ordonez, A. Vega and F. V. Diez, *Chemosphere,* vol. 58, pp. 9-17, 2005.

[26] J.-H. Park, J. Cho, Y. Kim, E. Kim, H. Han and C. Shin, *Applied Catalysis B: Environemental,* Vols. 160-161, pp. 135-143, 2014.

[27] F. Yin, S. Ji, P. Wu, F. Zhao, H. Liu and C. Li, *ChemSusChem,* vol. 1, p. 311–319, 2008.

[28] M. Monai, M. Montini , E. Fonda, R. Gorte and P. Fornasiero, *ChemCatChem,* vol. 6, pp. 1-14, 2014.

[29] Y. Madier, C. Descorme , A. Le Govic and D. Duprez, *J. Phys. Chem. B,* vol. 103, pp. 10999-11006, 1999.

[30] M. Lyubovsky, L. L. Smith, M. Castaldi, H. Karim, B. Nentwick, S. Etemad, R. LaPierre and W. C. Pfefferle, *Catalysis Today,* vol. 83, pp. 71-84, 2003.

[31] J. Kašpar, P. Fornasiero and N. Hickey, *Catalysis Today,* vol. 77, p. 419–449, 2003.

[32] H. Geng, Y. Zhongqing, L. Zhang, J. Ran and Y. Yunfei, *Energy Conversion and Menagement,* vol. 132, pp. 339-346, 2017.

Chapter 5

Effect of water on the stability and light-off performance of solution combustion synthesized $Pd/Ce_xZr_{1-x}O_2$ catalysts

Water poisoning represents a key issue for Pd-based catalysts due to the large amount of water vapor (10-15 vol.%) present in the exhaust gas stream. The investigation of the effect of water poisoning on the activity and durability of the series of $Pd/Ce_xZr_{1-x}O_2$ catalysts is the goal of this chapter. The regeneration of the water-poisoned catalysts is also addressed. The results are supported and discussed in light of FTIR and TEM analysis.

5.1. Catalytic performance in wet-lean conditions

5.1.1 Catalytic activity

The deactivation of Pd catalysts in the presence of external water was evaluated performing two oxidation cycles (heating/cooling) in wet atmosphere (0.5 CH_4, 2% O_2, 10 % H_2O(v) in He), named *cycle 1 H_2O* and *cycle 2 H_2O*. To check the reversibility of water poisoning, a third heating/cooling ramp (named *after H_2O*) in the absence of water (0.5 CH_4, 2% O_2, in He) was carried out. The second combustion cycle in dry-lean conditions (cycle 2 dry) is reported as a reference.

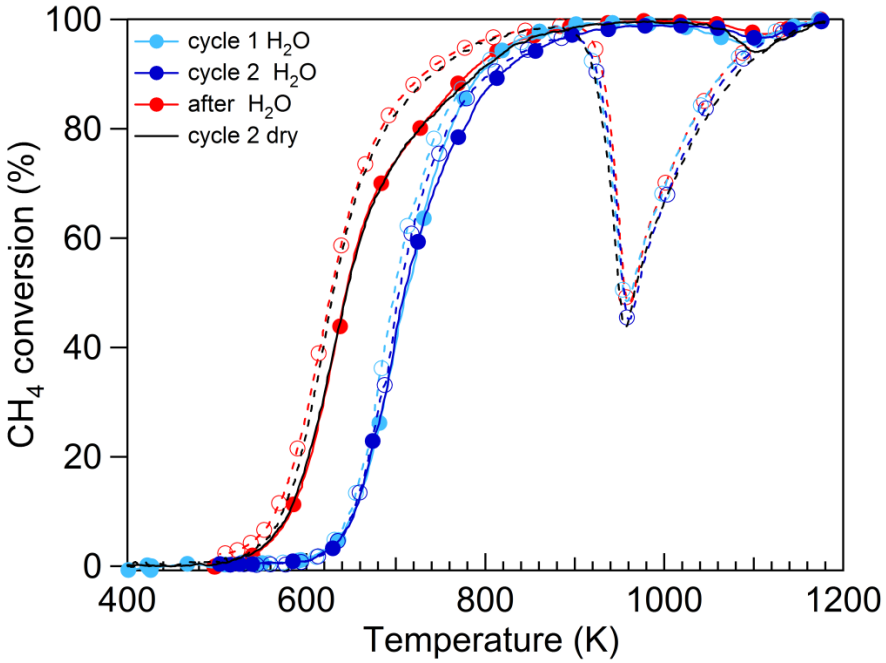

Figure 5.1: catalytic activity of 1PdCe SCS with and without water in lean conditions; closed symbols: heating; open symbols: cooling.

Figure 5.1 shows the light-off behavior during CH_4 oxidation in the presence and in the absence of water of 1PdCe SCS. When water is introduced in the gas stream, an increase of T_{10} from 581 K to 655 K and of T_{50} from 644 K to 710 K is observed, compared to cycle 2 dry. The catalytic performance in wet atmosphere is stable from cycle 1 to cycle 2: the two cycles are very similar to each other. It is worth noting that the activity drop during cooling is not affected by the presence of water vapor. When water is switched off, the catalytic activity is completely restored, and the light-off curve overlaps the curve recorded during cycle 2 in dry atmosphere.

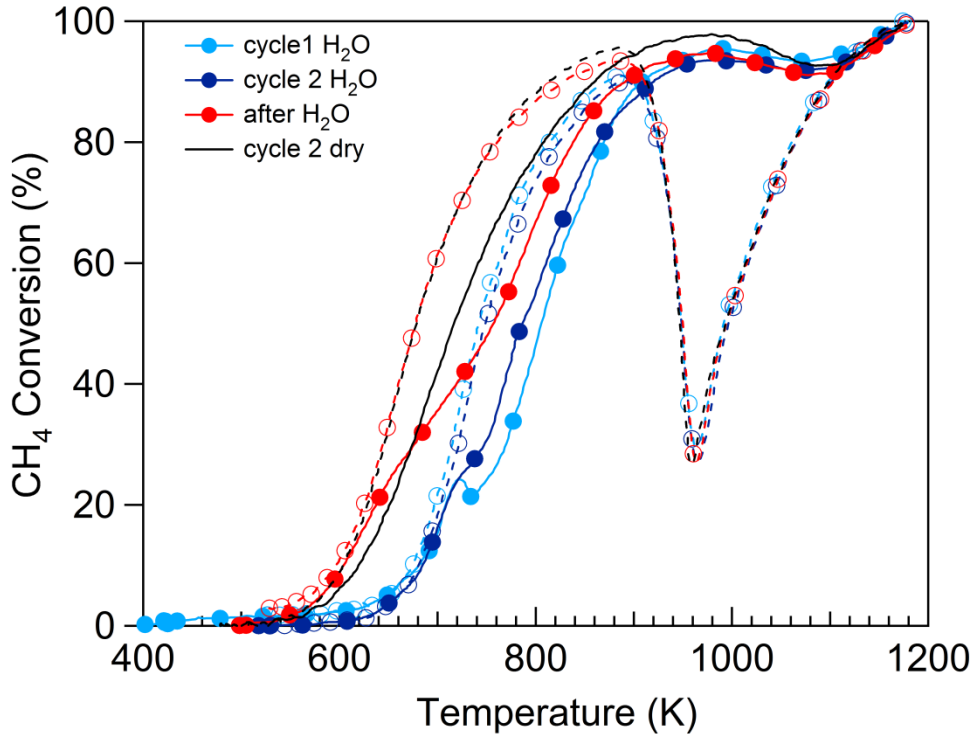

Figure 5.2: catalytic activity of 1PdCe IW with and without water; closed symbols: heating; open symbols: cooling.

1PdCe IW (Figure 5.2) displays also similar oxidation profiles throughout two heating/cooling ramps in wet conditions. In the presence of water T_{10} and T_{50} are shifted to higher temperature of 66 K and 70 K, respectively, with respect to dry atmosphere. After water removal the initial catalytic activity seems to be not fully restored during heating, with an increase of T_{50} of 40 K; however when the sample is cooled down the activity follows the same pattern observed in dry conditions. Again, no appreciable variations on the activity drop during cooling are detected upon water introduction and removal.

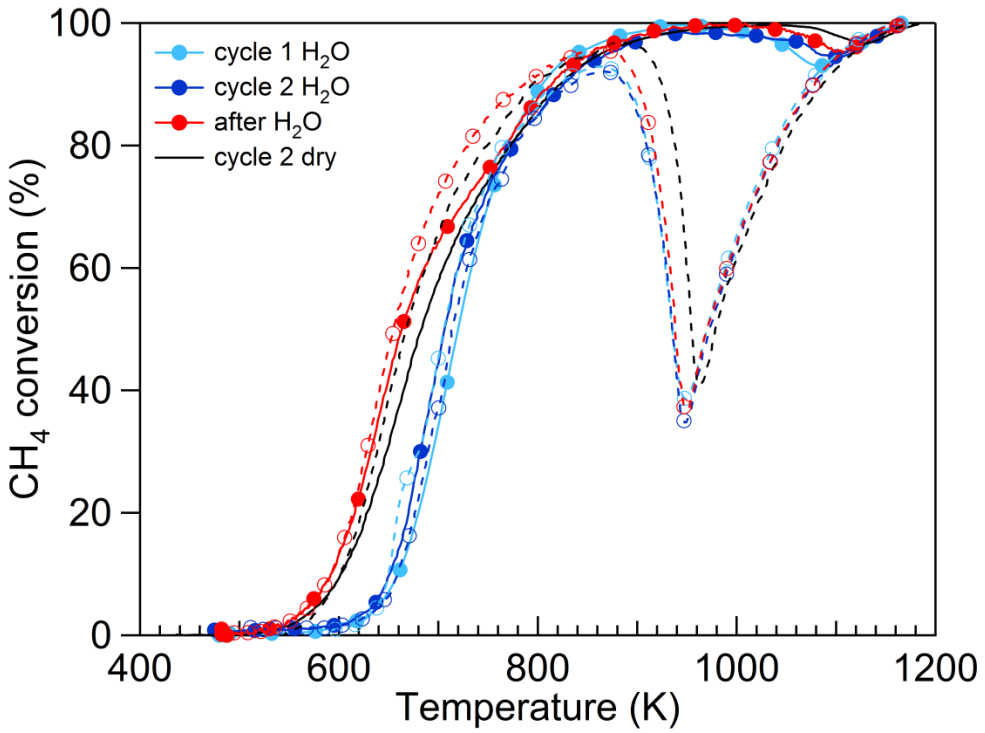

Figure 5.3: catalytic activity of 1PdCZ75 SCS with and without water; closed symbols: heating; open symbols: cooling.

The catalytic activity in wet atmosphere of 1PdCZ75 SCS is shown in Figure 5.3. The gap in terms of T_{10} between dry and wet curve is narrower with respect to the one measured for CeO_2-supported samples. At increasing temperature this gap is further reduced, with a shift of only 20 K for T_{50}. Looking at the cooling part of the cycle, the activity loss is slightly more pronounced than that in the absence of water, with a shift of the position of the minimum from 687 K to 677 K. When water is switched off, the activity is entirely recovered with a little improvement below 700 K compared to cycle 2 dry.

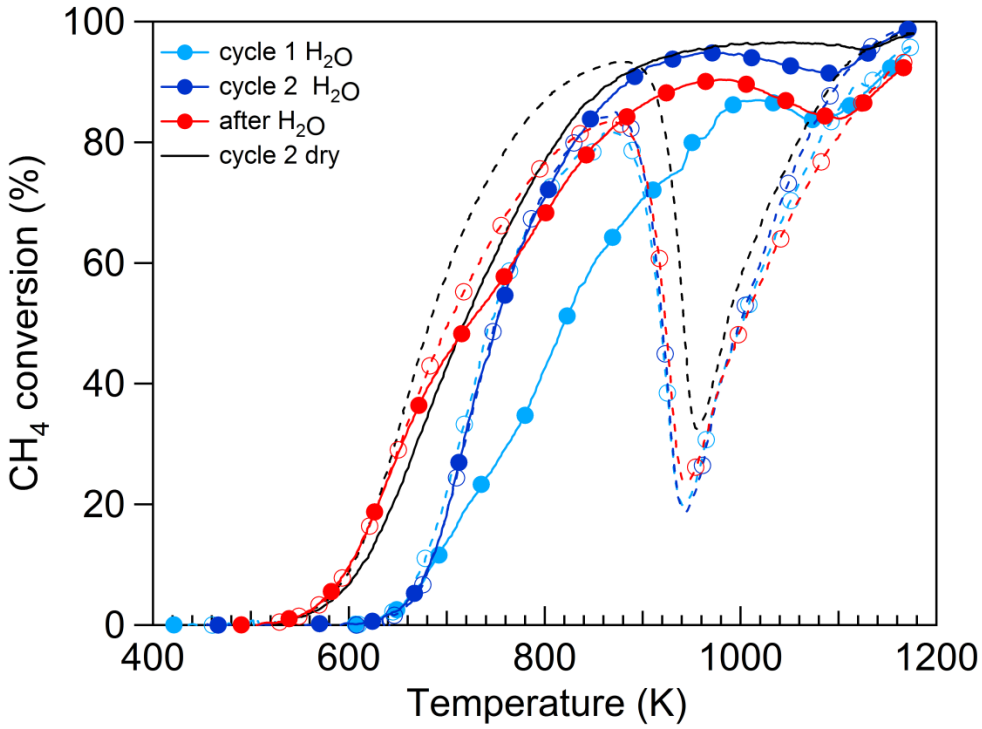

Figure 5.4: catalytic activity of 1PdCZ75 IW with and without water. Closed symbols: heating; open symbols: cooling.

For CZ75-based sample prepared by IW method (Figure 5.4), during cycle 1 H_2O the reaction starts at 680 K and 50% of CH_4 conversion is reached only at ~ 800 K. After the first run, the catalytic activity is considerably improved with an increase of T_{10} and T_{50} of only 70 K and 33 K, respectively, compared to dry conditions. In this case though, water not only affects the catalytic performance during the heating ramp but also in the cooling branch: methane conversion falls to 20% and Pd re-oxidation slightly moves to lower temperature ($T_{ox} \cong 941$ K against 956 K in dry conditions). When water is removed from the gas stream, the activity improves but does not recover completely compared to that in dry atmosphere, especially at high temperature where methane conversion hardly reaches 90% as maximum value.

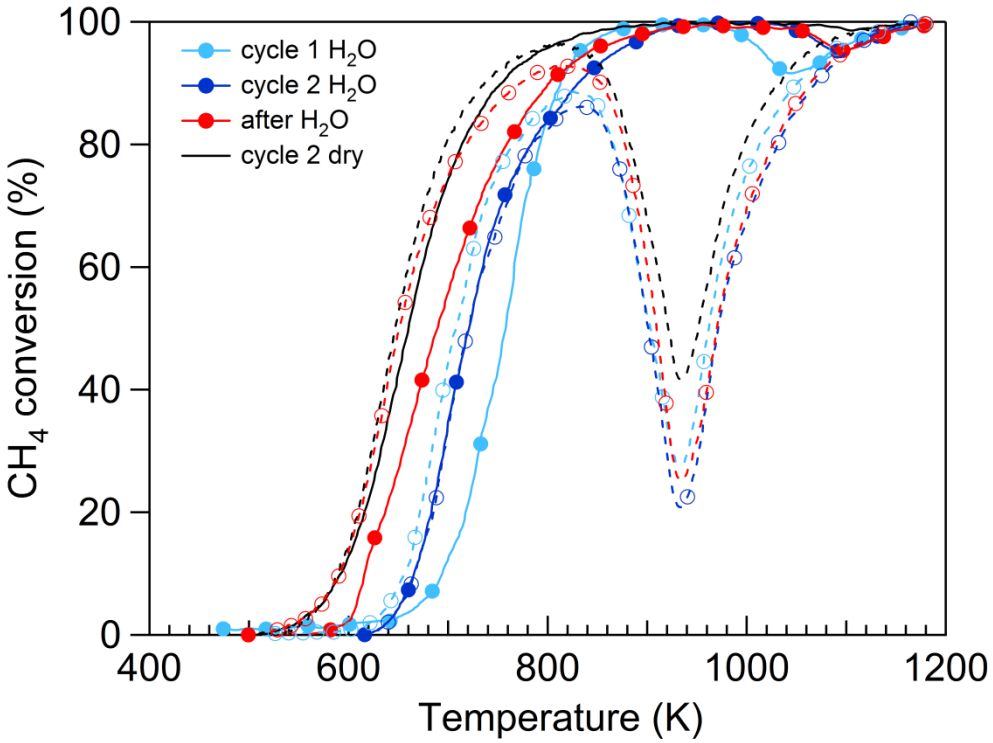

Figure 5.5: catalytic activity of 1PdZr SCS with and without water. Closed symbols: heating; open symbols: cooling.

The addition of water vapor has a strong effect on the catalytic activity of 1PdZr SCS (Figure 5.5): a severe water inhibition is observed during the first oxidation run where light-off of methane occurs at 695 K, showing a large hysteresis between heating and cooling ramp. When a second cycle is carried out, the catalytic behavior is improved with an increase of T_{10} of 71 K compared to dry conditions, with a smaller hysteresis. Focusing on the cooling part of the cycle, Pd re-oxidation takes place at 940 K with a critical drop of methane conversion to 20%. This could be caused by sintering mechanism after exposure to high temperature and promoted by the presence of water vapor [1]. When water is switched off, during the heating part of the cycle the activity remains lower compared to dry atmosphere, with T_{10} and T_{50} increasing of 21 K and 29 K, respectively. The activity loss continues to be more severe compared to cycle 2 dry; the initial level of activity is restored only upon cooling below 700 K.

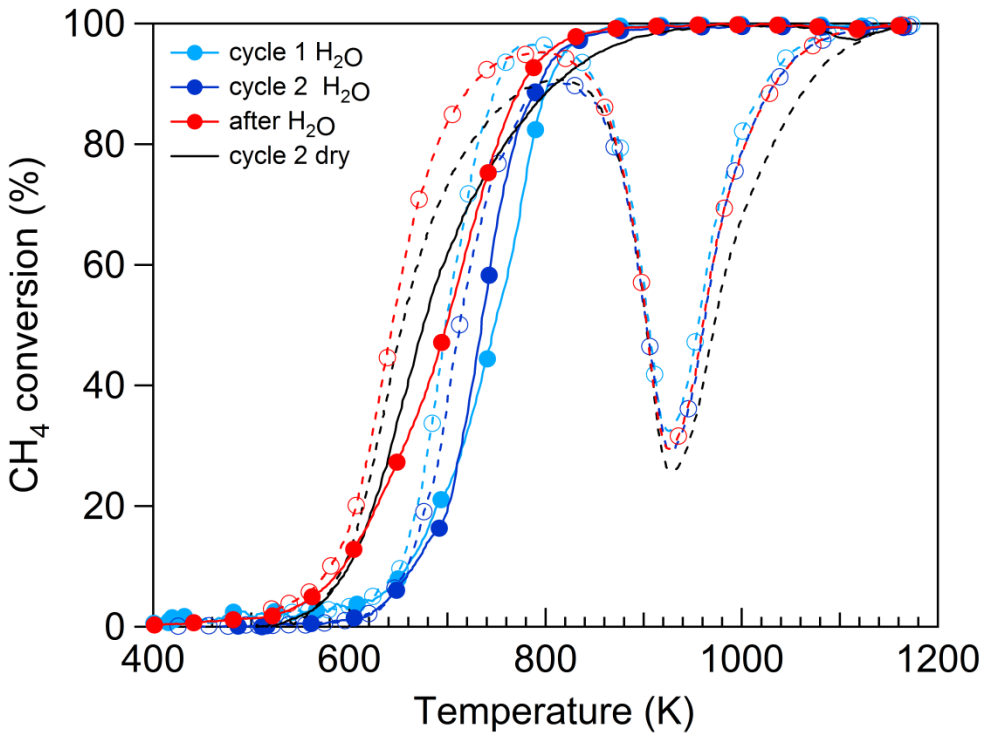

Figure 5.6: catalytic activity of 1PdZr IW with and without water. Closed symbols: heating; open symbols: cooling.

Looking at the results of 1PdZr IW (Figure 5.6), methane oxidation starts at 63 K higher than in the absence of water. Although a marked inhibition effect is observed during the heating segment, water has no significant influence on the high-temperature deactivation. Once water is removed, the activity is completely restored only during cooling with a slight improvement with respect to the cooling branch in dry atmosphere.

Table 5.1 summarizes the characteristic temperatures at which 10% and 50% of methane conversion is achieved with and without water for all samples.

Table 5.1: T_{10} and T_{50} performed during methane oxidation with and without water for 1% $Pd/Ce_xZr_{1-x}O_2$ catalysts

	T_{10} (K)			T_{50} (K)		
Catalyst	**dry**	**wet**	**after H_2O**	**dry**	**wet**	**after H_2O**
1PdCe SCS	581	655	583	644	710	645
1PdCZ75 SCS	602	654	592	684	703	664
1PdZr SCS	594	665	615	661	723	690
1PdCe IW	619	685	604	718	788	758
1PdCZ75 IW	614	683	602	718	751	724
1PdZr IW	601	664	595	676	735	700

By observing the values reported in Table 5.1, solution combustion synthesized samples demonstate a superior activity in wet conditions, especially when ceria is present in the

support: 1PdCe SCS and 1PdCZ75 SCS are significantly more active than their IW counterparts. As observed for the experiments carried out in dry atmosphere, for ZrO_2 supported samples the catalytic behavior is very similar between SCS and IW also in presence of water, showing close T_{10} and T_{50} values. This is a further confirmation that in the case of zirconia the preparation method does not have a strong influence on the catalytic performance, likely because Pd and zirconia do not interact as strongly as Pd-ceria.

The results obtained from catalytic tests in wet atmosphere indicate that water acts as a strong inhibitor of methane oxidation on Pd-based catalysts, especially at low temperature, and well in agreement with the published data [2, 3, 4, 5, 6, 7, 8]. The increase of the onset of methane oxidation has been attributed to the competitive adsorption between water and methane on active sites [3, 4, 8, 9], or to the formation of inactive $Pd(OH)_2$ by the reversible reaction of PdO with water molecules [10, 11], or to the suppression of oxygen exchange among Pd, gas phase-and support [12, 13]. When $Ce_{0.75}Zr_{0.25}O_2$ is used as support, the deactivation degree is less severe, irrespective of the preparation procedure. Ciuparu *et al.* attributed the better resistance to water poisoning of PdO/ceria-zirconia to the higher oxygen mobility of Ce-Zr mixed oxide. A fast oxygen exchange between the active phase and the support has been proposed to avoid a high hydroxyl coverage of the catalytic surface, thus enhancing the resistance to the deactivation caused by water [11, 12]. When water is switched off, the catalytic activity is restored more or less slowly to the initial value due to the desorption of hydroxyls from the catalytic surface [2, 4] or to the recovery of oxygen exchange process [12]. The catalytic performance on CeO_2-containing catalysts made by SCS, with higher oxygen exchange capability, is immediately recovered upon water removal, whereas for their corresponding IW ones the activity is recovered at low temperature but not over the entire cycle.

By looking at the catalytic results presented above, the effect of water on PdO-Pd-PdO phase transformation is not straightforward to define. For this reason we carried out also TPO experiments in presence of water. If we focus on the second TPO cycle performed in wet atmosphere (2% O_2/N_2, 10% H_2O) (Figure 5.7), it is possible to observe that water does not modify significantly the onset or the shape of PdO-Pd transformation, which occurs always in a single broad step on IW catalysts and in three well defined peaks on SCS samples. Also the cooling part of the cycle is not markedly affected by water addition; only for 1PdZr IW the oxygen amount consumed for PdO re-formation is reduced with respect to the dry pattern. However, the differences observed during transient tests indicate that the effect is more pronounced or it acts differently when methane oxidation takes place.

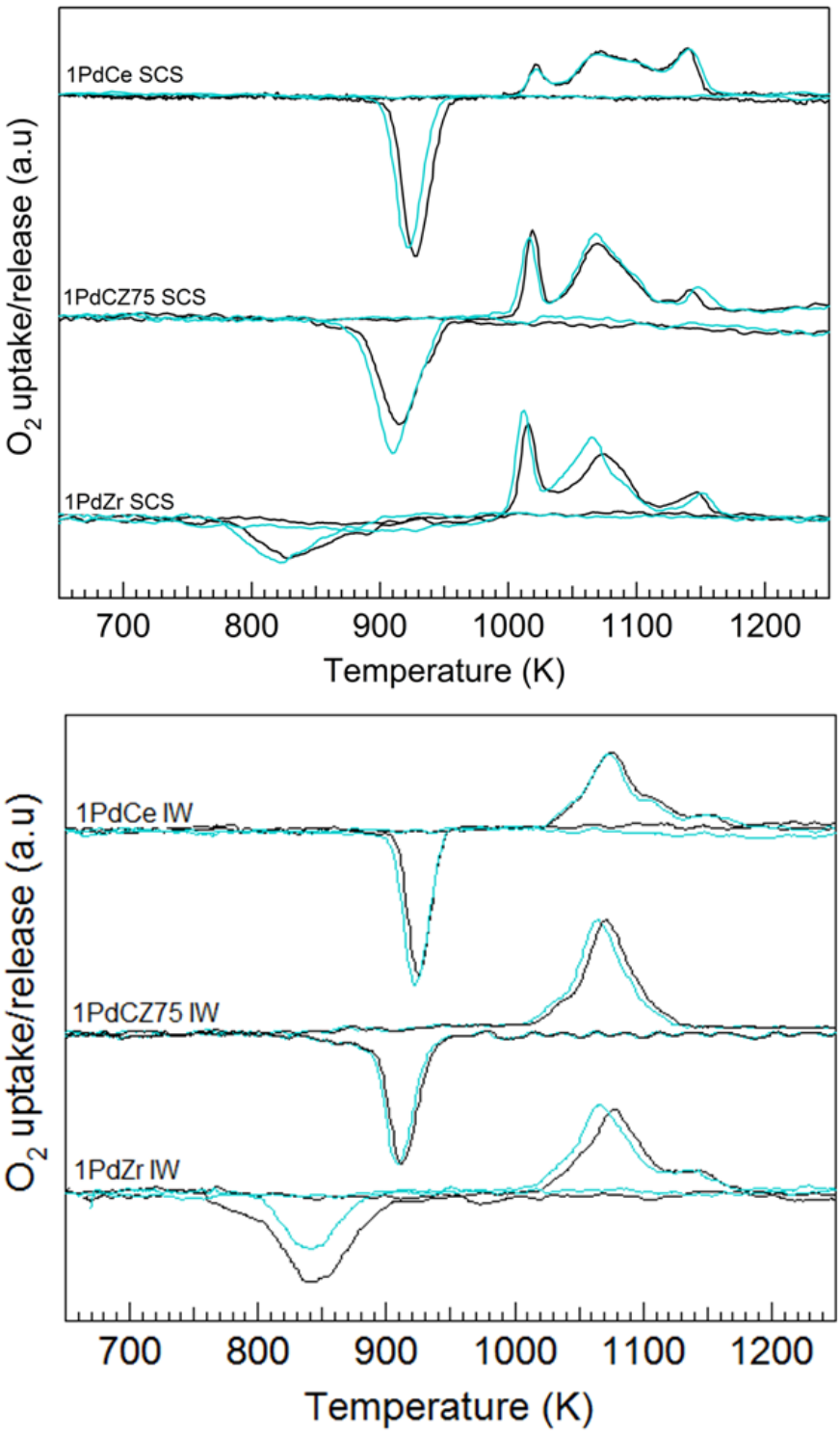

Figure 5.7: second TPO cycle with and without water for $Pd/Ce_xZr_{1-x}O_2$; black line: dry (2% O_2/N_2); light-blue line: wet (2 % O_2/N_2, 10% H_2O)

Figure 5.8 illustrates the comparison of second heating/cooling cycle in the presence of water of SCS catalysts.

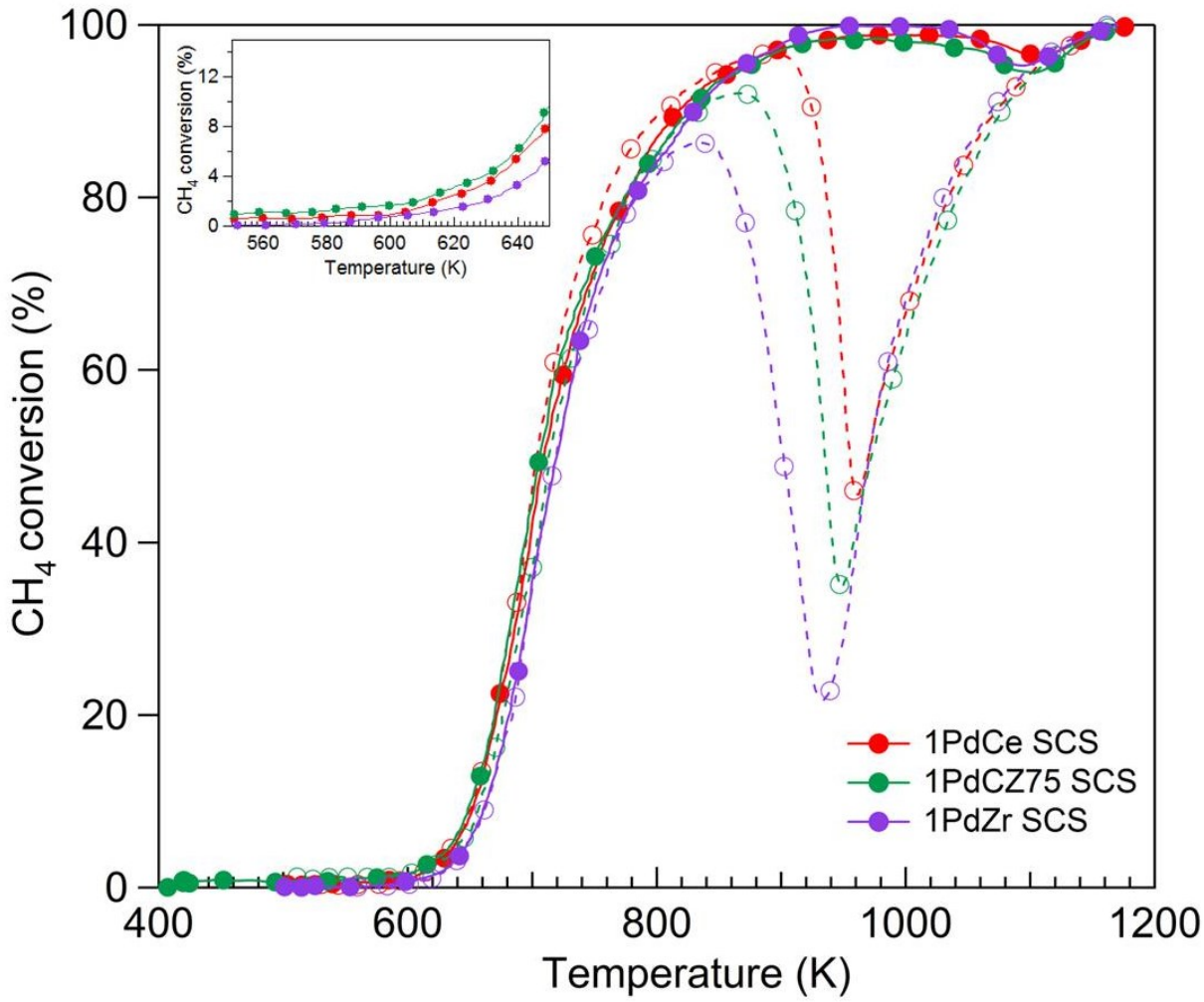

Figure 5.8: catalytic activity during the second heating/cooling ramp in wet conditions on SCS samples. Solid line, closed symbols: heating; dotted line, open symbols: cooling.

All samples show a similar light-off behavior during the heating ramp, with a slightly better performance in the low temperature region achieved by 1PdCZ75 SCS, followed by 1PdCe SCS, and 1PdZr SCS (see the inset of Figure 5.8). Focusing on the cooling branch, the effect of the support is clearly observable: re-oxidation of Pd to PdO takes place at higher temperatures when CeO_2 and CZ75 are used as carriers, and, thanks to this effect, the activity loss is considerably reduced compared to zirconia-supported sample.

5.1.2 *Study of the durability and regeneration of H_2O-poisoned catalysts*

The effect of water on the catalysts stability has been evaluated by time-on-stream measurements (TOS) at 723 K with a constant concentration of water vapor (10 vol.% (v)). The evolution of methane concentration has been continuously monitored with time-on-stream. The comparison between SCS and corresponding IW samples is made on the basis of normalized methane conversion, calculated as follows:

$$normalized\ \ CH_4\ conversion = \frac{X_{CH4}^{wet}(t)}{X_{CH4}^{wet}(0)}$$

where $X_{CH4}^{wet}(0)$ is the CH_4 conversion reached at the beginning of the test at 723 K. For sake of clarity, the stability curves collected without water ("dry mixture") and already shown in chapter 4, Figure 4.9 are added. Figure 5.9 shows the results of TOS experiments on 1PdCe IW and 1PdCe SCS in wet atmosphere.

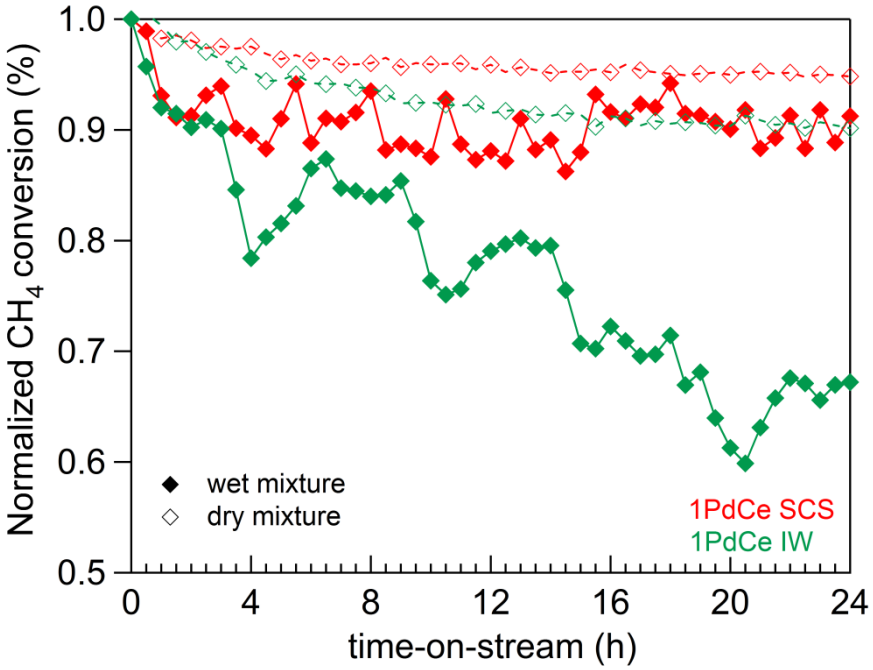

Figure 5.9: normalized CH_4 conversion versus time-on-stream for CeO_2 supported samples at 723 K in wet and dry atmosphere

As soon as water is introduced into the dry feed, 1PdCe IW is rapidly deactivated, according to the inhibition effect of water on methane oxidation. The activity is immediately deteriorated, and the conversion decreases to ~ 85% of the initial value in 8 hours, continuing to decline in the following hours. At the end of the test, the conversion decreases of about 40% with respect to the initial value (against 16 % in dry atmosphere). In the case of 1PdCe SCS instead, water affects only slightly the stability of the catalyst, losing only about 10% of the initial conversion. By looking at the stability curves of Ce-Zr-based samples (Figure 5.10), the introduction of water accelerates the deactivation of 1PdCZ75 SCS much more with respect to 1PdCe SCS,

causing a decrease of normalized methane conversion from 100% to 70% after 24 hours. Concerning 1PdCZ75 IW, in isothermal conditions it experiences a severe deactivation with time-on-stream, losing 40% of its initial activity, similarly to what observed for 1PdCe IW.

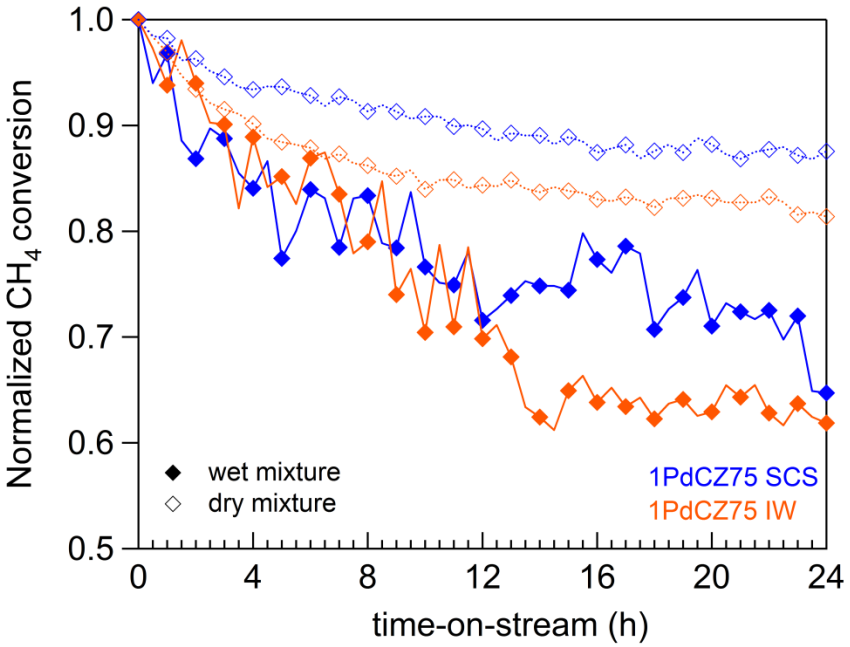

Figure 5.10: normalized CH_4 conversion versus time-on-stream for CZ75 supported samples at 723 K in wet and dry atmosphere

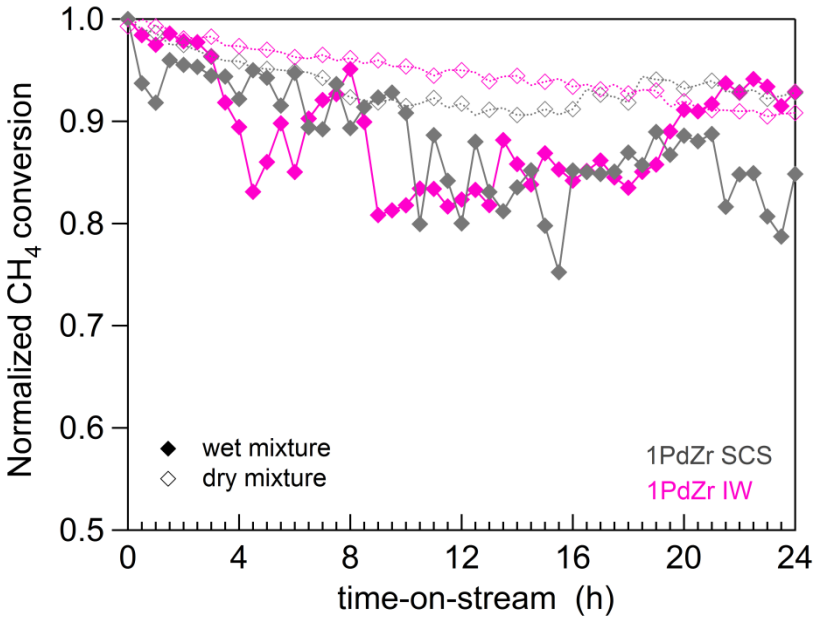

Figure 5.11: normalized CH_4 conversion versus time-on-stream for ZrO_2supported samples at 723 K in wet and dry atmosphere

In Figure 5.11 the comparison of time-on-stream behavior of ZrO_2-based catalysts is reported. At steady-state both samples show a good hydrothermal stability: the addition of water vapor into the gas feed seems to not affect the time-on-stream behavior of 1PdZr IW with an overall deactivation similar to that measured in dry feed (8 %). Also 1PdZr SCS is able to maintain a good stability during the hydro-treatment, losing 19% of initial conversion (vs 8% in dry feed).

It should be emphasized that the numbers are merely indicative, since the oscillations in water feed might affect the punctual conversion values; what is significant is the general trend which indicates a higher stability of 1PdCe SCS and Zr-supported catalysts among all samples considered in this study.

When water is introduced into the reaction feed, the synthesis procedure does not affect significantly the deactivation over time of ceria-zirconia samples, in contrast to what observed in dry conditions. In the case of pure ceria the difference between IW and SCS becomes instead much more pronounced than in dry feed, with the latter showing a much higher stability. For zirconia-supported catalysts the trend of deactivation observed without water is maintained in wet atmosphere with similar stability of both samples under steady-state conditions. The low deactivation of zirconia-based catalysts during hydro-aging is in agreement with other literature results. Some authors tentatively ascribed the stability of zirconia-supported catalysts to the high surface oxygen mobility, that might avoid the accumulation of OH on the surface of the catalyst [1, 13, 14]. Alternatively, physic-chemical properties of ZrO_2 (acid strength, hydrophobicity) were indicated to enhance the resistance to water poisoning [1, 15], but no conclusive explanation has been found yet.

In order to determine the reversibility of water deactivation during time-on-stream test, activity recovery experiments were carried out to study the regeneration of the H_2O-poisoned catalysts. These tests represent a key point to evaluate the stability of the catalysts upon cyclic wet/dry feed. The activity recovery experiments were performed at 723 K and each sample was subjected to cyclic feed stream from wet-lean to dry-lean feed, represented in the scheme reported in Chapter 2, Figure 2.6. The cooling branch of the second cycle carried out in dry condition ("cycle 2 dry cool") and the time-on-stream curve recorded in dry conditions ("723_dry 24 h") are also shown as references.

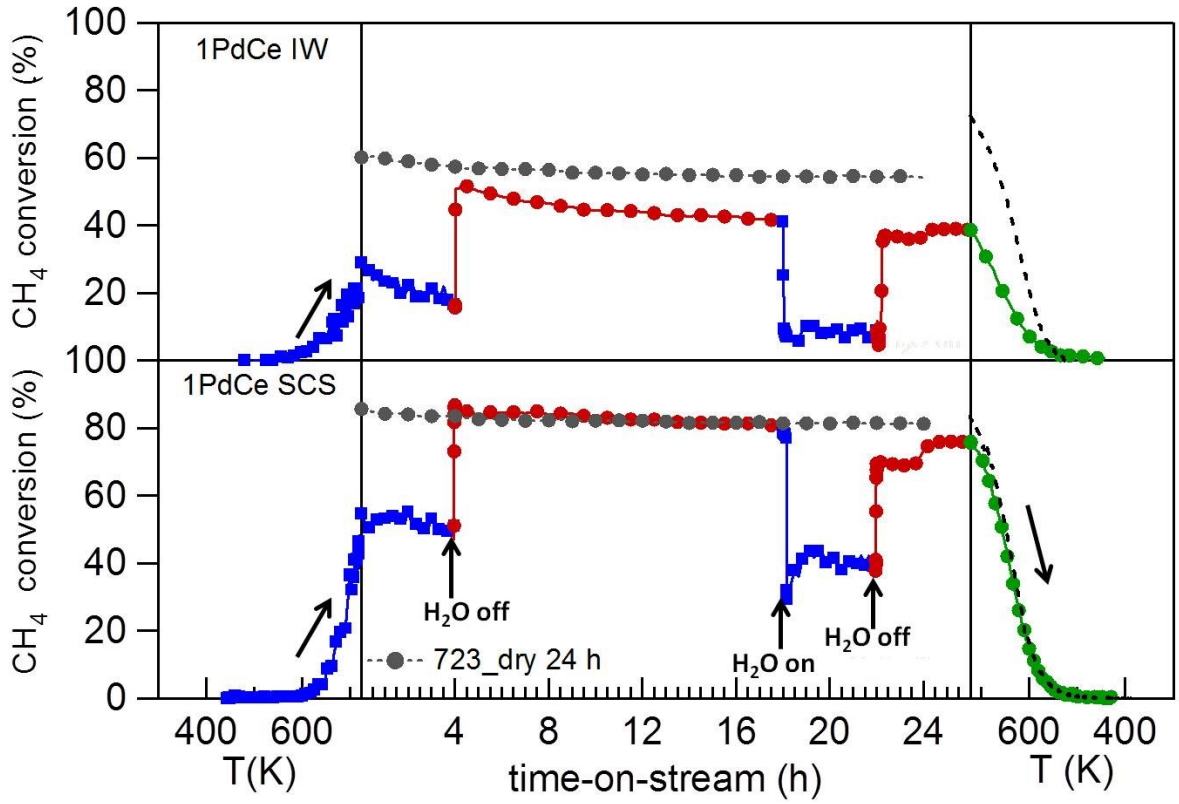

Figure 5.12: activity recovery test on CeO_2 supported samples; square symbols: wet; circular symbols: dry.

Figure 5.12 illustrates the behavior of ceria-based catalysts during the activity recovery test at 723 K. 1PdCe SCS, as already observed during TOS, shows a good stability in the presence of water, while 1PdCe IW progressively loses its activity with time. After removing water, leaving the catalysts in dry conditions for about 14 hours, SCS sample recovers completely the initial catalytic activity, even slightly improving for a short time its performance compared to dry conditions (grey curve), whereas 1PdCe IW is not able to recover its dry activity pattern. After a further addition of water, the methane conversion drops very quickly to ~ 40% and 15% for SCS and IW sample, respectively, and it remains almost constant during 4 hours. Removing water again, a quick increase in activity can be observed for both samples. The conversion of methane remains constant for about 1 h, then a further slight increase is recorded.

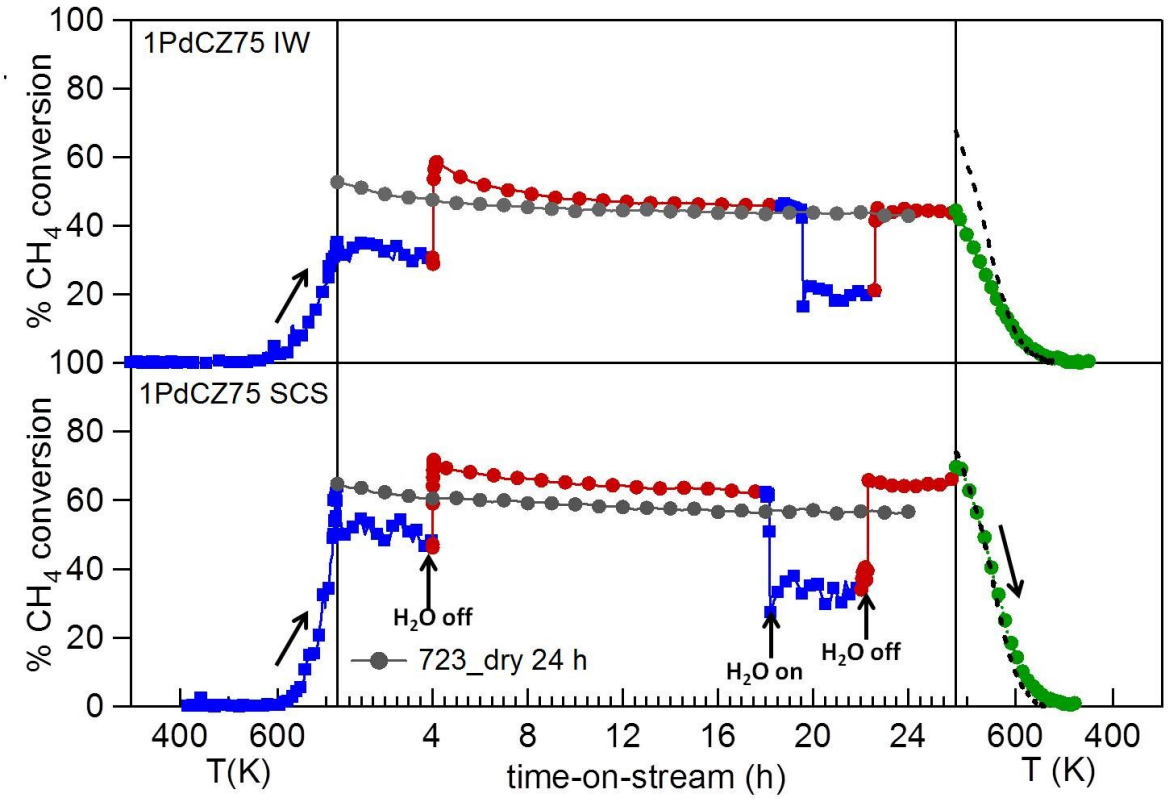

Figure 5.13: activity recovery test on CZ75 supported samples; square symbols: wet; circular symbols: dry.

Figure 5.13 illustrates the results for CZ75-supported samples. When water is switched off after 4 hours, both samples improve their performances compared to the respective dry activity (grey line), in line with the results obtained during activity tests. This effect is much more evident than for 1PdCe SCS, and for 1PdCZ75 SCS it is maintained during the 14 hours in dry atmosphere (methane conversion being always 10% higher than the time-on-stream dry conversion). 1PdCZ75 IW loses progressively its activity, going back to the values recorded during dry time-on-stream experiment. After a further water on/off cycle, 1PdCZ75 SCS slightly increases again its methane conversion compared to the last observed value before water introduction. As it was observed for ceria-supported samples, also in this case the SCS catalyst follows its dry cooling light-off curve while the IW one is highly deactivated.

The results of ZrO_2-supporting samples during regeneration tests are presented in Figure 5.14.

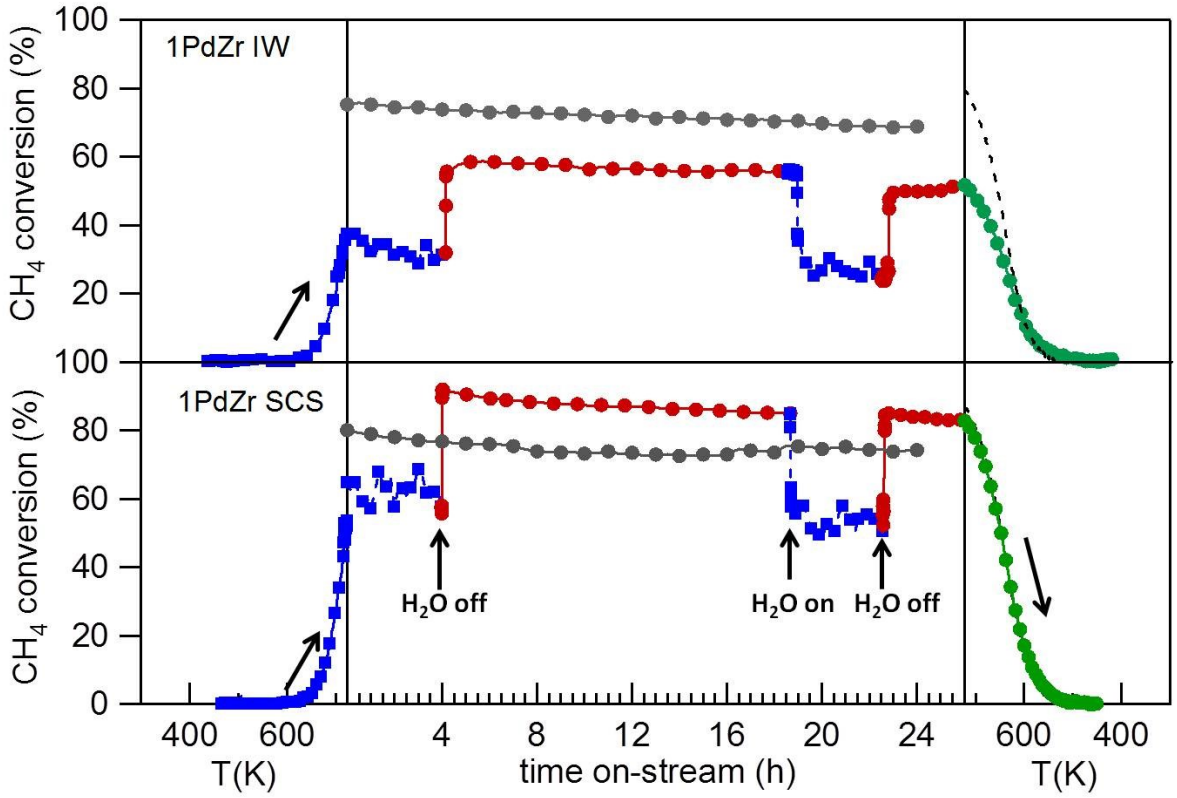

Figure 5.14: activity recovery test on ZrO_2 supported samples; square symbols: wet; circular symbols: dry.

During the first 4 hours in wet atmosphere, both samples exhibit a good hydrothermal stability, as assessed during TOS. Upon removing water, SCS catalyst is able not only to restore its initial conversion but also to show a considerable improvement of its performance compared to the behavior recorded in dry conditions (grey line). On the contrary, for 1PdZr IW only a partial restore is detected and the overall conversion remains ~20% lower than the dry time-on-stream test. Once water is re-introduced, methane conversion immediately drops to 60% and 35-40% for 1PdZr SCS and 1PdZr IW, respectively. Switching off water again, only 1PdZr SCS recovers completely its initial pattern. When the samples are cooled down, 1PdZr SCS follows the cool-down branch of cycle 2 dry, whereas the IW sample shows a permanent deactivation.

The recovery of activity is enhanced for ceria-zirconia-based catalysts: the addition of ZrO_2 into CeO_2 structure enhances the oxygen storage capacity (OSC) of CeO_2 and oxygen mobility [16], as measured by TPR (see Chapter 3): this has been indicated as a key factor to prevent or minimize the effects of deactivation by water [12, 13]. Indeed, a very good performance of ceria-zirconia based samples can be observed despite the preparation method. This result seems well in agreement with the mechanism of deactivation via suppression of oxygen exchange with the support proposed by Ciuparu *et al.* and recently by Schwartz *et al.* When Pd is supported on ceria-zirconia mixed oxide the deactivation operated by water is less severe likely due to the higher oxygen exchange capability of the oxide carrier which provide a better stability during

the reaction in wet atmosphere [12, 13]. The stabilizing role of zirconia is known to be beneficial for the activity of Pd-based catalysts in presence of water [14]. Indeed a very good performance has been observed also for 1PdZr SCS during time-on-stream experiments.

Furthermore, Stasinska *et al.* found a correlation between water deactivation and Pd particle size: catalysts with smaller PdO particles were found to be less affected by water poisoning [17]. This behavior has been attributed to a faster and easier oxygen exchange for small Pd crystallites, while for larger PdO particles a more severe deactivation was observed. A heterogeneous PdO size distribution and/or different PdO species on SCS samples, as inferred from TPO and TPR profiles, could explain their lower susceptibility to water deactivation, guaranteeing higher activity and stability.

In order to obtain a deeper understanding of the behavior of different catalysts, catalysts fresh and after activity recovery tests (aged) were characterized by means of FTIR spectroscopy and TEM analysis. Figure 5.15, 5.16 and 5.17 illustrate the IR spectra after the activity recovery tests of Pd catalysts supported on ceria, ceria-zirconia and zirconia, respectively.

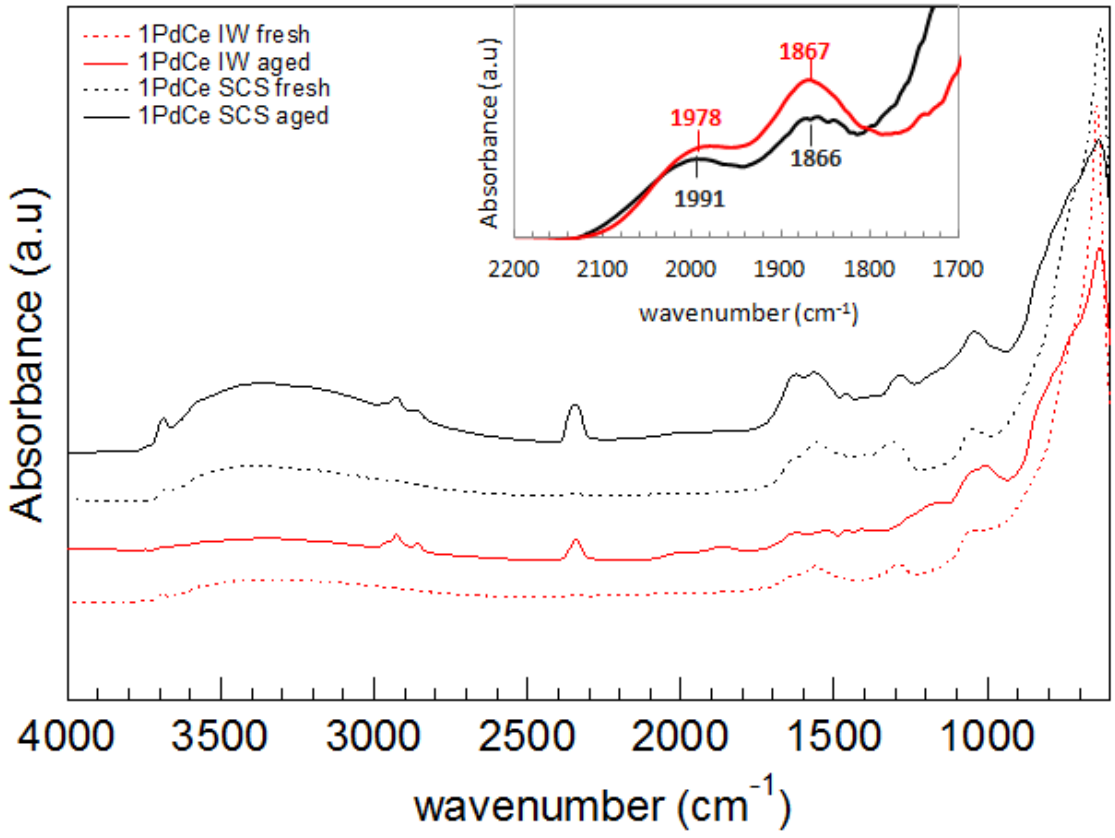

Figure 5.15: FTIR spectra of fresh (dotted line) and aged (solid line) CeO_2 supported samples in the range of 600-4000 cm^{-1}

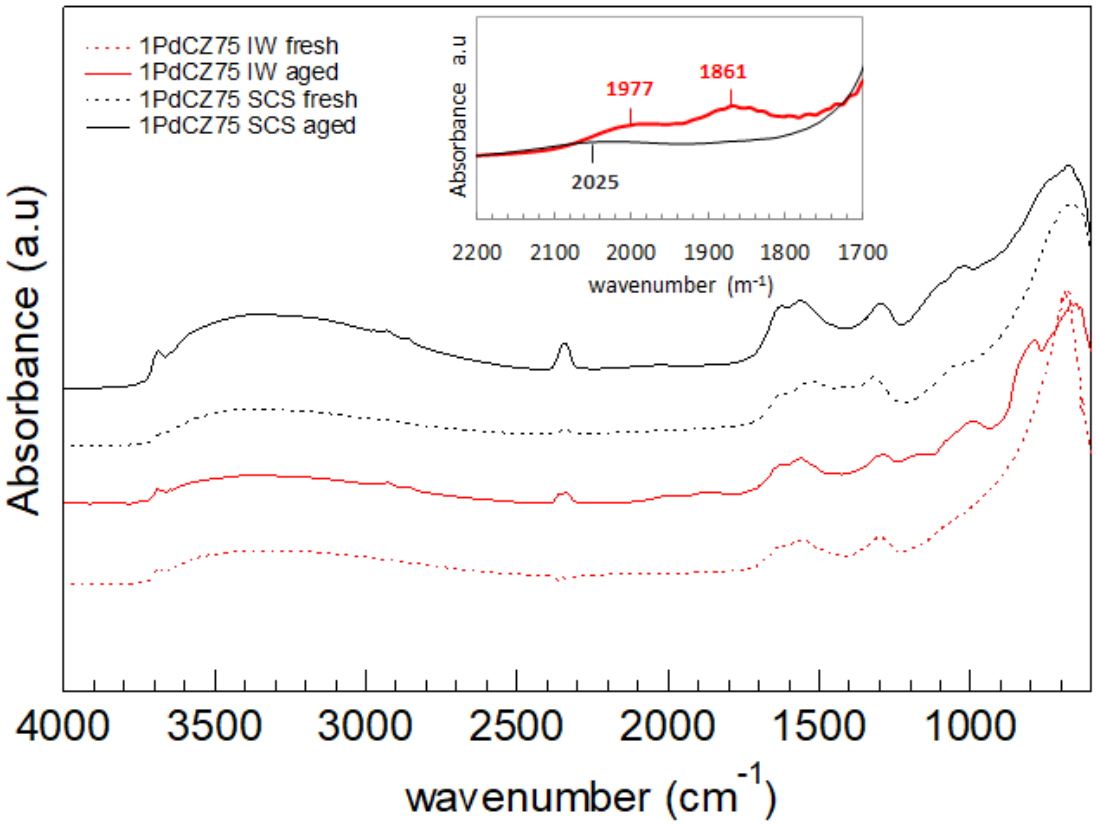

Figure 5.16: FTIR spectra of fresh (dotted line) and aged (solid line) CZ75 supported samples in the range of 600-4000 cm^{-1}

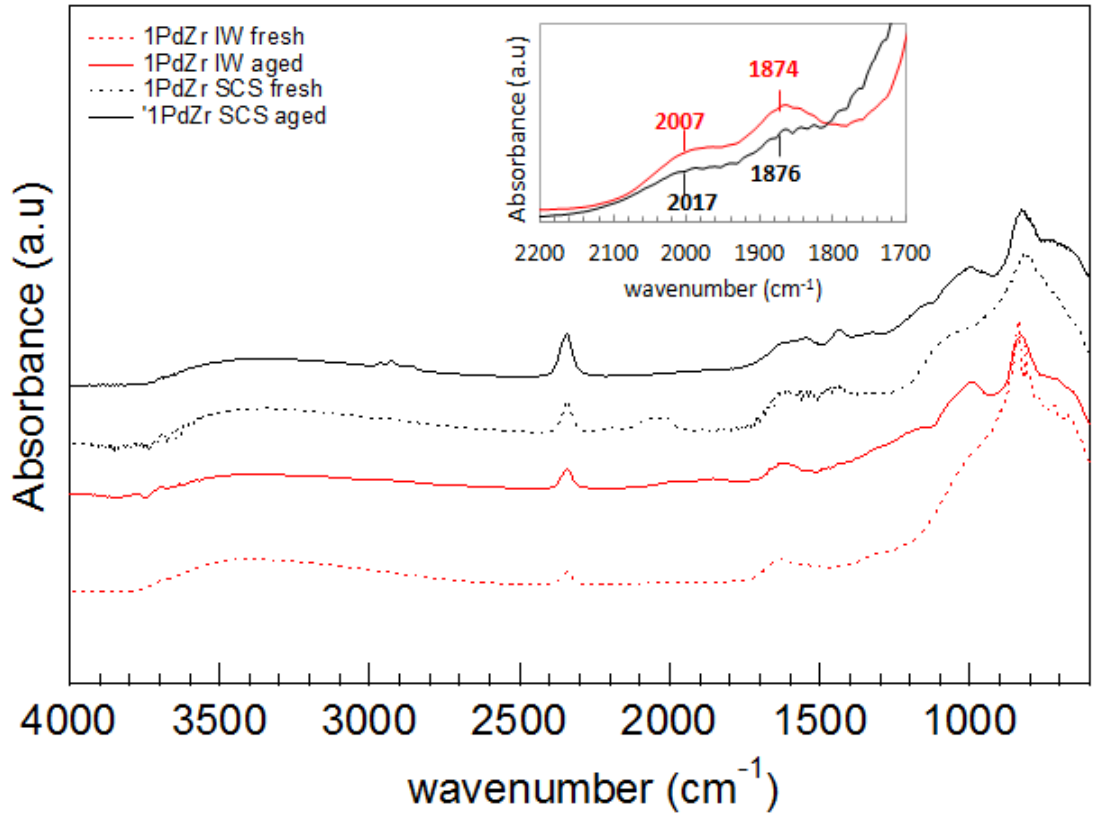

Figure 5.17: FTIR spectra of fresh (dotted line) and aged (solid line) ZrO_2 supported samples in the range of 600-4000 cm^{-1}

The IR patterns recorded before (fresh) and after activity recovery test (aged) show several adsorption bands in the range of 600-4000 cm^{-1}.

The fresh catalysts (dotted lines) show large bands in the range of 3700-3100 cm^{-1} belonging to the stretching of O-H species [18, 19, 20]. A small shoulder is present at ~ 3698 cm^{-1} which could be assigned to the surface OH groups on the support [19]. The sharp IR peak located at approximately 2400-2300 cm^{-1} corresponds to gaseous CO_2 [18]. Looking at the IR spectrum of the fresh 1PdZr SCS (Figure 5.17 dotted black line) a broader and not well defined IR band is observed in the range of 2160-1980 cm^{-1}: this large band can be attributed to CO coordinated to Pd and/or Zr^{4+} [19, 20].

The peaks in the region 1700-1000 cm^{-1} are generally assigned to the presence of various carbonates, hydrogenocarbonates and formates adsorbed on the support [21, 22, 23, 24]. These species trapped on the fresh catalysts can be originated from the thermal decomposition of precursors and organic fuel used for sample preparation. The strong adsorption bands at lower wavenumber (600-900 cm^{-1}) are characteristic of Ce-O and Zr-O stretching mode [25, 26, 27]. In particular the IR peak at ~ 750 cm^{-1} present on ZrO_2-supported catalysts is assigned to monoclinic ZrO_2.

Looking at the IR patterns of the aged samples (solid line), it is possible to observe that the absorption features relative to the support oxide are slightly modified upon aging, indicating that the vibrational modes of Ce-O and Zr-O are in some way affected by cyclic wet/dry treatment. The appearance of IR peaks in the region 3100-2600 cm^{-1} is detected and ascribed to C-H intermediates remained adsorbed on the surface after reaction. The main feature observed after the aging treatment consists in the bands corresponding to carbonyl species adsorbed on Pd^0 sites, that appear on all catalysts. The vibrational frequencies of C-O bond depend on the adsorption sites of carbon monoxide over Pd, whose identification is not straightforward due to the their close wavenumber. However, the band centred at ~ 1880-1870 cm^{-1} is generally characteristic of bridging CO over metallic Pd sites [19, 20, 22, 28], where CO molecule is coordinated to two-three Pd^0 sites, while the bands at about 2000 cm^{-1} can be attributed to linear Pd^0–CO complexes [21]. Irrespective of the support, on impregnated samples the bands relative to bridge Pd^0-CO are more intense than on SCS ones: this might evidence the presence of larger Pd particles or lower Pd dispersion after aging in IW catalysts. Also, on SCS samples a slight shift of the band at higher wavenumbers is observed, indicating the prevalence of linear bonded CO. It is worth noting that the IR pattern of aged 1PdCZ75 SCS does not reveal any band attributed to bridge Pd^0-CO.

In order to ascertain the hypothesis of higher dispersion on SCS samples after aging, and trying to further understand the deactivation mechanism, TEM characterization of aged CZ75-based samples has been carried out, measuring the average particle size of palladium particles before

and after aging. Figure 5.18 shows the TEM images of fresh and aged CZ75-based samples; black arrows indicate Pd particles. Pd particle size distribution before and after aging has also been calculated on the basis of TEM characterization and the results are reported in Figure 5.19.

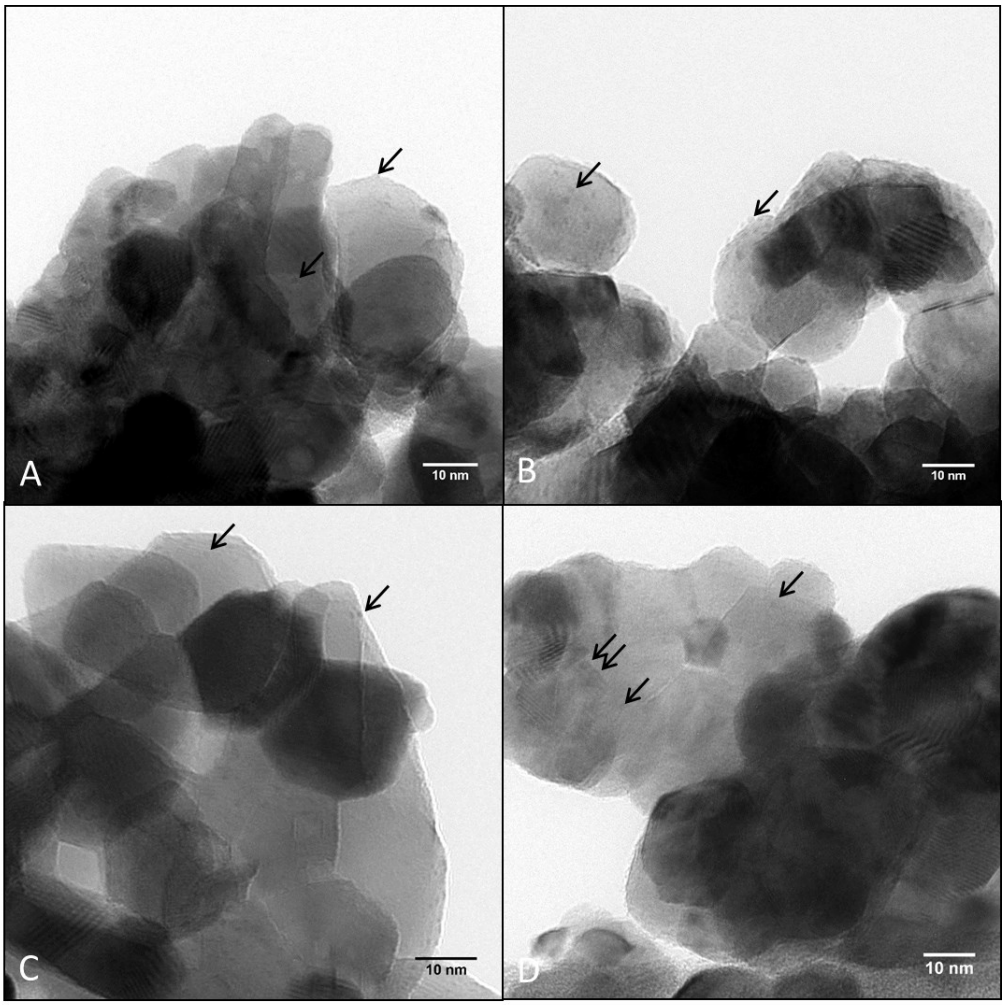

Figure 5.18: TEM images of fresh A) 1PdCZ75 SCS, B) 1PdCZ75 IW, aged C) 1PdCZ75 SCS and D) 1PdCZ75 IW

TEM images of fresh 1PdCZ75 SCS show that Pd particles are finely dispersed on the ceria-zirconia support and the mean size of Pd particles is of 0.80 nm, as inferred from Figure 5.19 (A). On the fresh 1PdCZ75 IW sample (Figure 5.19 (B)), palladium particles are larger with an average size of 1.22 nm. After aging, the mean particles size of Pd increases up to 0.90 nm and 1.90 nm on 1PdCZ75 SCS and 1PdCZ75 IW, respectively. The particle size range remains within 0-2 nm on 1PdCZ75 SCS before and after aging, whereas for its IW counterpart there is a significant increase from 0.5-2 nm to 1-3.5 nm, as it is shown in Figure 5.19.

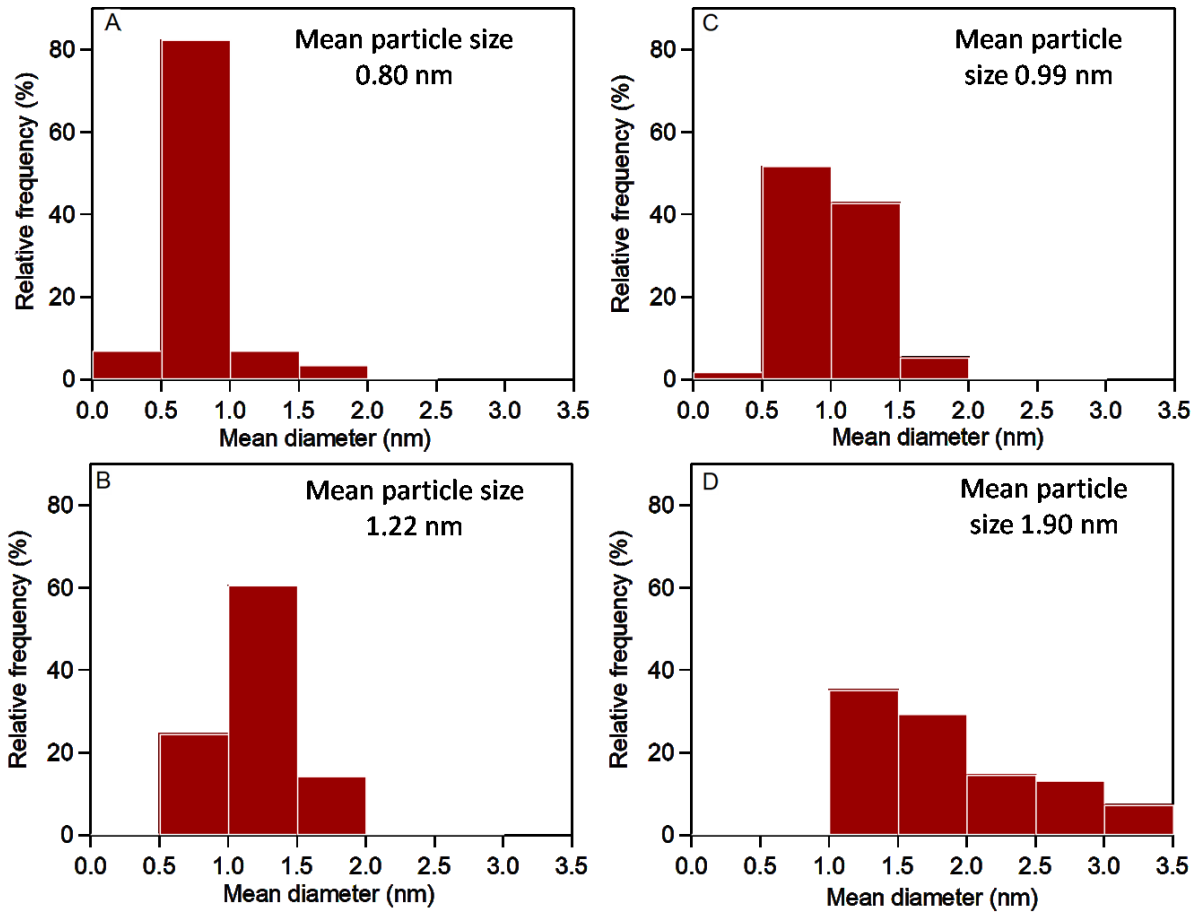

Figure 5.19: Pd particle size distribution of CZ75-based samples; A) fresh 1PdCZ75 SCS, B) fresh 1PdCZ75 IW, C) aged 1PdCZ75 SCS and D) aged 1PdCZ75 IW

TEM results seem to be consistent with the ones obtained by IR characterization. The particle size of palladium and its dispersion on the catalytic surface can change after aging [29, 30, 31]. The growth of noble metal particles after aging treatment is more pronounced for impregnated samples: the formation of Pd-O-Ce linkages via strong metal-support interaction for solution combustion synthesized Ce-containing samples might prevent the sintering of Pd particles and maintain Pd highly dispersed on the support. High dispersion and smaller particles of palladium have been indicated to enhance the catalytic activity [17, 30] and are less susceptible to deactivation in the presence of water [17].

5.2 Catalytic performance in wet-stoichiometric conditions

In order to study the effect of oxygen concentration on water poisoning, the catalytic performance of 1PdCe SCS and 1PdCZ75 SCS has been investigated also in oxygen-deficient conditions (0.5% CH_4, 1.0% O_2 with 10 vol.% of H_2O in He), following the same experimental procedure used for wet-lean experiments.

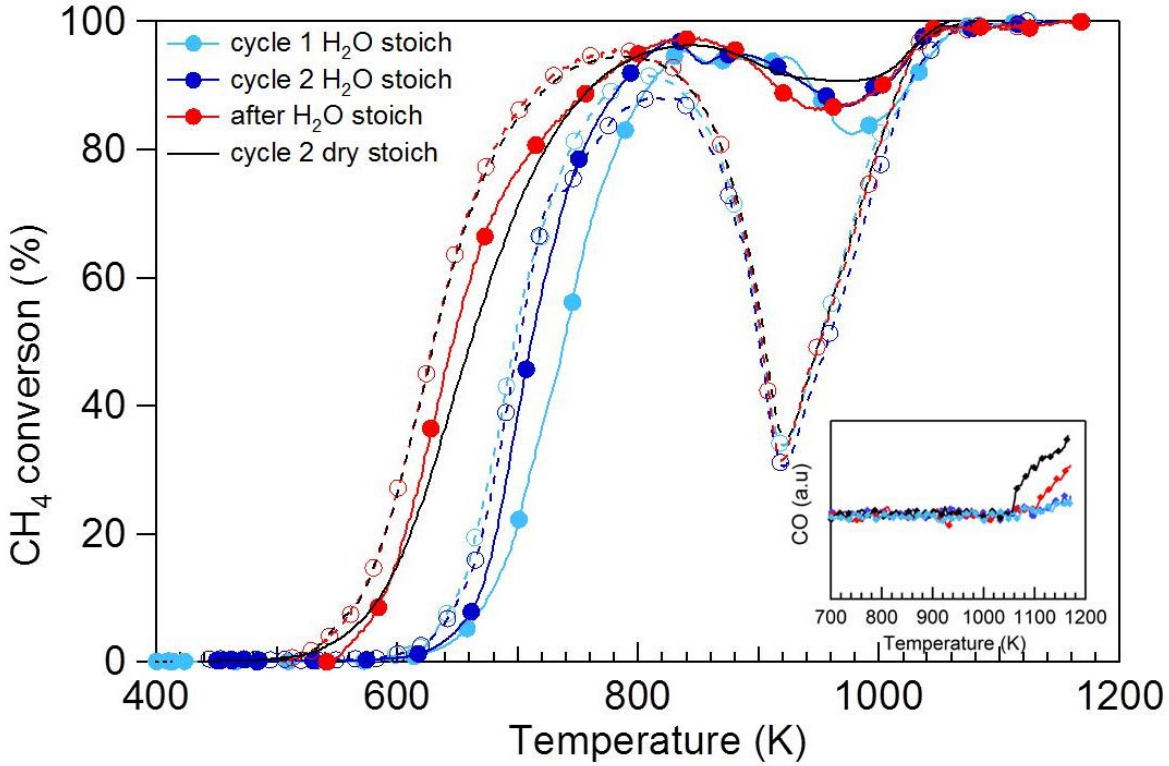

Figure 5.20: catalytic activity of 1PdCe SCS with and without water in stoichiometric conditions; closed symbols: heating; open symbols: cooling.

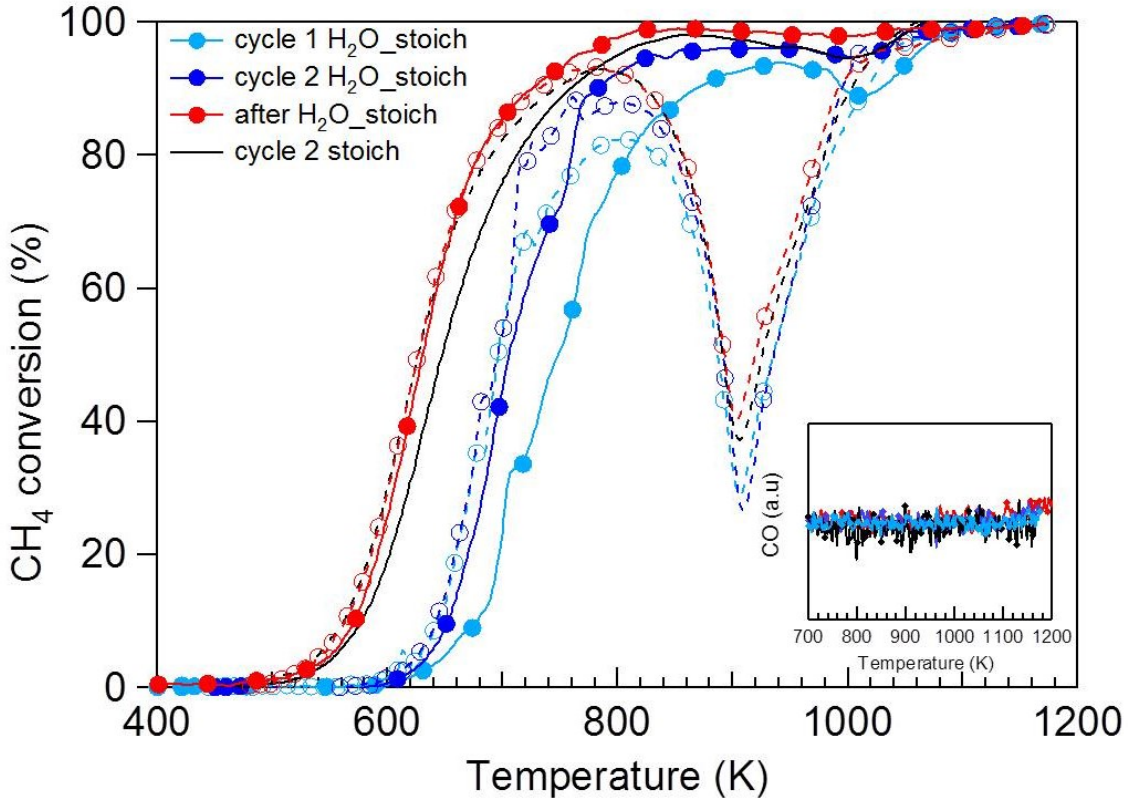

Figure 5.21: catalytic activity of 1PdCZ75 SCS with and without water in stoichiometric conditions; solid line, closed symbols: heating; dotted line, open symbols: cooling.

As observed in lean conditions, the addition of water into the reaction mixture deactivates the catalysts, increasing the temperature of the onset of methane oxidation. During the first cycle, for both samples the addition of water into the gas stream negatively affects methane oxidation with a large thermal hysteresis between heating and cooling ramp. Performing a new cycle on the used catalysts, T_{10} is delayed of approximately 80 K and T_{50} increases of only ~ 50 K with respect to dry conditions. Looking at the light-off curves of 1PdCZ75 SCS, a strong deactivation of the catalyst during the first cycle is observed. The delay becomes less pronounced during the second wet cycle where T_{10} and T_{50} increases of 78 K and 57 K compared to dry conditions; the presence of steam negatively affects Pd re-oxidation during cooling, causing a drop of CH_4 conversion to 26 %. However, for both catalysts the deactivation is completely reversible and the patterns in dry conditions are quickly recovered once water is removed from the reaction mixture, with a slight improvement of activity during the heating ramp.

In order to further examine the effect of water under different oxygen partial pressure, the temperature difference in terms of T_{10} and T_{50} recorded during the second heating ramp in dry and wet feed is illustrated in Figure 5.22.

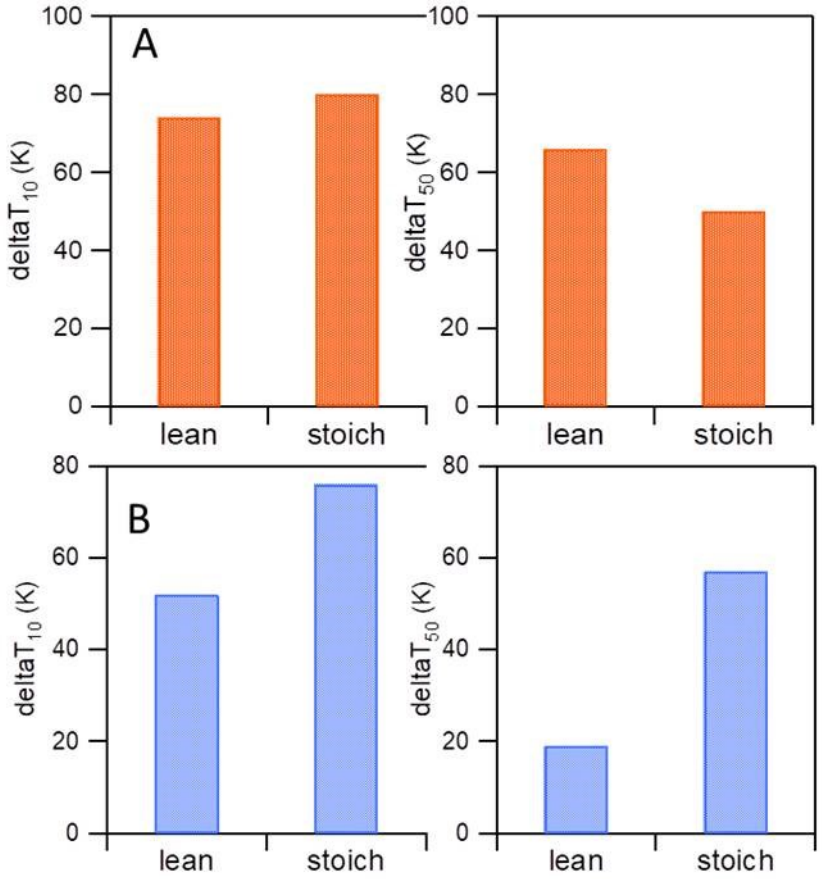

Figure 5.22: temperature difference for 10 % and 50 % methane conversion between dry and wet feed during the second heating ramp in stoichiometric and lean conditions; A) 1PdCe SCS and B) 1PdCZ75 SCS

For 1PdCe SCS, the oxygen partial pressure does not affect significantly the temperature difference between dry and wet feed at 10% and 50% of conversion, showing a similar deactivation in lean and stoichiometric oxidation. Regarding 1PdCZ75 SCS instead, the oxygen partial pressure seems to have a stronger effect: a higher deactivation degree is observed in stoichiometric conditions for both T_{10} and T_{50}.

The results seem in contrast with those obtained by Mihai *et al.* who observed a more marked deactivation using high oxygen concentration. This discrepancy can be related to the different experimental conditions used to evaluate the catalytic activity (catalyst: Pd/Al_2O_3, 5% H_2O with reducing/oxidizing steps used to pre-treat catalyst before activity test) [32].

Looking at the inset of Figure 5.20, it is possible to observe the formation of small traces of carbon monoxide during cycle 1 and 2 H_2O beyond 1000 K but in lower amount compared to that measured in dry conditions (i.e cycle 2 dry and after H_2O). This is in line with the results obtained by Mihai *et al.* who measured a higher amount of CO produced in dry conditions than in the presence of water [32]. When oxygen becomes the limiting reactant, water present in the gas stream might participate during methane oxidation through steam reforming or water gas shift reaction [32]. Again, for CZ-supported catalyst the formation of CO is not detected. However, these results need further investigation to assess the occurrence of additional reactions when methane oxidation is carried out in wet and oxygen-deficient conditions.

Conclusions

The effect of water poisoning on the series of $Pd/Ce_xZr_{1-x}O_2$ catalysts was evaluated both in transient and steady-state conditions. The results can be summarized in the following points:

- the presence of water in the reaction mixture inhibits the oxidation of methane, causing an increase of the light-off temperature. The deactivation becomes less severe when Ce-Zr is used as a support; in particular for 1PdCZ75 SCS, T_{10} and T_{50} increase of only 52 K and 19 K, respectively, against 60-70 K measured for other samples.
- Water has some effect also on PdO-Pd-PdO phase transformation but only when the reaction takes place. However for 1PdCe SCS and 1PdCZ75 SCS samples, the initial activity is completely restored upon water removal, while for their corresponding IW counterparts water poisoning is not completely reversible over the entire cycle.
- During time-on-stream tests, the presence of water accelerates the deactivation of the catalysts, especially in the case of impregnated samples. When zirconium oxide is used as a carrier, the catalysts exhibit a high resistance to hydrothermal aging, maintaining a high conversion level throughout the test.

- The difference between SCS and IW samples becomes even more clear during the activity recovery experiments. The cyclic wet/dry treatment does not suppress the activity of SCS samples: they are able to restore quickly the conversion recorded in dry conditions after being subjected to wet atmosphere. On the contrary, for IW catalysts the activity remains lower than that observed without water, confirming the results obtained during temperature programmed experiments.
- FTIR analysis on the aged catalysts evidences the presence of linearly and bridging CO coordinated to metallic Pd sites; in particular, on IW catalysts CO occupies mainly bridging sites. TEM characterization of CZ75-based catalysts confirms the results of FTIR analysis: after aging treatment, Pd particles size increases much more on the sample prepared by impregnation method, suggesting that the deactivation during cyclic wet/dry aging can be attributed to the sintering of noble metal particles. The strong Pd/ceria interaction obtained with SCS procedure might suppress the sintering of Pd species, thus accounting for the very good dispersion maintained by 1PdCZ75 SCS after the aging cycles as confirmed by FTIR (prevalence of linear bonded CO) and TEM.

Therefore, we can conclude that solution combustion synthesized catalysts demonstrate to have a superior activity under different reaction conditions (dry and wet) with an improved resistance to hydrothermal ageing compared to their IW counterparts. When ceria is present in the support, the intimate Pd-ceria contact, the presence of various PdO species (as inferred from TPO and TPR patterns (Chapter 3, Figure 3.11 and Figure 3.13)) and stable, smaller Pd particles (as inferred from FTIR and TEM analysis), can be considered the main responsible of their higher tolerance to water poisoning. In particular the use of supports with high oxygen mobility like ceria-zirconia mixed oxide reveals to be an interesting approach to minimize the effect of water deactivation. However, we obtained interesting results also in the case of 1PdZr SCS, which shows a good resistance to cyclic wet/dry treatment with a complete recovery of its initial conversion level and a good stability with time-on-stream. As for other solution combustion synthesized catalysts, different PdO species have been identified by TPO and TPR experiments (Chapter 3, Figure 3.11 and Figure 3.13), but they might not explain entirely the behavior observed. Noble metal-zirconia interaction can effectively reduce the deactivation induced by aging [33]. Moreover, the structural difference of zirconia support (more tetragonal in the case of 1PdZr SCS) could play a role in the degree of deactivation and improve somehow the resistance to hydrothermal aging as suggested by some authors [34].

Regarding the experiments in oxygen-deficient conditions, the presence of water continues to affect negatively the catalytic performance with a shift of light-off temperatures towards higher

values. When Pd is supported on pure ceria, the change in gas composition does not significantly modify the degree of deactivation. Contrarily, for 1PdCZ75 SCS the deactivation under stoichiometric conditions appears to be more severe, but the activity is complete reversible upon water removal, as observed during lean oxidation. Furthermore, side reactions like steam reforming, partial oxidation or water-gas shift can occur depending on the temperature and catalysts composition.

References

[1] R. Gholami, M. Alyani and K. J. Smith, *Catalysts,* vol. 5, pp. 561-594, 2015.

[2] P. Hurtado, S. Ordonez, H. Sastre and F. V. Diez, *Applied Catalysis B: Environmental,* vol. 47, p. 85–93, 2004.

[3] P. Hurtado, S. Ordonez, H. Sastre and F. V. Diez, *Applied Catalysis B: Environmental,* vol. 51, p. 229–238, 2004.

[4] R. Kikuchi, S. Maeda, K. Sasaki, S. Wennerstrom and K. Eguchi, *Applied Catalysis A: General,* vol. 232, p. 23–28, 2002.

[5] M. Monai, T. Montini, C. Chen, E. Fonda, R. Gorte and P. Fornasiero, *ChemCatChem 2014,* vol. 6, p. 1–10 , 2014.

[6] J. Park, J. Ahn, H. Sim, G. Seo, H. Han and C. Shin, *Catalysis Communications,* vol. 56, pp. 157-163, 2014.

[7] A. Setiawan, J. Friggieri, E. Kennedy, B. Dlugogorski and M. Stockenhuber, *Catal. Sci. Technol.,* vol. 4, p. 1793 –1802 , 2014.

[8] F.H. Ribeiro, M. Chow and R. Dalla Betta, *Journal of Catalysis,* vol. 146, pp. 537-544, 1994.

[9] F. Zhang, C. Hakanoglu, J. Hinojosa and J. Weaver, *Surface Science,* vol. 617, pp. 249-255, 2013.

[10] C. Cullis, T. Nevell and D. Trimm, *J. Chem. Soc., Faraday Trans. 1,* vol. 68, pp. 1406-1412, 1972.

[11] R. Burch, F. Urbano and P. Loader, *Applied Catalysis A: General,* vol. 123, pp. 173-184, 1995.

[12] W.R. Schwartz, D. Ciuparu, and L.D. Pfefferle, *J. Phys. Chem. C,*vol. 116, pp. 8587-8593, 2012.

[13] D. Ciuparu, E. Perkins and L.D. Pfefferle, *Applied Catalysis A: General,* vol. 263, pp. 145-153, 2004.

[14] C. Chen, Y. Yeh, M. Cargnello, C. Murray, P. Fornasiero and R. Gorte , *ACS Catal.,* vol. 4, p. 3902–3909, 2014.

[15] K. Nomura, K. Noro, Y. Nakamura, H. Yoshida, A. Satsuma and T. Hattori, *Catalysis Letters,* vol. 58, p. 127–130, 1999.

[16] Y. Madier, C. Descorme , A. Le Govic and D. Duprez, *J. Phys. Chem. B,* vol. 103, pp. 10999-11006, 1999.

[17] B. Stasinska, A. Machocki, K. Antoniak, M. Rotko, J. Figueiredo and F. Goncalves, *Catalysis Today,* vol. 137, pp. 329-334, 2008.

[18] M. Richard, D. Duprez, N. Bion and F. Can, *ChemSusChem,* vol. 10, p. 210–219, 2017.

[19] S. Specchia, E. Finocchio , G. Busca, P. Palmisano and V. Specchia , *Journal of Catalysis,* vol. 263, pp. 134-145, 2009.

[20] S. Specchia, C. Galletti and V. Specchia, *Studies in Surface Science and Catalysis,* vol. 175, pp. 59-67, 2010.

[21] O. Demoulin, M. Navez and P. Ruiz, *Applied Catlysis A: General,* vol. 295, pp. 59-70, 2005.

[22] L. Zenboury, B. Azambre and J. Weber, *Catalysis Today,* vol. 137, pp. 167-173, 2008.

[23] P. Jodlowski, R. Jedrzejczyk, D. Chlebda, M. Gierada and J. Lojewska, *Journal of Catalysis ,* vol. 350, pp. 1-12, 2017.

[24] M. Lin, J. Wan, S. Liu, R. Ran e D. Weng, *Catalysis Today,* vol. 242, pp. 322-328, 2015.

[25] M. Palard, J. Balencie, A. Maguer and J.-F. Hochepied, *Materials Chemistry and Physics,* vol. 120, pp. 79-88, 2010.

[26] S. Khan, M. Faisal, M. Rahman and A. Jamal, *Science of the Total Environment,* vol. 409, pp. 2987-2992, 2011.

[27] H. Altass and A. E. R. S. Khder, *Journal of Molecular Catalysis A: Chemical,* vol. 411, pp. 138-145, 2016.

[28] M. Yang, M. Shen, J. Wang, J. Wen, M. Zhao, J. Wang and W. Wang, *J. Phys. Chem. C ,* vol. 113, pp. 12778-12789, 2009.

[29] X. Chen, Y. Cheng, C. Yup Seo, J. W. Schwank and R. W. McCabe, *Applied Catalysis B: Environmental,* vol. 163, pp. 499-509, 2015.

[30] Y. Cao, R. Ran, X. Wu, B. Zjao, J. Wan and D. Weng, *Applied Catalysis A: General,* vol. 457, pp. 52-61, 2013.

[31] B. Zhang, X. Wang, O. M'Ramadj, D. Li, H. Zhang and G. Lu, *Journal of Natural Gas Chemistry,* vol. 17, p. 87–92, 2008.

[32] O. Mihai, G. Smedler, U. Nylen, M. Olofsson and L. Olsson, *Catalysis Science & Technology,* pp. 1-34, 2017.

[33] Y. Cao, R. Ran, X. Wu, J. Wan and D. Weng, *Catalysis Today,* vol. 281, pp. 490-499, 2017.

[34] I. Heo, D.Y. Yoon, B. K. Cho , I.-S. Nam, J. W. Choung and S. Yoo, *Applied Catalysis B: Environmental,* Vols. 121-122, pp. 75-87, 2012.

Chapter 6

Effect of SiO_2 and Al_2O_3 addition on the structural and redox behavior of Pd/CeO_2 catalysts

This chapter addresses the discussion of the structural and morphological characterization of Pd-ceria catalysts doped with different amount of silica and alumina prepared by solution combustion synthesis. BET surface area measurements and XRD analysis have been employed to characterize the catalysts by a morphological point of view. The second part of the chapter is focused on the investigation of PdO thermal stability in 2% O_2/N_2 mixture with the aim to study the influence of the introduction of SiO_2 and Al_2O_3 on the dynamics of PdO-Pd-PdO phase transformation. To gain further insights into the redox properties of these samples the results of H_2-TPR characterization are also presented.

6.1. Surface area and X-ray diffraction analysis

Catalysts compositions, BET surface area and mean particle size of the catalysts (D), calculated by Scherrer's equation from the line broadening of the most intense diffraction peak (2θ = 28.2°), are summarized in Table 6.1.

Table 6.1: characteristics of Ce-Si and Ce-Al supported catalysts

		SiO_2/Al_2O_3 content (nominal)		BET surface area (m^2/g)	D (nm)
Catalyst	**Sample name**	**wt.%**	**mol. %**		
1%Pd/CeO_2	1PdCe SCS	-	-	6.6	46
1%Pd/CeO_2-2% SiO_2	1PdCeSi2 SCS	2	5.5	14.4	34
1%Pd/CeO_2-5% SiO_2	1PdCeSi5 SCS	5	13	12.7	40
1%Pd/CeO_2-13% SiO_2	1PdCeSi13 SCS	13	29	11.4	30
1%Pd/CeO_2-20% SiO_2	1PdCeSi20 SCS	20	41	7.8	42
1%Pd/CeO_2-13% Al_2O_3	1PdCeAl13 SCS	13	20	7.4	31

The surface area of all samples is quite low, due to the high temperature reached during combustion synthesis, but the addition of SiO_2 increases the surface area of 1PdCe SCS (6.6 m^2/g). Silica, in fact, acts a surface area-stabilizer for ceria support [1]. The improvement, however, decreases with increasing amount of silica, and this can be due to the segregation of some silicon oxide at higher SiO_2 loadings (see the XRD patterns). Also for the Al-doped sample the surface area is slightly higher than that measured for 1PdCe SCS, due to the stabilization effect of Al_2O_3 on CeO_2 support upon severe treatment during the synthesis [2].
XRD characterization (Figure 6.1) of Si-containing catalysts shows sharp diffraction peaks relative to cubic ceria, suggesting the sintering of CeO_2 as a result of the severe conditions reached during combustion synthesis [3].

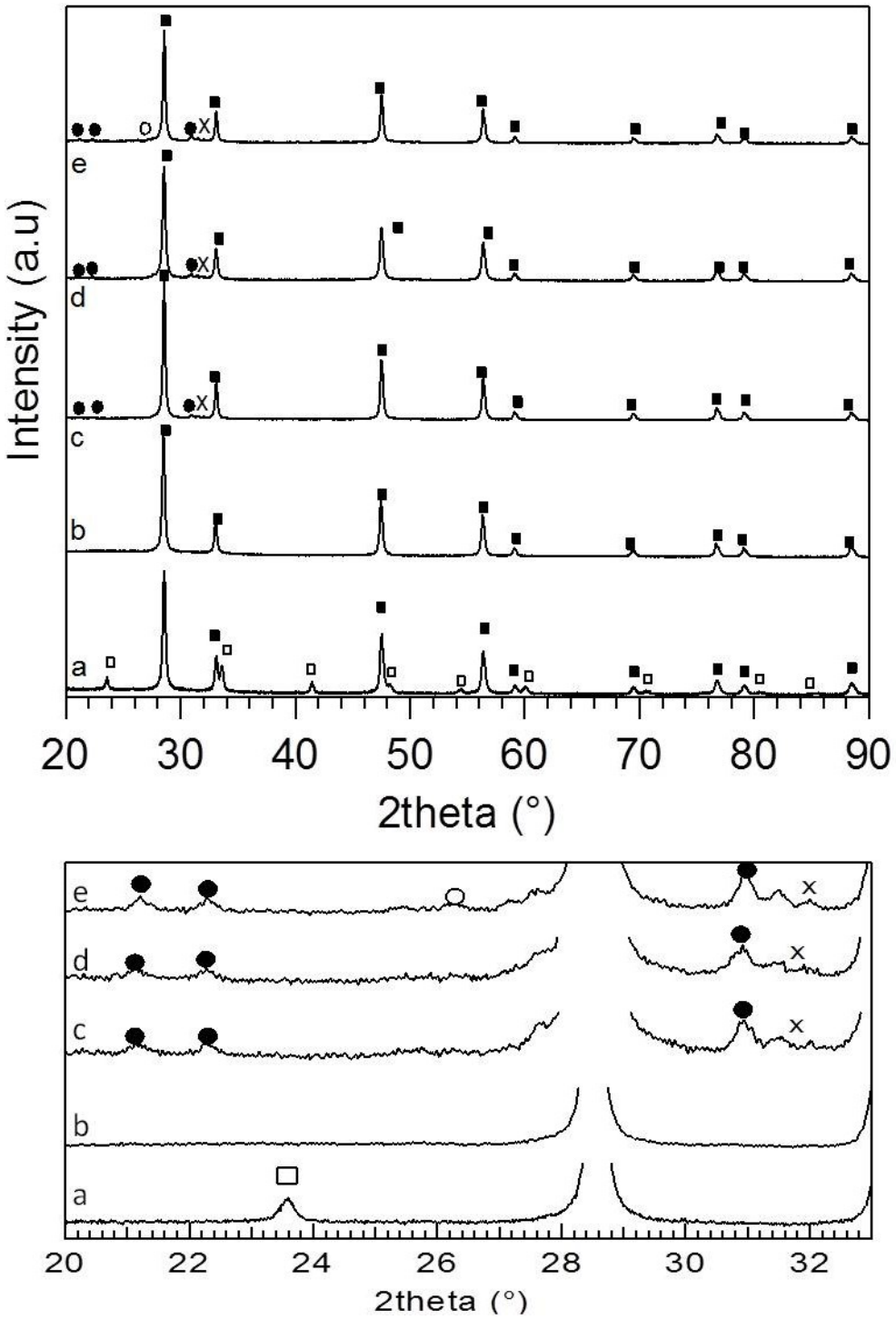

Figure 6.1: XRD patterns of all catalysts: (a) 1PdCeAl13 SCS, (b) 1PdCeSi2 SCS, (c) 1PdCeSi5 SCS, (d) 1PdCeSi13 SCS (e) 1PdCeSi20 SCS; ■ CeO_2, ●$Ce_{4.94}Si_3O_{13}$, □ $CeAlO_3$; x SiO_2 tetragonal; ○ SiO_2 hexagonal (top); XRD spectra in the range of 20°< 2θ < 35° (bottom)

On the samples with SiO_2 loading higher than 2 wt.%, weak peaks are detected at 21.2°, 22.4° and 30.9° belonging to a hexagonal cerium silicate phase (possibly $Ce_{4.94}Si_3O_{13}$), more visible in Figure 6.1 (bottom). No indication of the presence of ceria-silica alloy is observed on 1PdCeSi2 SCS likely due the low SiO_2 loading and/or to the high dispersion of this phase (see TPO profile for more details). At 31.4° ceria-silica support shows the typical diffraction bands of

tetragonal SiO_2; for 1PdCeSi20 SCS an additional peak at 26.5° is observable corresponding to hexagonal SiO_2. When ceria is doped with alumina, the oxide carrier shows the characteristic peaks of cubic ceria and small peaks relative to the formation crystalline $CeAlO_3$ in tetragonal structure. No obvious diffraction peak belonging to Pd or PdO phase is observable from XRD profile due to the high dispersion and/or to the low loading of the active phase.

The presence of $CeAlO_3$ and cerium silicate has been already observed in previous works from ours and other groups. Trovarelli and co-workers, through morphological investigation by HRTEM and XRD analysis on CeO_2/SiO_2 oxides, found the formation of $Ce_{9.33}(SiO_4)_6O_2$ phase upon reduction treatment and reported its progressive decomposition in oxidizing atmosphere at T > 873 K [4]. In some previous works, our group investigated a series of CeO_2/Al_2O_3 mixed oxides. After treatment in reductive atmosphere, it was observed the formation of ceria-alumina binary oxide, i.e $CeAlO_3$ phase, attributed to a strong ceria-alumina interaction [2]. Similar observations have been reported by Damyanova *et al.:* these authors suggested the occurrence of a strong ceria-alumina interaction in reducing atmosphere above 800 K. Ce-Al interaction leads to the formation of $CeAlO_3$ mixed oxide due to a facile diffusion of Al^{3+} ions into CeO_{2-x} lattice [5]. Also Liotta *et al*. found the presence of $CeAlO_3$ phase: after treatment in reducing conditions, they detected the evidence of crystalline $CeAlO_3$ on noble metal-free CeZrAl washcoat [6], promoted by the reaction of Ce^{3+} with alumina.

In our case, solution combustion synthesis involves a redox reaction between salts precursors and organic fuel and very high temperatures (> 1273 K) can be easily reached in the furnace [3, 7, 8]. Therefore, it is reasonable to attribute the origin of these Ce-based compounds to a strong Ce-Si and Ce-Al interaction promoted by redox conditions achieved during the synthesis. The presence of $CeAlO_3$ and cerium silicate ($Ce_{4.94}Si_3O_{13}$) indicates that ceria is stabilized in 3+ form [2, 4 ,6].

6.2 Redox behavior in oxidizing and reducing atmosphere

6.2.1 TPO experiments

The stability of palladium oxide has been evaluated through TPO experiments in 2 vol.% O_2/N_2 mixture. For each sample three decomposition/re-oxidation cycles have been performed up to 1273 K, monitoring continuously the oxygen concentration at increasing/decreasing temperature. The main goal is to study the influence of silica/alumina doping on the dynamics of PdO-Pd-PdO phase transformation. The qualitative oxygen uptake/release profile during the three TPO cycles of 1PdCeSi13 SCS is reported in Figure 6.2, as an example for silica-doped catalysts.

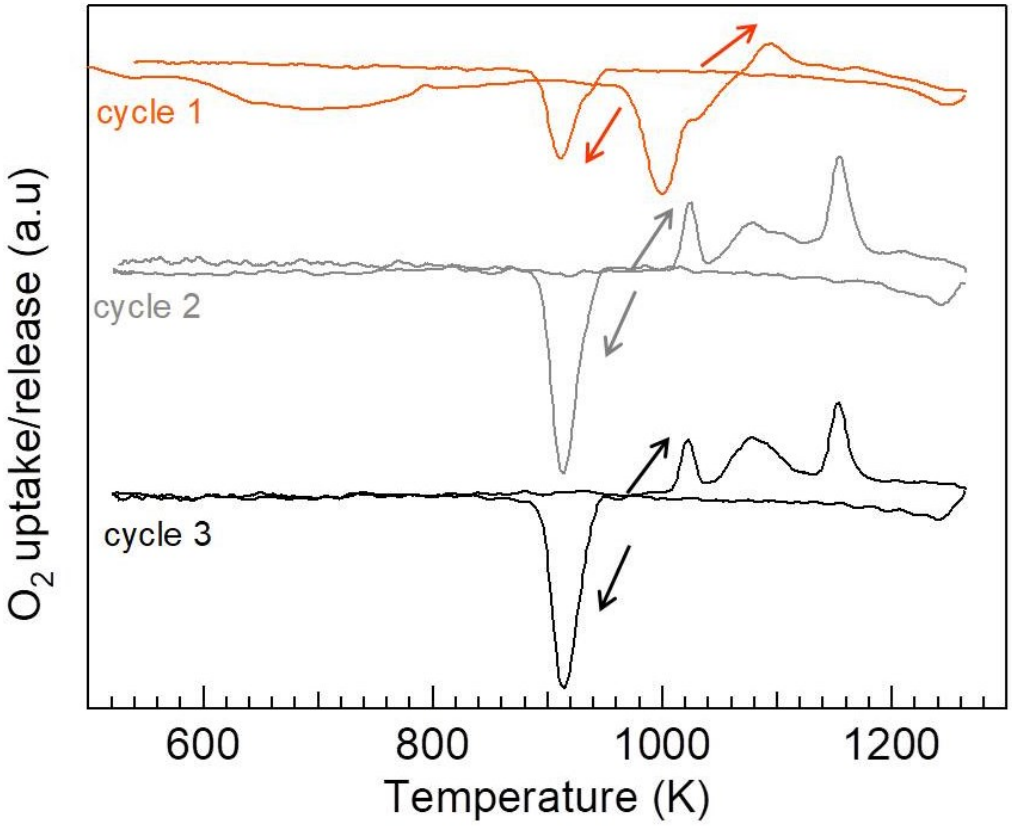

Figure 6.2: O_2 uptake/release during the three TPO cycles for 1PdCeSi13 SCS in 2 vol.% O_2/N_2

Focusing on the heating part of cycle 1, a broad negative peak in the range of 600-800 K is observable likely due to the oxidation of metal Pd particles, not visible by XRD analysis due to their high dispersion or small size. At further increasing temperature, in the range 960 K-1050 K, a sharp oxygen uptake is present and a small one appears above 1050 K, which corresponds to PdO decomposition. In the cooling part of TPO cycle a single oxygen uptake with a minimum at 911 K appears whose threshold does not change in the following cycles. The qualitative oxygen profile recorded during the heating part of the 2^{nd} and 3^{rd} cycle is completely different from the first one since PdO-Pd transformation takes place in three well defined steps with the maximum at 1021 K, 1078 K and 1153 K, respectively.

Figure 6.4 illustrates the comparison of the oxygen uptake/release profile during the first TPO cycle of all Si-containing samples.

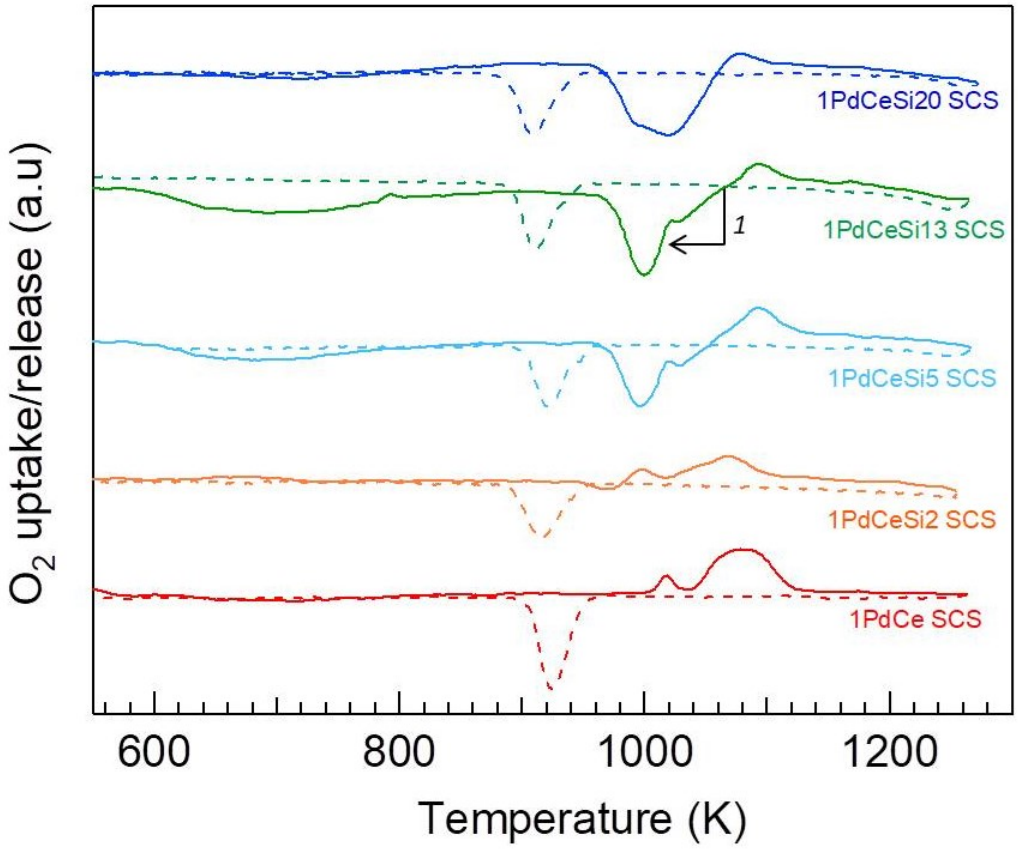

Figure 6.3: comparison of the 1st TPO cycle of all Si-doped catalysts in 2 vol.% O_2/N_2; heating: solid line, cooling: dotted line

The shape of PdO decomposition is strongly modified upon SiO_2 addition: only the dynamics of PdO-Pd transition of 1PdCeSi2 SCS appears similar to 1PdCe SCS with two oxygen release peaks centred at 1006 K and 1076 K with an additional weak oxygen uptake between 960 K and 987 K. At increasing SiO_2 amount, two main features deserve to be highlighted: *i)* the negative peak before PdO decomposition becomes larger at increasing SiO_2 content and *ii)* the oxygen release step, associated to the decomposition of PdO to Pd, becomes less defined due to the overlapping with the oxygen uptake peak. Looking at the cooling branch, the onset of Pd re-oxidation (~ 950 K) does not change significantly.

Trying to assess the nature of the oxygen uptake peak between 947-1053 K, the heating ramp was stopped at 1053 K (first TPO cycle stopped@1053 (*point 1)* in Figure 6.3) and the sample was cooled down in pure nitrogen to be collected for XRD and HRTEM analysis. The results of XRD analysis of 1PdCeSi13 SCS are reported as an example in Figure 6.4.

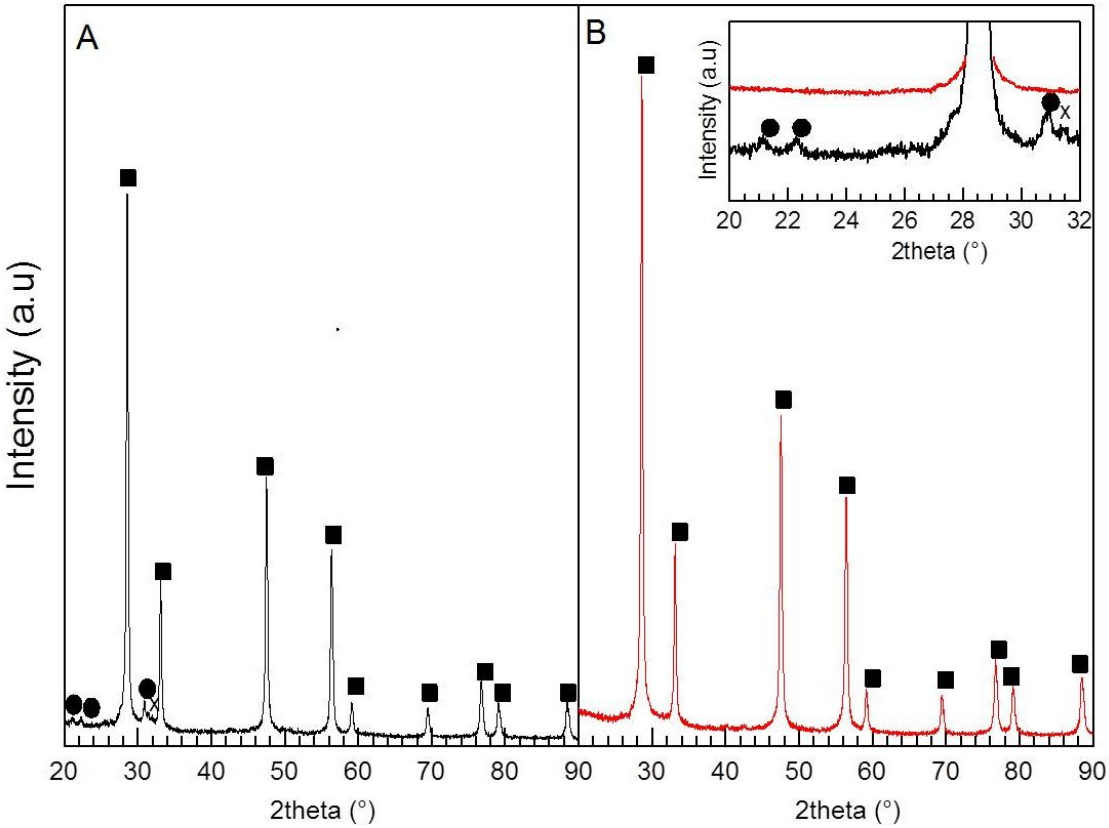

Figure 6.4: XRD patterns of (A) fresh and (B) after first TPO cycle stopped@1053.

On the sample collected after TPO stopped@1053 (pattern B), the diffraction peaks belonging to the cerium silicate phase and tetragonal SiO_2 disappear, as inferred by the magnification showed in the inset of Figure 6.4, with the increase of the intensity of the peak relative to cubic ceria.

These results seem to be in agreement with the ones obtained by Rocchini *et al.* Upon reduction of CeO_2-13 wt.% SiO_2 oxide, they detected the formation of $Ce_{9.33}(SiO_4)_6O_2$ phase, that decomposed into CeO_2 and amorphous SiO_2 after oxidation at T > 873 K. This conclusion has been suggested by the progressive increase of the intensity of X-ray diffraction peaks of cubic ceria and the disappearance of the characteristic bands of cerium-silicate [9]. Therefore, the oxygen uptake in the range of 947-1053 K can be assigned to the decomposition of cerium-silicate compound into ceria and silica.

The results of HRTEM characterization, that confirm this observation, are shown in Figure 6.5.

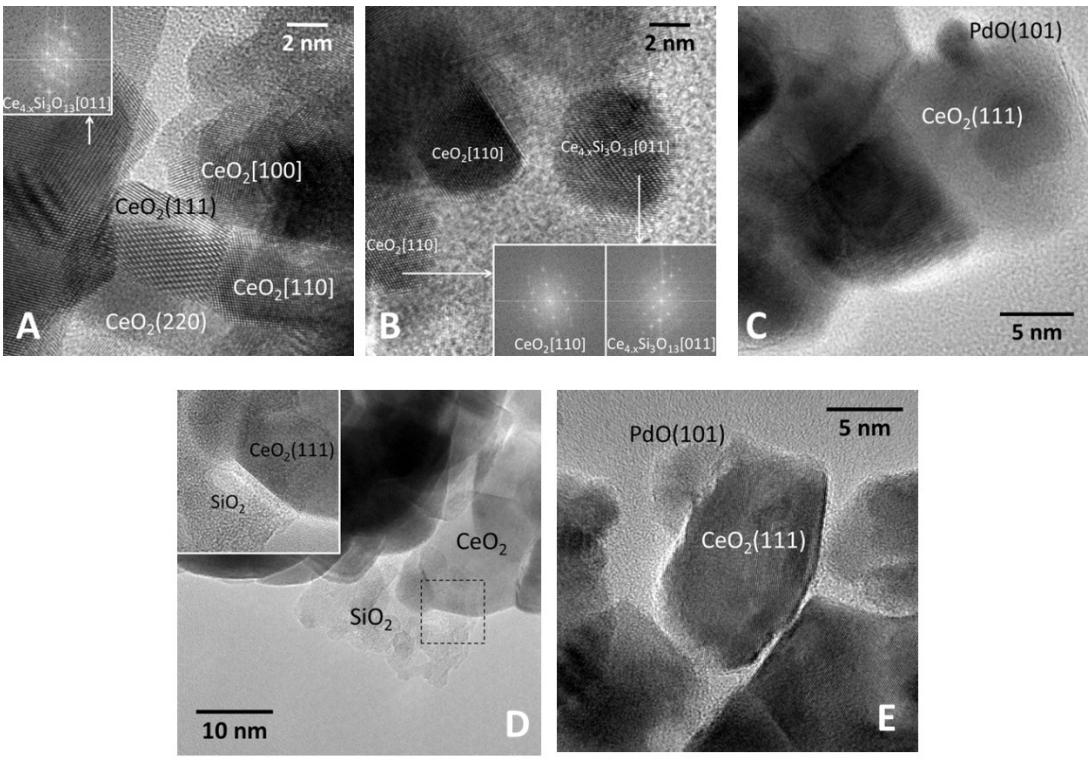

Figure 6.5: HRTEM images of (A,B,C) fresh 1PdCeSi13 SCS and (D,E) after first TPO stopped@1153

All particles are highly crystalline. A careful analysis of the lattice fringes reveals the presence of ceria crystallites in a large extent, whereas much less abundant crystallites of cerium silicate are observed (Figures 6.5 (A) and Figures 6.5 (B)). In Figure 6.5 (B), the particle labeled $Ce_{4-x}Si_3O_{13}$ is oriented along the [011] crystallographic direction as deduced from the Fourier Transform (FT) image. It is not possible to distinguish between different cerium silicates, such as $Ce_{4.94}Si_3O_{13}$ or $Ce_{4.67}Si_3O_{13}$, indicated by Rocchini *et al.* [4]. Concerning palladium, it occurs mostly as PdO as individual nanoparticles of about 2-5 nm in size (Figure 6.5 (C)).

The most important effect of oxidation up to 1053 K during the first TPO cycle (Figure 6.5 (D) and (E)) is the disappearance of the cerium silicate phase, which is transformed into ceria and silica. In Figure 6.5 (D), only ceria crystallites are visible along with amorphous patches of silica, as indicated in the figure. The inset shows an enlargement of the area enclosed in the black rectangle. The (111) lattice fringes of ceria at 3.12 Å are clearly seen in contact with amorphous silica (with lower electron contrast). Figure 6.5 (E), shows the occurrence of a PdO nanoparticle, showing the (101) crystallographic planes at 2.65 Å, in contact with a ceria crystallite ((111) planes at 3.12 Å).

The results of HRTEM characterization confirm the ones obtained from XRD analysis, and thus the oxygen uptake observed during the first TPO cycle can be unequivocally assigned to the decomposition of cerium-silicate phase into ceria and amorphous silica, in agreement with the results reported in the literature by Rocchini and co-workers [4].

The thermal stability of palladium oxide over 1PdCeAl13 SCS has been investigated with the same experimental procedure performing three reduction/oxidation cycles and the results are reported in Figure 6.6.

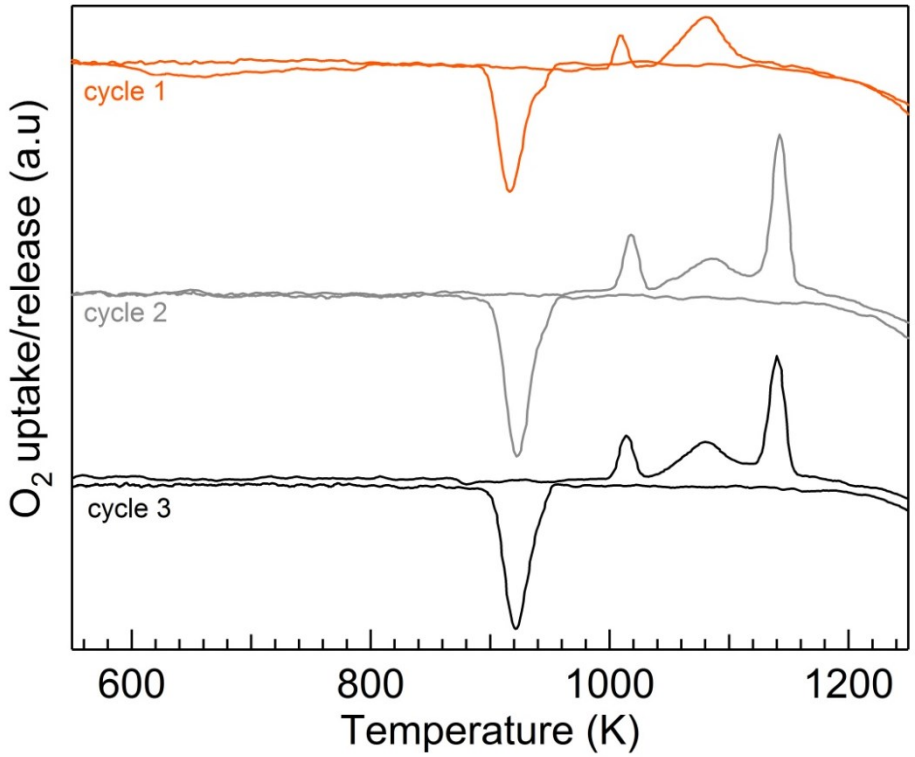

Figure 6.6: O_2 uptake/release during the three TPO cycles for 1PdCeAl13 SCS in 2 vol.% O_2/N_2

During the first TPO run, two separate oxygen release steps can be identified: the first one at lower temperature (1013 K) and a second one at high temperature (1085 K). During the following cycles three steps relative to PdO decomposition can be clearly distinguished: a first O_2 release occurs with maximum at 1018 K, whose area increases from cycle 1 to cycle 3, a second release peak at 1085 K and a last one at higher temperature (1145 K) with a sharp release peak, whose intensity slightly decreases from cycle 2 to cycle 3. During the cooling branch, PdO re-formation occurs in a single step at about 924 K, not showing significant modification during the entire TPO measurements.

Since from the second TPO cycle onward no further modifications are detected in the qualitative oxygen/release profile, the comparison of redox behavior is made on the basis of the 3rd cycle; the corresponding results for 1PdCe SCS are added as reference in Figure 6.7.

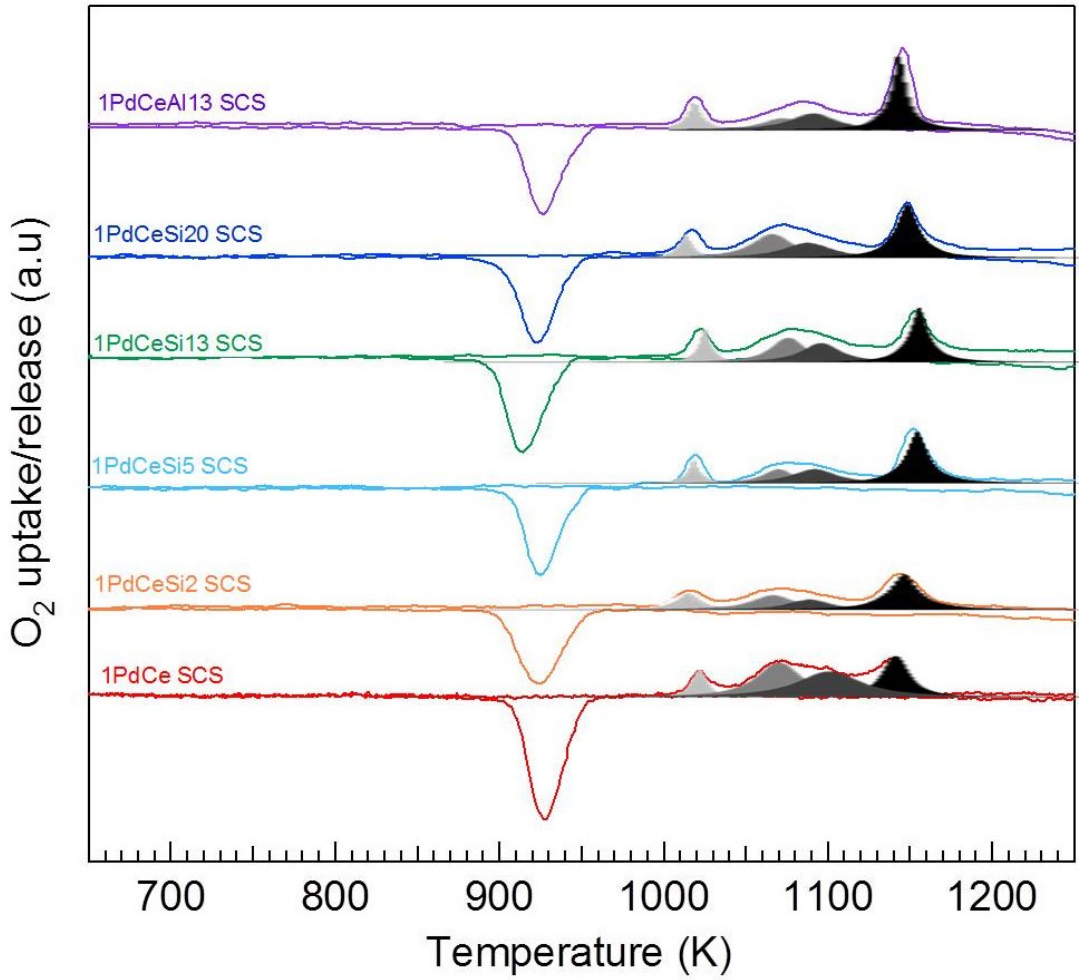

Figure 6.7: comparison of the 3rd TPO cycle on Si- and Al-doped catalysts in 2 vol.% O_2/N_2

Table 6.2: quantitative analysis of the 3rd TPO cycle (2% O_2/N_2) for Si- and Al-doped catalysts

Sample	T_{max} of first oxygen release peak (K)	T_{max} of re-oxidation peak (K)	µmol $O_2/g_{Pd}\times10^{-3}$ release	µmol $O_2/g_{Pd}\times10^{-3}$ uptake	% PdO red.[a]	%PdO ox. [a]
1PdCeSi2 SCS	1013	926	3.59	2.92	70	62
1PdCeSi5 SCS	1020	926	3.53	3.27	75	70
1PdCeSi13 SCS	1021	917	3.47	3.50	73	67
1PdCeSi20 SCS	1019	924	3.82	3.60	81	77
1PdCeAl13 SCS	1018	924	3.78	3.07	81	65

[a] PdO red: amount of PdO reduced during heating; PdO ox.: amount of Pd re-oxidized during cooling

By looking at the heating part of the third TPO cycle, all catalysts show a similar dynamic behavior during PdO-Pd transformation. The first positive peak, typical of solution combustion synthesized catalysts, is located at about 1020 K, as inferred in Table 6.2, and likely corresponds to the oxygen release from the smaller PdO particles. The second large oxygen release peak reaches a maximum at ~ 1070 K and contains the contribution of bulk PdO or larger PdO clusters [10]. The peak at high temperature can be attributed to the stabilization of

palladium oxide operated by ceria [10, 11] or to the core of bigger PdO particles as suggested by Chen *et al.* [12]. The doping of Pd/ceria with silica or alumina does not influence the decomposition threshold, confirming that PdO-Pd transformation is a process ruled by the thermodynamics of PdO/O_2 system [10], but it has an effect on the amount of PdO decomposed in each step, as clearly observed by the fitting of TPO patterns shown in Figure 6.6. When silica or alumina are present on the support, the contribution of the last peak represents about 35-45 % of the entire PdO against 24% on 1PdCe SCS. This suggests an improvement of PdO stability upon SiO_2 and Al_2O_3 introduction.

In the cooling part of the cycle PdO re-generation starts at ~ 950 K and is completed at ~ 900 K, occurring with a single oxygen uptake peak. The position of the minimum is set almost at the same temperature ($T_{ox} \cong 925$ K) and similar to that observed on 1PdCe SCS; only for the sample with 13 wt.% of SiO_2, Pd-PdO transition is slightly delayed, showing a larger hysteresis with respect to the decomposition process. The re-oxidation of Pd to PdO has been determined to be a kinetic-ruled process where diffusion kinetics of oxygen [10], OSC of the support and particle size play a key role in the threshold and the extent of Pd-PdO transformation [13].

6.2.2 H_2-TPR

H_2-TPR experiments have been performed to investigate the redox properties of the catalysts and to gain further insights on the metal-support interaction. The reducibility of Pd-based catalysts has been evaluated in 4.5% H_2/N_2 reaction mixture, monitoring the hydrogen uptake/release at increasing temperature. In Figure 6.8 the profile of H_2 uptake/release is plotted against temperature, and the corresponding reduction profile of 1PdCe SCS is reported as reference. Table 6.4 reports the quantitative analysis of hydrogen consumed and the degree of reduction of ceria calculated after subtracting the contribution of H_2 due to PdO reduction.

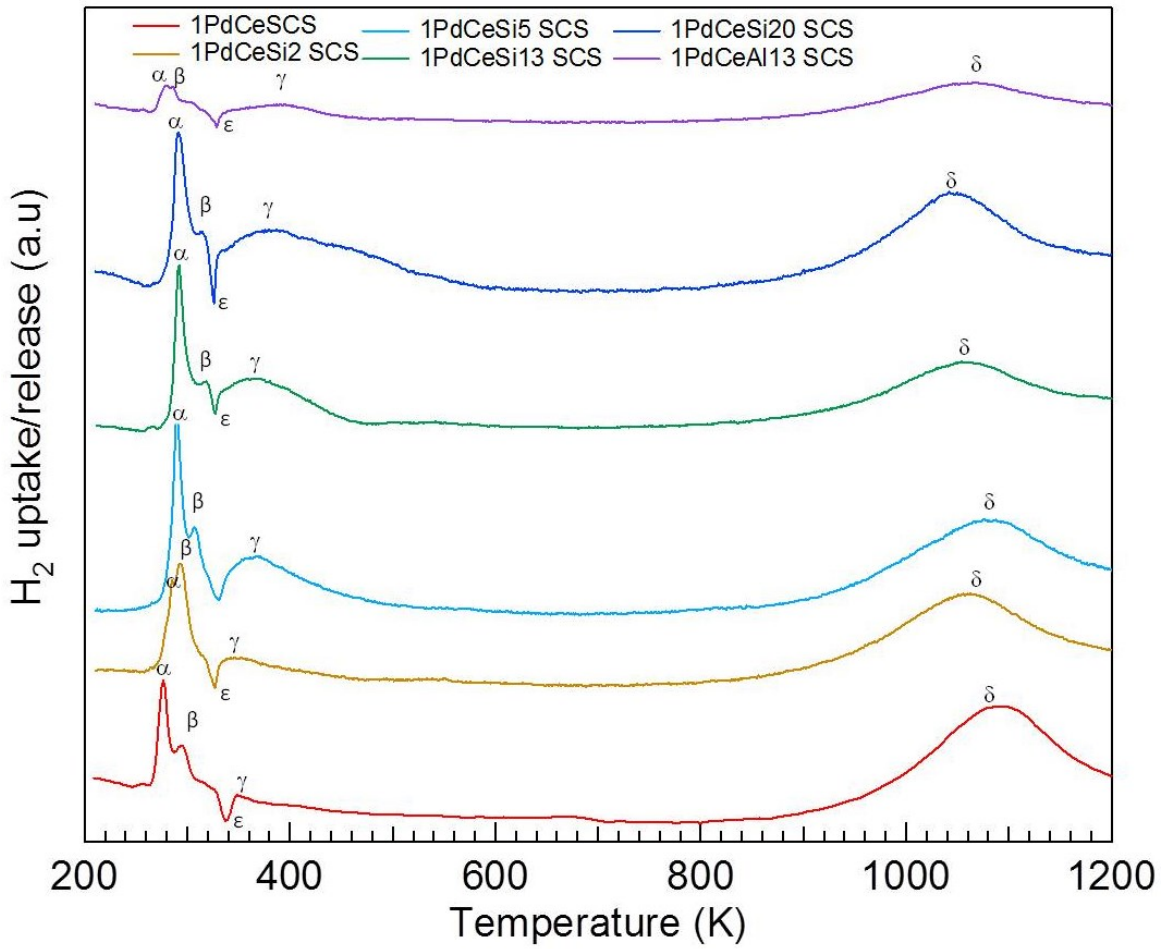

Figure 6.8: H_2-TPR profiles of all Si- and Al-doped catalysts

Table 6.3: quantitative analysis for TPR experiments

Sample	**μmolH_2/g_{cat} up to 723 K**	**x in CeO_{2-x} up to 723 K[a]**
1PdCe SCS	111	0.004
1PdCeSi2 SCS	194	0.017
1PdCeSi5 SCS	363	0.055
1PdCeSi13 SCS	492	0.080
1PdCeSi20 SCS	392	0.065
1PdCeAl13 SCS	144	0.011

[a] calculated as $CeO_2 + xH_2 \rightarrow CeO_{2-x} + xH_2O$ up to 723 K

All catalysts, irrespective of the composition, exhibits four hydrogen consumption peaks (peak α, β, γ and δ) and one hydrogen release peak (peak ε). The large hydrogen consumption peak near room temperature (260-320 K) is attributed to the reduction of PdO to metallic Pd and to the simultaneous reduction of part of the support, due to the well-known spillover phenomenon [14, 15, 16]. The peak is splitted into two features (indicated as α and β) which have been attributed to different types and/or a heterogeneous particle size distribution of palladium oxide [17, 18, 19, 20, 21] The peak located at ~ 280K (peak α) likely contains the

contribution of small PdO particles or particles finely dispersed on the surface of the support [17, 19]. The second one (~ 300 K) (peak β) might be assigned to the reduction of more stable or larger PdO clusters [20]. Peak γ located at around 360 K and barely present on 1PdCe SCS likely contains the contribution of PdO particles in strong interaction with the oxide carrier [17, 19]. This peak should account also for a partial reduction of surface Ce^{4+}, facilitated by the hydrogen activation promoted by noble metal and its migration to the support (spillover) [14, 15, 16]. The low-temperature peak on Al-doped sample consists of two poor-resolved peaks centred at ca. 279 K and ca. 286 K. At high temperature, a broad hydrogen consumption (peak δ) is observed in the range of 1040-1080 K and it is ascribed to the reduction of the ceria bulk [14]. The maximum of this peak is shifted to lower values with respect to 1PdCe SCS, especially for high SiO_2 loading, i.e 13 wt.% and 20 wt.%. The decomposition of β-hydride species (PdH_2), resulting from hydrogen adsorption/diffusion in the metallic Pd particles [22], occurs with a negative peak (peak ε) at around 340 K. For 1PdCeSi20 SCS, peak ε appears to be sharp if compared to other catalysts, likely indicating a partial sintering of Pd [21].

The incorporation of SiO_2 into CeO_2 support strongly modifies the reduction profile of Pd/CeO_2 catalysts, especially for dopant concentration of 5-20 wt.%. The hydrogen consumption, estimated by the integration of the peak area between 200 K and 723 K, is higher than the theoretical value (~ 87 μmol H_2/g_{cat}) implying the occurrence of surface ceria reduction, originated by the hydrogen spillover from the noble metal to the support [19, 22]; the hydrogen amount consumed within this range progressively increases with SiO_2 content. The reduction degree *(x* in Table 6.3) calculated up to 723 K is one order of magnitude higher on Si-containing samples; the highest ceria reduction degree corresponds to SiO_2 amount of 13 wt.%. Similar results have been obtained by Rocchini *et al.* who observed a marked increase of reducibility of CeO_2 doped with 13 wt. % of silica [4].

When Al_2O_3 is used as dopant, the hydrogen amount consumed up to 723 K is higher than for 1PdCe SCS, but the area of the high temperature peak (peak δ) is definitely lower than in pure Pd/CeO_2. The TPR patterns displayed by Si-modified catalysts are very similar to that observed for Pd catalysts supported on $Ce_{0.75}Zr_{0.25}O_2$ mixed oxides (Chapter 3, Figure 3.13). This suggests that the addition of SiO_2 into ceria support enhances the reducibility of CeO_2, promoting the oxygen mobility of pure ceria. This behaviour though is not a result of a perturbation of the ceria lattice as in the case of ceria-zirconia oxides but it is due to the formation of ceria-silica phase ($Ce_{9.33}(SiO_4)_6O_2$) [9]. In our case cerium silicate is present on the catalysts as-prepared and likely formed by strong ceria-silica interaction upon redox conditions and high temperatures achieved during SCS procedure [3].

Conclusions

Silica and alumina-modified catalysts were characterized by the structural point of view by means of BET surface area and X-ray Powder Diffraction analysis. The doping of Pd/ceria with SiO_2 and Al_2O_3 induces important structural modifications. XRD analysis revealed on Si-doped and Al-doped catalysts the presence of new phases, namely cerium silicate (likely $Ce_{4.94}Si_3O_{13}$) phase and $CeAlO_3$, likely generated by the strong interaction of ceria-silica and ceria-alumina which stabilize Ce in the 3+ form. The formation of these phases can be promoted by the high temperatures and redox conditions realized during combustion synthesis. The presence of cerium-silicate phase affects the TPO profile of Pd-based samples: during the first heating/cooling ramp all catalysts show an oxygen uptake in the range of 950-1050 K, which becomes larger at increasing SiO_2 amount and likely corresponds to the decomposition of $Ce_{4.94}Si_3O_{13}$ phase into ceria and silica crystallites, as inferred from XRD and HRTEM analysis.

The shape as well as the dynamics of PdO-Pd transformation showed during the third TPO cycle is typical of solution combustion synthesized catalysts where three-well defined decomposition steps can be distinguished: the occurrence of separate steps can be ascribed to various kinds of PdO species with different phase boundary or particle size. The nature of the support does not affect the onset of Pd decomposition/oxidation, but only the amount of PdO decomposed/re-oxidized in each step.

The introduction of SiO_2 increases the reducibility of bare Pd/ceria sample, as observed for Pd/ceria-zirconia. The presence of SiO_2 enhances the interaction of ceria with hydrogen, promoting the reducibility of surface ceria at lower temperature. This behavior is not the result of a structural modification of the ceria lattice, as it happens in the case of ceria-zirconia, but of the formation of cerium-silicate phase.

References

[1] L. Bonneau, T. Chopin and O. Touret.U.S Patent 529, 969, 1996.

[2] A. Piras, S. Colussi, A. Trovarelli, V. Sergo, J. Llorca, R. Psaro and L. Sordelli, *J. Phys. Chem. B,* vol. 109, pp. 11110-11118, 2005.

[3] S. Specchia, C. Galletti and V. Specchia, *Studies in Surface Science and Catalysis,* vol. 175, pp. 59-67, 2010.

[4] E. Rocchini, A. Trovarelli, J. Llorca, G. W. Graham, W. H. Weber, M. Maciejewski and A. Beiker, *Journal of Catalysis,* vol. 194, pp. 461-478, 2000.

[5] S. Damyanova, C. Perez, M. Schmal and J. Bueno, *Applied Catalysis A: General,* vol. 234, p. 271–282, 2002.

[6] L.F. Liotta, A. Longo, G. Pantaleo, G. Di Carlo, A. Martorana, S. Cimino, G. Russo and G. Deganello, *Applied Catalysis B: Environmental,* vol. 90, pp. 470-477, 2009.

[7] S.L. Gonzales-Cortes and F. E. Imbert, *Applied Catalysis A: General,* vol. 452, pp. 117-131, 2013.

[8] A. Varma, A. S. Mukasyan, A. Rogachev S. and K. V. Manukyan, *Chem. Rev.,* vol. 116, p. 14493–14586, 2016.

[9] E. Rocchini, M. Vicario, J. Llorca, C. De Leitenburg, G. Dolcetti, and A. Trovarelli, *Journal of Catalysis,* vol. 211, pp. 407-421, 2002.

[10] S. Colussi, A. Trovarelli, E. Vesselli, A. Baraldi, G. Comelli, G. Groppi and J. Llorca, *Applied Catlysis A: General,* vol. 390, pp. 1-10, 2010.

[11] S. Colussi, A. Trovarelli and J. Llorca, *Catalysis Communications,* vol. 8, pp. 1263-1266, 2007.

[12] X. Chen , J. Schwank, G. Fisher, Y. Cheng, M. Jagner and R. McCabe, *Applied Catalysis A: General,* vol. 475, pp. 420–426, 2014.

[13] Y.-H. (Cathi) Chin , M. Garcia-Dieguez and E. Iglesia, *J. Phys. Chem. C,* vol. 120, pp. 1446–1460, 2016 .

[14] A. Trovarelli, *Catalysis Reviews Science and Engineering,* vol. 38, no. 4, pp. 439 - 520, 1996.

[15] P. Fornasiero, R. Di Monte, G. Ranga Rao, J. Kaspar, S. Meriani, A. Trovarelli and M. Graziani, *Journal of Catalysis,* vol. 151, pp. 168-177, 1995.

[16] J. Cunnhingam, D. Cullinane, J. Sanz, J. Rojo, X. Soria and J. Fierro, *J. Chem. Soc. Faraday Trans.,* vol. 88, no. 21, pp. 3233-3240 , 1992.

[17] S. Lin, L. Yang, X. Yang and R. Zhou, *Applied Surface Science,* vol. 305, pp. 642-649, 2014.

[18] S. Lin, L. Yang, X. Yang and R. Zhou, *Chemical Engineering Journal,* vol. 247, pp. 42-9, 2014.

[19] Q. Wang, Z. Li, B. Zhao, G. Li and R. Zhou, *Journal of Molecular Catalysis A,* vol. 339, pp. 132-137, 2011.

[20] S. Gil, J. M. Garcia-Vargas, L. F. Liotta, G. Pantaleo, M. Ousmane, L. Retailleau and A. Giroir-Fendler, *Catalysts,* vol. 5, pp. 671-689, 2015.

[21] Y. Cao, R. Ran, X. Wu, B. Zjao, J. Wan and D. Weng, *Applied Catalysis A: General,* vol. 457, pp. 52-61, 2013.

[22] A. Baylet, P. Marecot, D. Duprez, P. Castellazzi, G. Groppi and . P. Forzatti, *Phys. Chem. Chem. Phys,* vol. 13, p. 4607–4613, 2011.

Chapter 7

Catalytic performance of Si- and Al-doped Pd/CeO_2 catalysts in methane oxidation in the absence and in the presence of water

This chapter presents the results of the catalytic performance of the series 1 wt.% Pd supported on Si- and Al-modified ceria catalysts prepared by solution combustion synthesis. The catalytic behavior of various samples was examined during cyclic temperature programmed combustion experiments up to 1173 K, both in lean and stoichiometric reaction conditions, in the absence and in the presence of water. To understand deeply the catalytic behavior in the presence of water, the results obtained from TPO experiments in wet atmosphere are illustrated and supported by HRTEM analysis.

The catalysts deactivation under long-time exposure to lean reaction mixture has been evaluated by time-on-stream experiments at 723 K for 24 hours.

7.1 Catalytic methane oxidation in the absence of water

7.1.1 Catalytic activity and stability in lean reaction conditions

In order to investigate the activity for methane oxidation, two heating/cooling ramps up to 1173 K were performed for each sample. Figure 7.1 presents the methane conversion profiles obtained during two heating/cooling cycles for various samples.

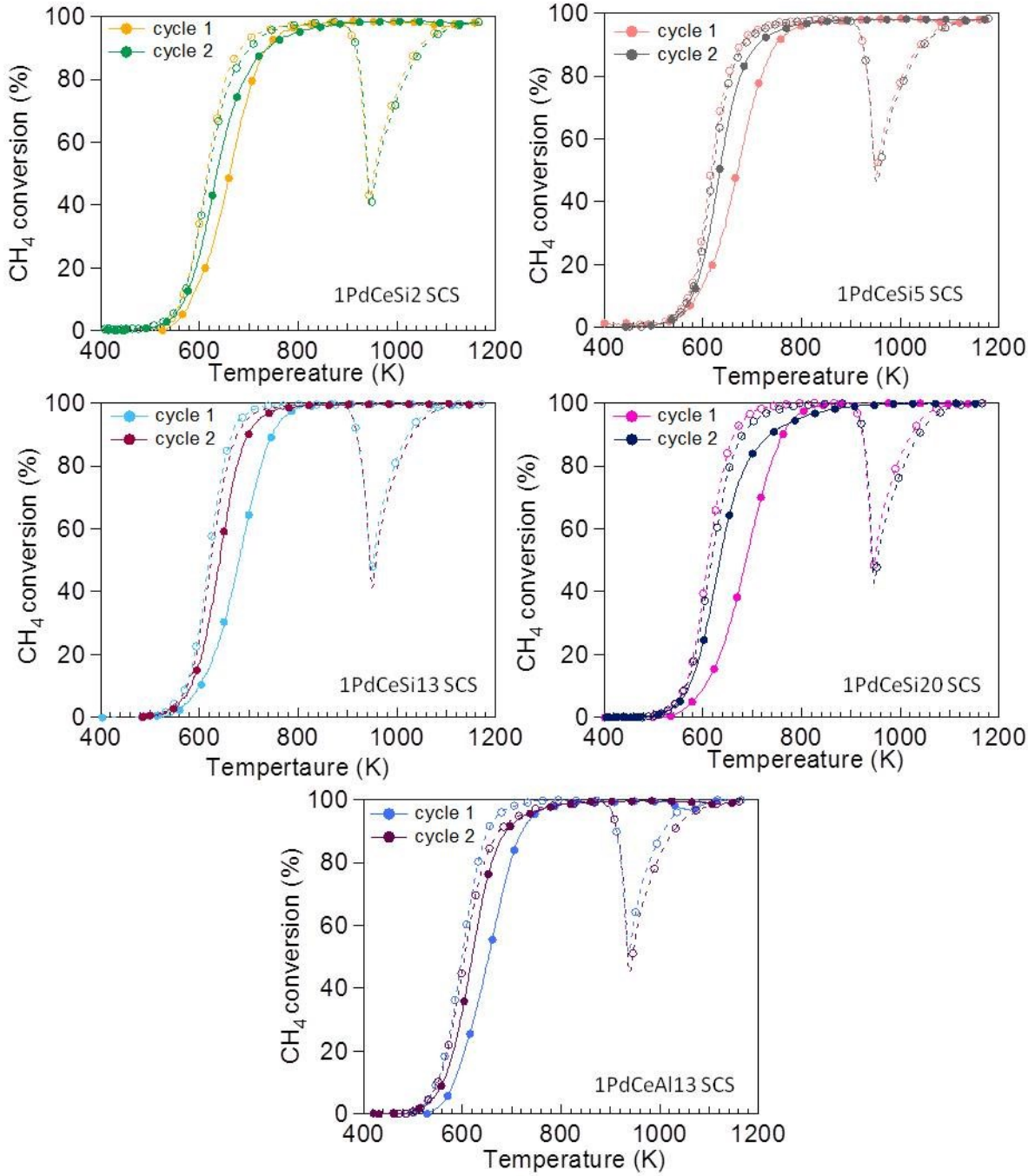

Figure 7.1: catalytic activity of CeO_2-SiO_2 and CeO_2-Al_2O_3 supported catalysts during two heating/cooling cycles for lean methane oxidation; solid line, filled symbols: heating; dotted line, open symbols: cooling

All samples show the typical hysteresis behavior of Pd-based catalysts during cyclic methane oxidation. Regardless of the catalyst composition, the hysteresis between heating and cooling branch markedly changes from one cycle to another: the hysteresis effect is larger during the first heating/cooling cycle, becoming narrower int the next one. For an easier comparison, the thermal hysteresis have been calculated as temperature difference in terms of T_{50} between the heating and cooling segment, according to the equation below:

$$\Delta T_{50} = T_{50\,(heat)} - T_{50(cool)}$$

The values are shown in Figure 7.2 for all samples.

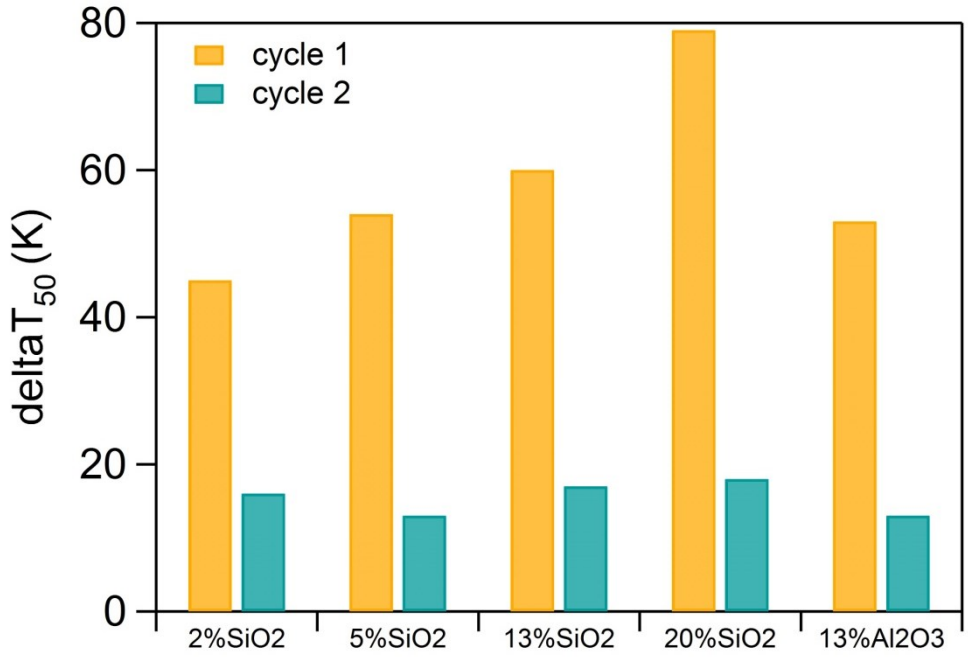

Figure 7.2: thermal hysteresis values (ΔT_{50}) for the first and second oxidation cycles for all samples

As clearly illustrated in Figure 7.2, a larger difference of T_{50} values is observed during the first oxidation cycle and ΔT_{50} progressively increases at increasing SiO_2 loading, reaching a maximum of 79 K for 1PdCeSi20 SCS. During the second run, the hysteresis becomes smaller and equal to about 13-18 K for all samples. Similar results are obtained for the Al-doped sample: the hysteresis is equal to 53 K in the first oxidation cycle, then decreases to 15 K.

Performing a new oxidation cycle on the used catalysts results in an enhancement of the catalytic activity. The behavior of Si-modified catalysts can be explained taking into account the results of TPO measurements (Chapter 6). PdO-Pd phase transformation in fact evolves differently during the first and second/third TPO cycle. When silica is added to ceria support, the first TPO run is characterized by the decomposition of $Ce_{4.94}Si_3O_{13}$ phase, followed by a not well defined PdO decomposition peak. The second (and third) cycle, which represents the state of PdO during the second light-off cycle, shows three well-defined steps of PdO decomposition. Therefore, the different hysteresis behavior between the first and second light-

off curve might be attributed to the different thermal treatment of Pd particles in air during the synthesis and under reaction mixture [1, 2, 3]. In the case of Ce-Si-based samples the situation is much more evident with respect to non-doped Pd-ceria catalysts (Chapter 4).
Figure 7.3 compares the heating and cooling part of the second oxidation cycle for Si-doped samples.

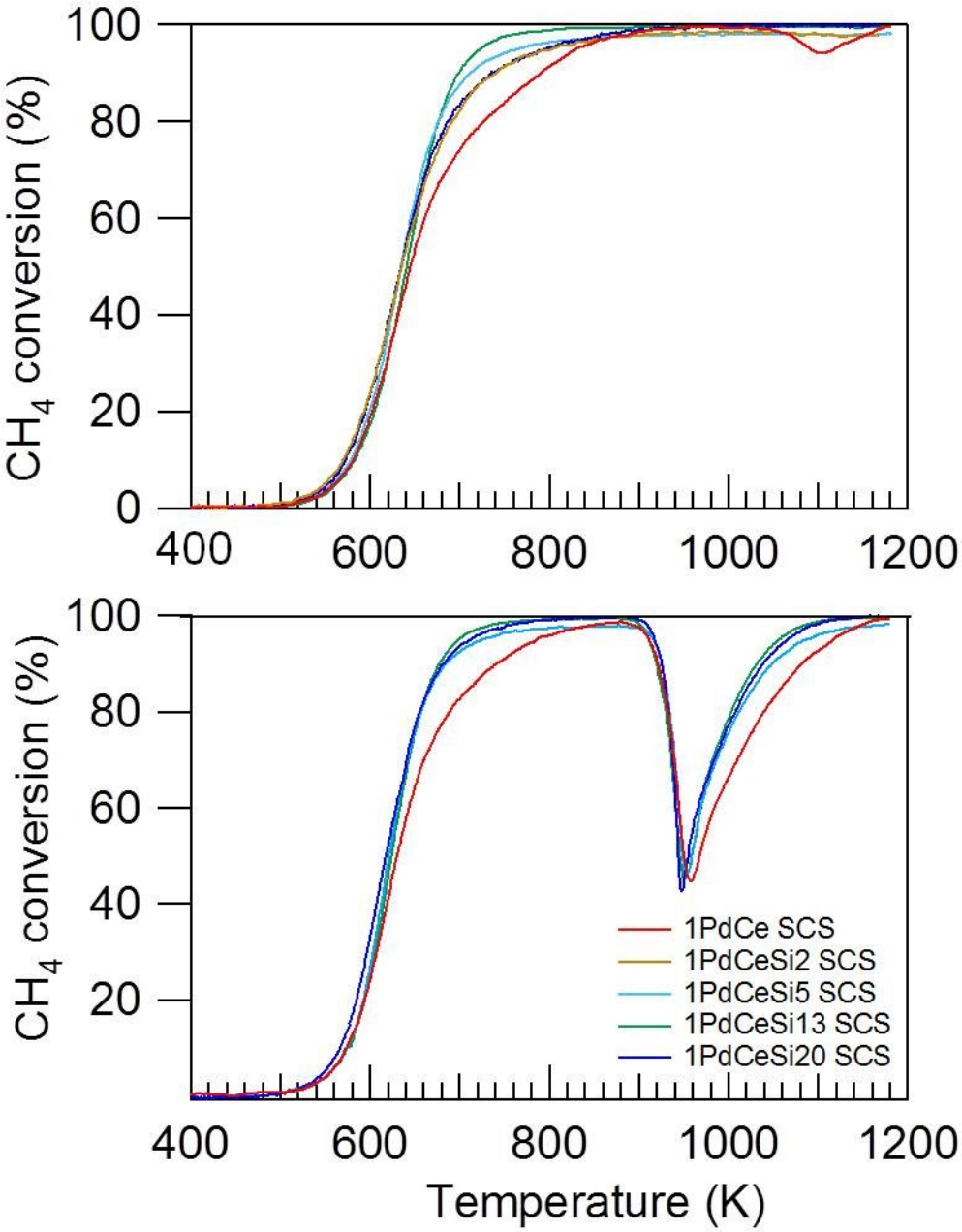

Figure 7.3: comparison of the heating (top) and cooling (bottom) light-off curves during the second methane oxidation cycle for all Si-doped catalysts

During the heating ramp, all silica-doped catalysts show a similar light-off behavior up to ~ 700 K. At increasing temperature, 1PdCeSi13 SCS considerably exceeds the performance of the other samples, reaching 100% conversion around 800 K; the samples containing 2 wt. % and 20 wt.% of SiO_2, instead, reach the full conversion at ~ 920 K. By observing the cooling part of the

curve (Figure 7.3 (bottom)), the conversion profiles present a pronounced minimum, attributed to the presence of metallic Pd at high temperature [4, 5, 6]. The presence of SiO_2 slightly delays Pd-PdO transformation, but the amount of silica does not have a strong effect as all catalysts behave similarly. Also the minimum value of CH_4 conversion does not change significantly with catalyst composition and is equal to 40-45%. After Pd re-oxidation the conversion starts again to increase, reaching the full conversion around 900 K: Si-containing catalysts maintain high conversion values up to 720 K, while for 1PdCe SCS the activity decreases immediately below 900 K. However, the light-off curves continue to be very similar to each other below 620 K.

Figure 7.4 compares the light-off behavior of doped samples with the same amount of dopant (Si or Al) with that of 1PdCe SCS.

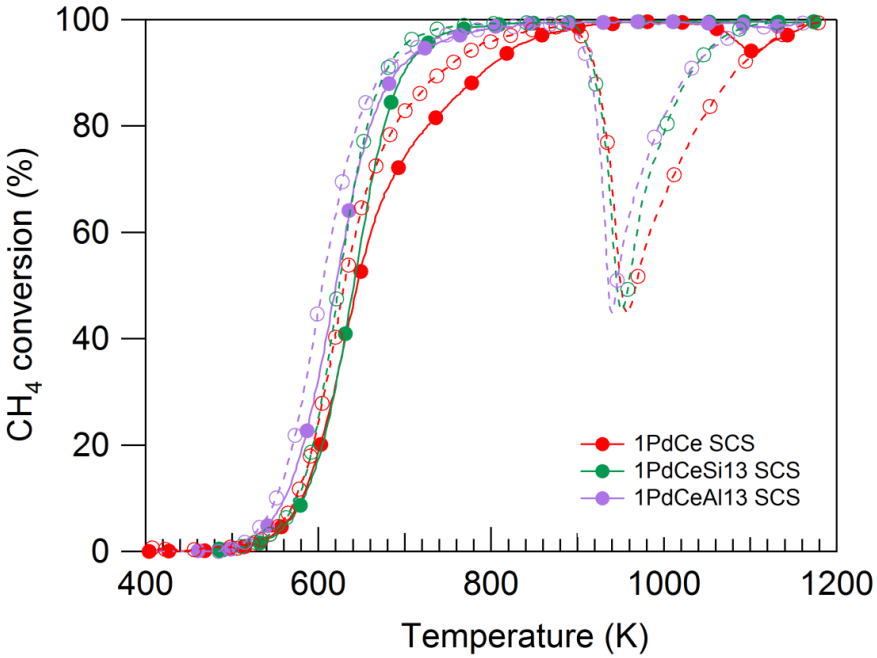

Figure 7.4: comparison of the second light-off cycle on 1PdCeSi13 SCS, 1PdCeAl13 SCS and 1PdCe SCS; solid line, closed symbols: heating; dotted line, open symbols: cooling.

Focusing on the heating part of the cycle, in the kinetically-limited region, 1PdCeAl13 SCS exhibits a superior activity towards methane oxidation. On doped-samples, the full CH_4 conversion is achieved at ~ 780 K, 140 K lower with respect to that observed for 1PdCe SCS. Beside a slight temperature shift, the shape of the activity loss as well as the minimum in CH_4 conversion are not affected by the composition of the support. After PdO re-formation, the catalytic activity is quickly recovered for doped catalysts, reaching again 100% of conversion, with a slight improvement of performance during the cooling step.

In order to understand quantitatively the difference among various samples, the activities were compared in terms of reaction rates calculated at 623 K, using the recycle apparatus described in section 2.6. During kinetic measurements, the recycle ratio was maintained at high value (R=25), with the purpose to ensure the occurrence of differential conditions and, thus,

performing a correct kinetic analysis. The results are reported in Table 7.1 in terms of CH_4 moles reacted per unit of time and gram of Pd.

Table 7.1: reaction rates at 623 K on Si- and Al-doped samples for methane oxidation in lean conditions

sample	**Rate@623 K (μmol CH_4/g_{Pd}*s)**
1PdCe SCS	111.4
1PdCeSi2 SCS	132.9
1PdCeSi5 SCS	146.4
1PdCeSi13 SCS	108.7
1PdCeSi20 SCS	147.9
1PdCeAl13SCS	218.3

Taking 1PdCe SCS as reference, the samples doped with 2, 5 and 20 wt.% of SiO_2, show a higher efficiency towards methane oxidation. For the sample containing 13 wt.% of SiO_2, instead, the moles of CH_4 reacted per unit of time are very similar to those observed for undoped sample, as suggested by light-off experiments. The positive effect of silica introduction to Pd/CeO_2 towards methane oxidation has been also highlighted by Hoffmann *et al.:* they obtained a series of catalysts with a superior activity towards methane oxidation with respect to pure Pd/CeO_2 [7]. When ceria is doped with alumina, the difference becomes more marked, where the reaction rate is approximately twice than that measured for 1PdCe SCS and sensibly higher with respect to silica-containing samples. Considering the TPO profiles performed during the third heating/cooling cycle (Chapter 6, Figure 6.7), the introduction of SiO_2 and Al_2O_3 leads to an increase of the fraction of palladium oxide interacting with the support and this might explain the increase of reaction rate for doped-samples.

The stability of different Si- and Al-modified samples has been evaluated by time-on-stream tests in order to check the catalysts deactivation over time. Figure 7.5 illustrates the deactivation profile of all Pd-based catalysts measured at 723 K for 24 hours, where normalized methane conversion is plotted against time-on-stream.

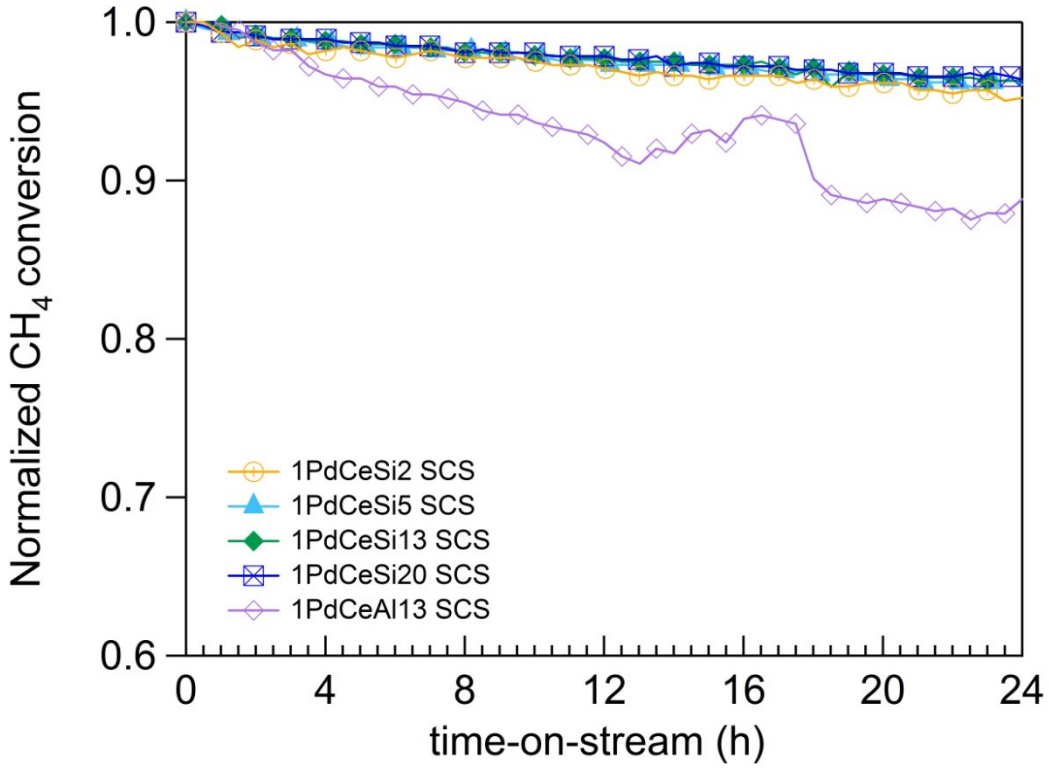

Figure 7.5: stability of Al- and Si-modified catalysts at 723 K in lean methane oxidation

All Si-containing catalysts show a good stability during the entire time-on-stream test: after 24 hours the catalytic activity decreases of only 3-5%, indicating no severe deactivation. For Al-doped sample instead, during the first half of the test methane conversion rapidly decreases of about 10% with respect to the initial conversion value. In the following hours the deactivation further proceeds on but more slowly, with a residual activity equal to 88% of the initial value after 24 hours. The decrease of activity with time might be ascribed to the build-up of water molecules on the catalytic surface produced from methane oxidation, whose desorption has been demonstrated being very slow [8]. The poor stability of Al-containing sample is in line with the published data, which report the severe deactivation of Pd catalysts supported on alumina in steady-state conditions [9, 10, 11]. The high affinity of alumina for water has been suggested to cause the decrease of stability when Al_2O_3 is used as support [10, 11].

7.1.2 Catalytic activity in stoichiometric conditions

The activity of 1PdCeSi13 SCS and 1PdCeAl13 SCS has been evaluated under stoichiometric reaction conditions (O_2/CH_4 = 2) during two heating/cooling cycles. The characteristic temperatures measured on each sample are reported in Table 7.2.

Table 7.2: T_{10} and T_{50} measured on 1 PdCeSi13 SCS and 1PdCeAl13 SCS during the heating ramps of subsequent two oxidation cycles (O_2/CH_4 = 2)

	Cycle 1		Cycle 2	
Sample	**T_{10} (K)**	**T_{50} (K)**	**T_{10} (K)**	**T_{50} (K)**
1PdCeSi13 SCS	620	711	567	626
1PdCeAl13 SCS	663	734	627	676

Both samples present a remarkable improvement of activity during the second cycle, as already observed under lean reaction conditions (Figure 7.1). In particular, for Si-doped sample T_{10} and T_{50} decrease of 53 K and 85 K, respectively, while for Al-doped one T_{10} and T_{50} are lowered of 36 K and 58 K, respectively. Figure 7.6 shows the effect of oxygen concentration on the evolution of CH_4 conversion with temperature for 1PdCeSi13 SCS.

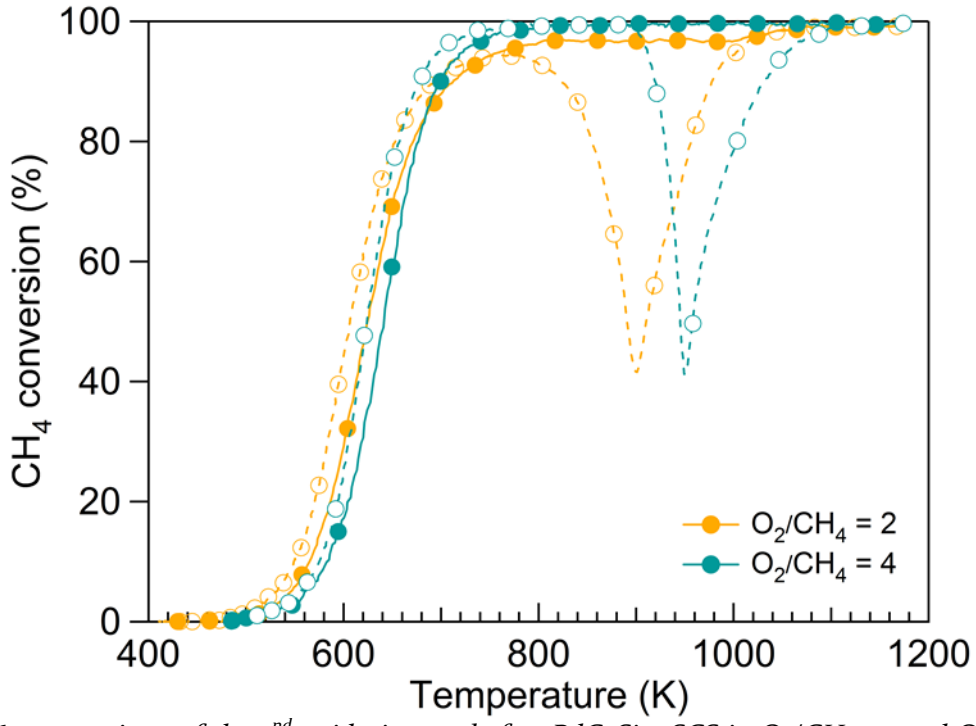

Figure 7.6: comparison of the 2nd oxidation cycle for 1PdCeSi13 SCS in O_2/CH_4= 2 and O_2/CH_4= 4 reaction mixture; solid line, closed symbols: heating; dotted line, open symbols: cooling.

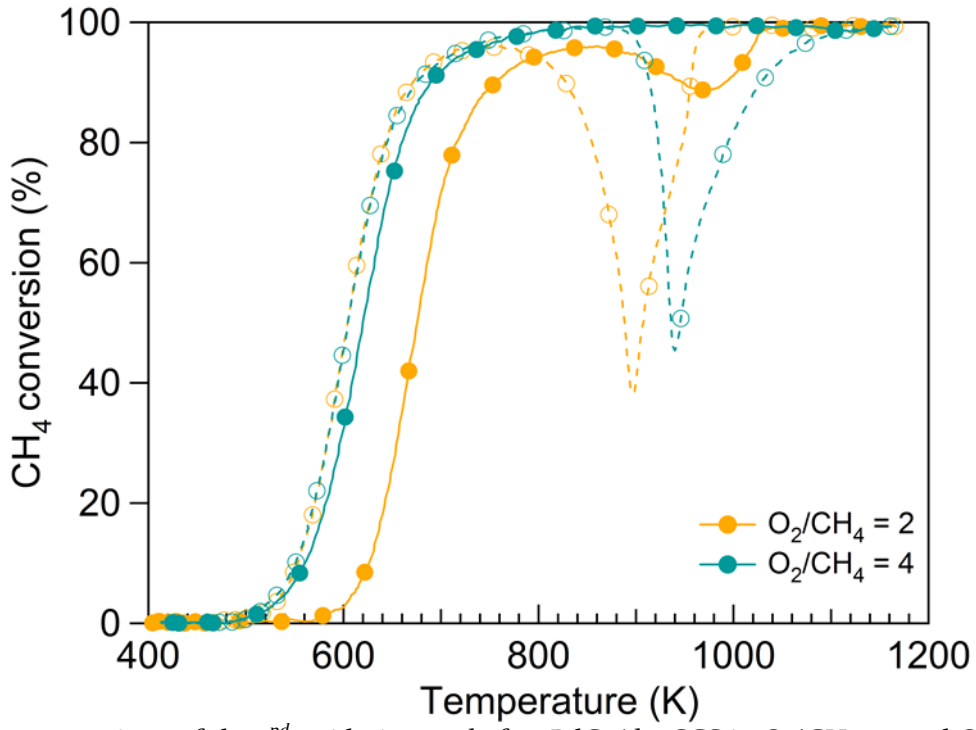

Figure 7.7: comparison of the 2nd oxidation cycle for 1PdCeAl13 SCS in O_2/CH_4= 2 and O_2/CH_4= 4 reaction mixture; solid line, closed symbols: heating; dotted line, open symbols: cooling.

For Si-doped sample, the decrease of the oxygen amount in the feed does not change significantly the catalytic performance during the heating ramp, with similar T_{10} and T_{50} values in lean and stoichiometric conditions. The main effect of varying oxygen partial pressure is observed during the cooling part of the cycle, where the re-oxidation of Pd to PdO takes place 50 K lower than in oxygen-rich atmosphere, but the minimum in methane conversion remains unchanged (38 %).

Differently from what observed for Si-doped sample, the activity of 1PdCeAl13 SCS (Figure 7.7) is strongly affected by the feed composition: the threshold of methane oxidation moves towards higher temperature during stoichiometric operation, where T_{10} and T_{50} increases of 64 K and 56 K, respectively. Above 860 K, when oxygen becomes the limiting reagent, the activity falls down sharply to rise again above ~ 1020 K (homogeneous reaction). Upon cooling, the activity reaches a minimum of 37 % at 900 K, against 44% at 940 K in oxygen-rich atmosphere. Furthermore, the hysteresis during cyclic oxidation becomes larger when oxygen partial pressure decreases; this might be due to a different reconstruction of Pd/PdO particles on alumina under lower oxygen concentration. For both samples, the decrease of oxygen partial pressure leads to a delay of Pd re-oxidation, pushing the position of the minima to lower values, according to the results obtained previously by ours and other research groups [5, 12, 13]. These results confirm the essential presence of high oxygen concentration to maintain palladium as PdO in the high-temperature region. Figure 7.8 shows the comparison of the second light-off curve with the one of 1PdCe SCS obtained in stoichiometric conditions.

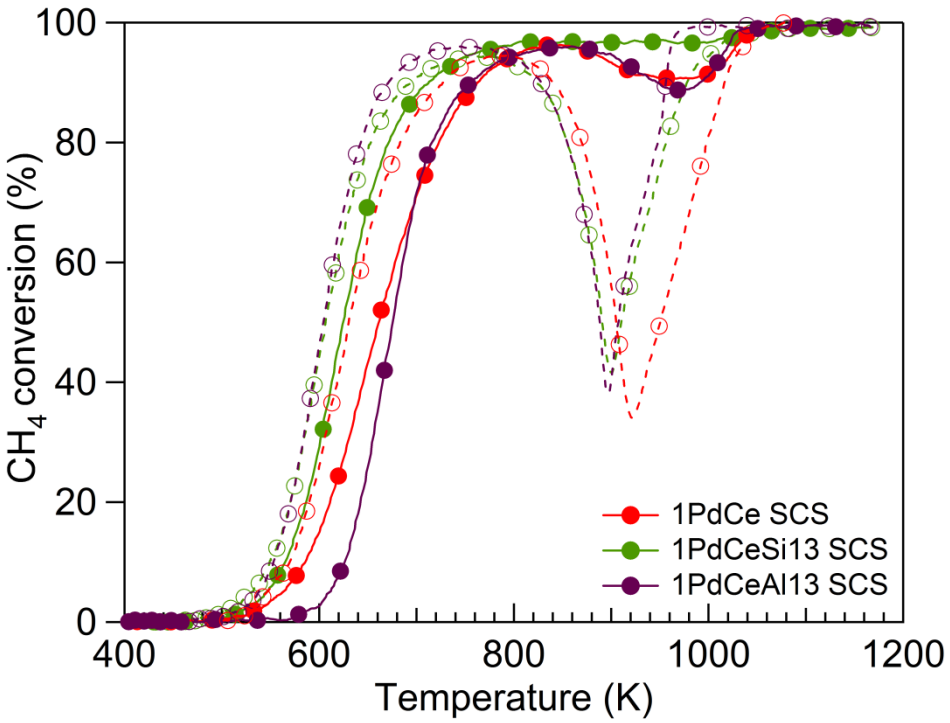

Figure 7.8: comparison of the second oxidation cycle for 1PdCe SCS, 1PdCeSi13 SCS and 1PdCeAl13 SCS during methane oxidation in stoichiomtric conditions; solid line, closed symbols: heating; dotted line, open symbols: cooling.

The light-off temperatures increase in the following order: 1PdCeSi13 SCS < 1PdCe SCS < 1PdCeAl13 SCS, and Si-doped sample has the best catalytic performance over the entire temperature range. The trend of activity changes completely with respect to lean conditions (Figure 7.4): the best light-off performance is obtained for Si-containing sample, whereas Al-doped one is less active for CH_4 oxidation in these reaction conditions. In the present study we are not able to state which is the active form of palladium in these reaction conditions and the debate about the active phase (Pd, PdO or a mixture of PdO/Pd) under stoichiometric/rich methane oxidation is still open [14]. However, the mechanism and kinetics of methane oxidation can change when O_2/CH_4 ratio is switched from lean to stoichiometric/rich regime, where reforming reactions and WGS might occur at increasing/decreasing temperature [15, 16, 17].

7.2 Catalytic methane oxidation in the presence of water

7.2.1 Catalytic activity and stability in lean reaction conditions

Similarly to what reported for ceria-zirconia supported catalysts, also on these samples the deactivation in the presence of external water was investigated. Briefly, two subsequent oxidation cycles (heating/cooling) were performed in the presence of water (0.5 CH_4, 2% O_2, 10 % H_2O(v) in He), named *cycle 1 H_2O* and *cycle 2 H_2O*. In order to assess the reversibility of water poisoning, a third cycle (named *after H_2O*) was carried out without water in the feed (0.5 CH_4, 2% O_2, in He). The second oxidation cycle in dry-lean conditions (*cycle 2 dry*) is added as reference one.

Figure 7.9 presents the activity of 1PdCeSi2 SCS in the presence and in the absence of water vapor in the feed.

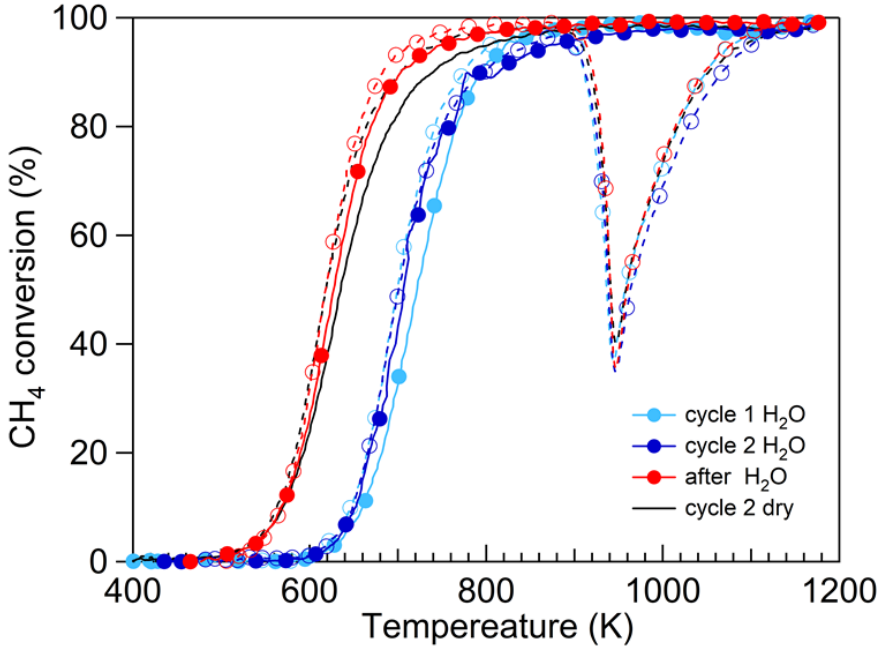

Figure 7.9: catalytic activity of 1PdCeSi2 SCS with and without water in lean conditions; closed symbols, solid line: heating; open symbols, dotted line: cooling.

When water is added into the gas stream, T_{10} and T_{50} increase of 80 K and 70 K, respectively, compared to cycle 2 dry, where the two oxidation cycles appeared almost identical to each other (see Figure 7.9). In wet atmosphere, no significant changes are detected on the activity loss during cooling as well as on the temperature of Pd re-oxidation. When water is removed from the gas stream (red curve), the catalytic activity is completely restored with a slight improvement of performance during heating above 600 K.

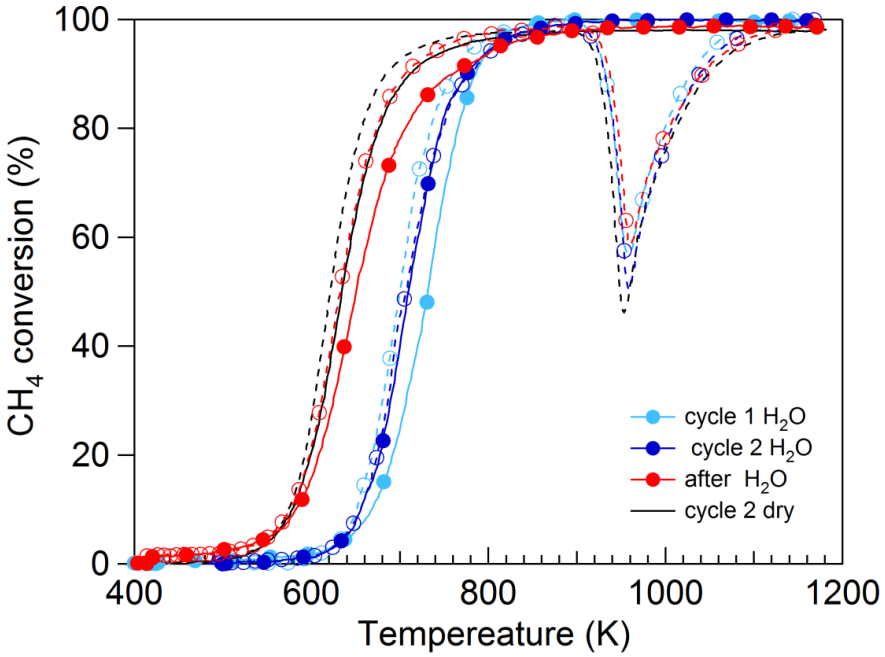

Figure 7.10: catalytic activity of 1PdCeSi5 SCS with and without water; closed symbols, solid line: heating; open symbols, dotted line: cooling.

1PdCeSi5 SCS (Figure 7.10) displays a stable catalytic activity throughout two heating/cooling ramps with the second cycle more active than the first one and very narrow thermal hysteresis. After removing water, the heating ramp is slightly shifted to higher temperatures with an increase of T_{50} from 635 K (cycle 2 dry) to 652 K: this suggests that water deactivation is not immediately reversible for this sample. It is interesting to observe that in the presence of water and, in particular, after water removal the size of the activity loss due to Pd-PdO transformation is smaller than in dry conditions: the position of the minima is the same that in dry conditions (962 K) but the value reached in "after H_2O" cycle is equal to 60% against 46% in dry atmosphere.

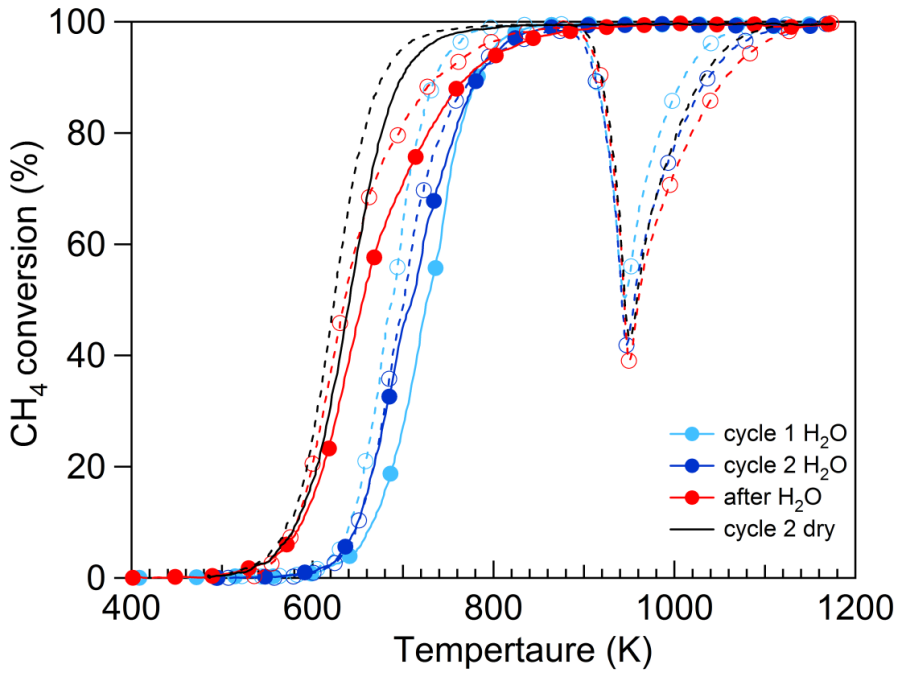

Figure 7.11: catalytic activity of 1PdCeSi13 SCS with and without water; closed symbols, solid line: heating; open symbols, dotted line: cooling.

The oxidation profiles in wet atmosphere of 1PdCeSi13 SCS are illustrated in Figure 7.11. The deactivation caused by water is less severe in terms of T_{10} with respect to other silica-doped samples: the gap between dry and second wet light-off curve is equal to 66 K. As detected for the sample with 5% of SiO_2, the loss in conversion during cooling is slightly reduced in the presence of water, especially during cycle 1 H_2O; this reduction, however, is not maintained after water removal.

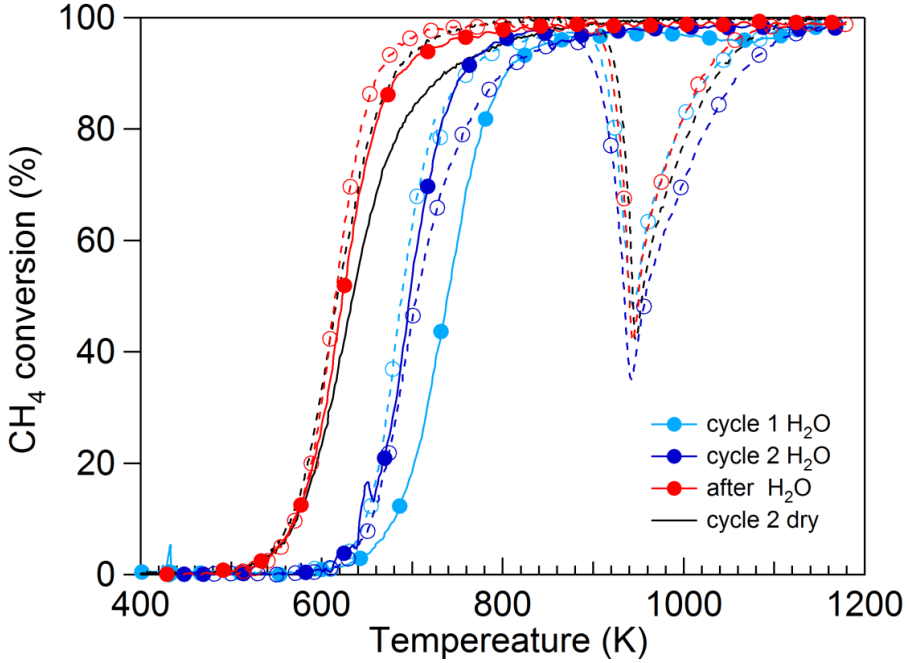

Figure 7.12: catalytic activity of 1PdCeSi20 SCS with and without water; closed symbols, solid line: heating; open symbols, dotted line: cooling.

For the catalysts doped with 20 wt.% of SiO_2 (Figure 7.12), a strong deactivation is observed during the first oxidation cycle with a shift of T_{10} and T_{50} of 93 K and 86 K, respectively, compared to dry conditions. After performing another cycle on the used sample, the catalytic activity is considerably improved with T_{10} and T_{50} decreased of 32 K and 53 K, respectively. Nevertheless, by observing the cooling part of cycle 2 H_2O, a strong deactivation is observed when Pd is present in metallic form reaching a minimum of 34% at 942 K. Below this temperature, upon PdO re-formation, the activity is not completely restored with the cooling segment less active than the heating one. After two heating/cooling cycles in the presence of water, the activity is better than in dry atmosphere during heating, overlapping with the cooling segment of cycle 2 dry when the temperature is decreased.

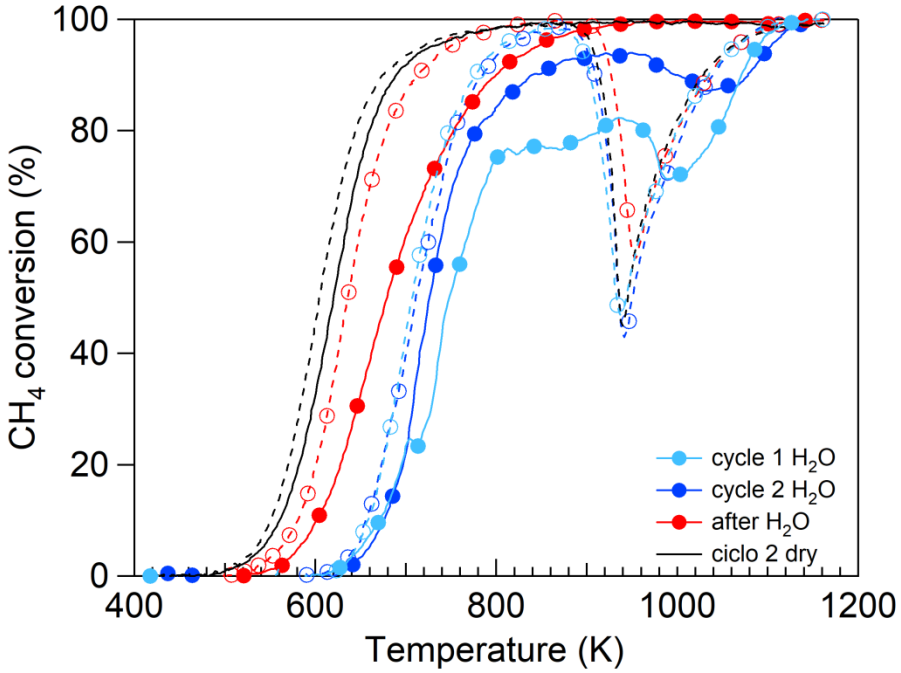

Figure 7.13: catalytic activity of 1PdCeAl13 SCS with and without water; closed symbols, solid line: heating; open symbols, dotted line: cooling.

As soon as water is added into the gas feed, the catalytic activity of 1PdCeAl13 SCS is definitely deteriorated during the first cycle (Figure 7.13): a strong deactivation operated by water is observed with an increase of T_{10} of 116 K. In the following cycle, the catalytic activity is improved, with a smaller thermal hysteresis between heating and cooling branch. Above ~ 920 K, a dramatic drop in methane conversion is detected due to the decomposition of PdO to metallic Pd. Despite a strong inhibition effect during the heating segment, water has no effect neither on temperature of Pd re-oxidation nor on the size of activity loss during cooling. If we look at the light-off behavior after two cycles in wet atmosphere, the poisoning is not reversible and the conversion level remains lower with respect cycle 2 dry: 10% and 50% of conversion are achieved at 39 K and 60 K higher than in dry conditions, respectively.

Surprisingly, the size of activity loss is significantly reduced, reaching a minimum of 60% against 44% during cycle 2 dry.

The behavior displayed by 1PdCeAl13 SCS well reflects the poor activity of alumina-supported catalysts in the presence of water with a strong deterioration of catalytic activity [1, 18, 19]. The storage of water in the support, the high affinity of alumina for water molecules and its low oxygen mobility can explain the severe deactivation when Pd is supported on alumina-containing oxides [10, 19, 20, 21]. Also the acid/base properties of the support might influence the activity towards methane oxidation and could play an important role on the deactivation induced by water [22, 23]. In our case it is difficult to assess the role of acidity/basicity of dopants as both Al_2O_3 and SiO_2 are mainly acidic, but their effect is somehow opposite on methane oxidation in presence of water.

Table 7.3 reports the difference in the characteristic temperatures measured during "cycle 2 dry" and "cycle 2 H_2O" of all doped-catalysts, where ΔT_{10} and ΔT_{50} have been calculated as follows:

$$\Delta T_{10} = T_{10,cycle2H2O} - T_{10,cycle2dry}$$
$$\Delta T_{50} = T_{50,cycle2H2O} - T_{50,cycle2dry}$$

Table 7.3: T_{10} and T_{50} measured with and without water in the feed

	T_{10} (K)			T_{50} (K)		
	cycle 2 dry	**cycle 2 H_2O**	**ΔT_{10}**	**cycle 2 dry**	**cycle 2 H_2O**	**ΔT_{50}**
1PdCeSi2 SCS	570	650	80	635	705	70
1PdCeSi5 SCS	579	657	78	635	710	75
1PdCeSi13 SCS	585	651	66	641	712	71
1PdCeSi20 SCS	584	652	68	655	698	43
1PdCeAl13 SCS	560	676	116	620	727	107

The increase of light-off temperatures in the presence of water is almost similar for all silica-doped catalysts and equal to 70-80 K; only for 1PdCeSi20 SCS the increase in T_{50} is lower with respect to the other samples. By comparing the temperatures achieved in wet atmosphere, no influence of different SiO_2 loadings can be detected on the catalytic activity, showing close T_{10} and T_{50} values. When water is added to reaction feed, Al-doped sample is less active towards methane oxidation, differently from what observed in the absence of water (Figure 7.4).

Since during light-off experiments the activity loss showed some changes upon water addition and removal, TPO experiments were performed in wet atmosphere (2% O_2/N_2, 10% H_2O) in order to evaluate the effect of water on PdO-Pd-PdO phase transformation. Similar to activity tests, for each sample two TPO cycles were carried out in wet atmosphere (only the second one

is shown) followed by a cycle without water (2% O_2/N_2) (*after H_2O*). The TPO profiles of 1PdCeSi13 SCS obtained with and without water in the feed are shown as an example (Figure 7.14). The points marked with an arrow (2, 2' and 3) indicate the temperatures at which the TPO was stopped and samples for HRTEM analysis were collected (see below).

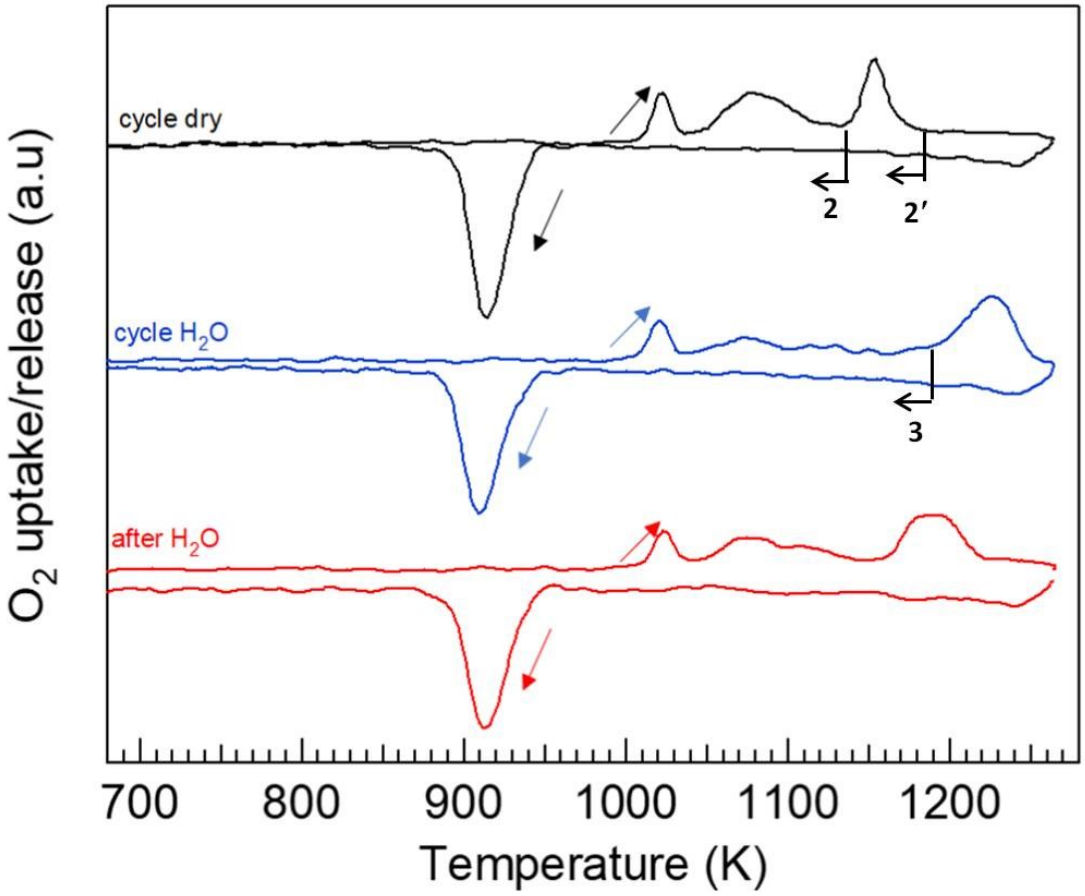

Figure 7.14: TPO profile of 1PdCeSi13 SCS with and without water in the feed

Differently from the results obtained for Pd/$Ce_xZr_{1-x}O_2$ samples (Chapter 5, Figure 5.7), the qualitative oxygen release/uptake profile is clearly affected by the addition of water. PdO-Pd phase transformation continues to be characterized by three separate oxygen release steps but the shape as well the position of the maxima markedly change. During cycle 2 H_2O, no change in the decomposition threshold of first oxygen release peak can be observed, and its maximum is set at 1021 K; the second step, instead, which likely correspond to the decomposition of bulk PdO [12], becomes broader and less defined. The main effect caused by water is related to the shift of the position of third oxygen release peak, corresponding to PdO species in strong interaction with the support [12]: the decomposition of the stable PdO species moves towards higher temperature (~ 70 K) with respect to the one in dry conditions. Focusing on the cooling part of the cycle, apparently no differences can be detected on the re-oxidation of metallic Pd.

When water is removed from the feed, the qualitative oxygen/release profile continue to be different from that obtained in dry atmosphere: the position of the third oxygen release peak is

shifted to higher temperature, likely due to the slow desorption rate of hydroxyls groups from the catalytic surface that slows the return of the TPO to the dry profile.

Figure 7.15 illustrates the comparison of the second TPO cycle of Si- and Al-doped samples carried out in the presence and in the absence of water.

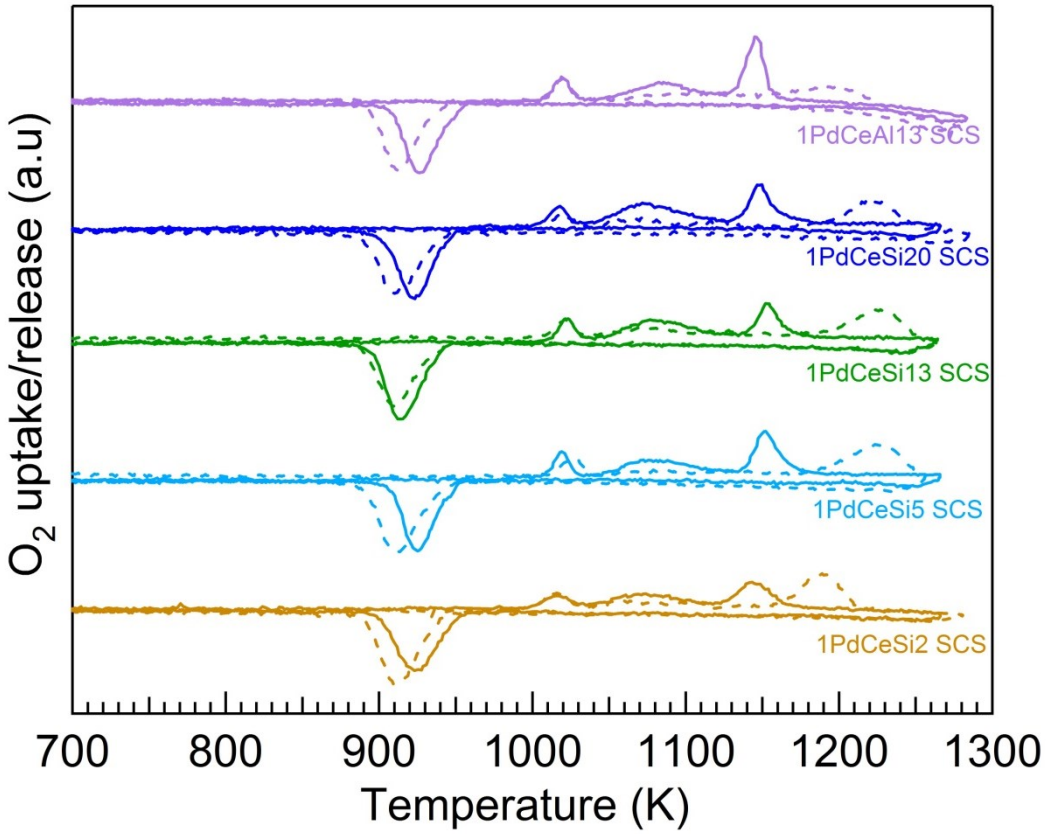

Figure 7.15: second TPO cycle with and without water for Si- and Al-doped samples; solid line: dry (2% O_2/N_2); dotted line: wet (2 % O_2/N_2, 10% H_2O)

When water is present in the feed gas, the dynamic of PdO-Pd transformation evolves differently for all catalysts. Two main effects have to be highlighted: *i)* the decomposition of the stable PdO species takes place at higher temperature, irrespective of the composition of the support, whereas no effect operated by water is detected on the decomposition threshold of the first and second step; *ii)* the second oxygen release peak becomes broader and less defined. For 1PdCeSi2 SCS, the decomposition of the third PdO species takes place with maximum at 1189 K, 46 K higher than during cycle 2 dry. A similar behavior can be observed for the other Si-based catalysts but the maximum of the third step is delayed of about 70 K at higher silica loadings. Analogues considerations can be done for the Al-doped sample: when water is added into the feed stream, the temperature of the maximum of the third oxygen release peak increases of 54 K with respect to the one in dry atmosphere. The introduction of water modifies also the distribution of the different steps: for Si-doped catalysts the contribution of the high temperature step becomes even more pronounced; on the contrary, for Al-doped sample the area of the high temperature peak is reduced and this might explain

its poor activity in the presence of water (Figure 7.13). Looking at the cooling part of the cycle, the oxygen uptake due to Pd re-oxidation is slightly shifted to lower temperatures: this behaviour might be related to a possible suppression of PdO re-formation due to the inhibition of oxygen mobility caused by water vapor [19].

In order to shade some light on the dynamic of PdO-Pd transformation in the presence of water, the heating ramp during the second TPO cycle was stopped at different fixed temperatures, the sample was cooled down quickly in pure nitrogen and then collected for HRTEM analysis following a procedure reported in the literature [24]. During cycle 2 dry, the collection temperatures for HRTEM were approximately 1123 K (second dry TPO cycle stopped@1123 (*point 2)* in Figure 7.14), before the third decomposition peak, and at around 1180 K (second dry TPO cycle stopped@*1180 (point 2')* in Figure 7.14). With the same procedure, during cycle 2 H_2O the heating ramp was stopped at around 1153 K (second wet TPO cycle stopped@1153 *(point 3)* in Figure 7.14), corresponding to an intermediate situation before the third PdO decomposition step. The samples so collected were characterized by HRTEM analysis and the results are illustrated in Figure 7.16.

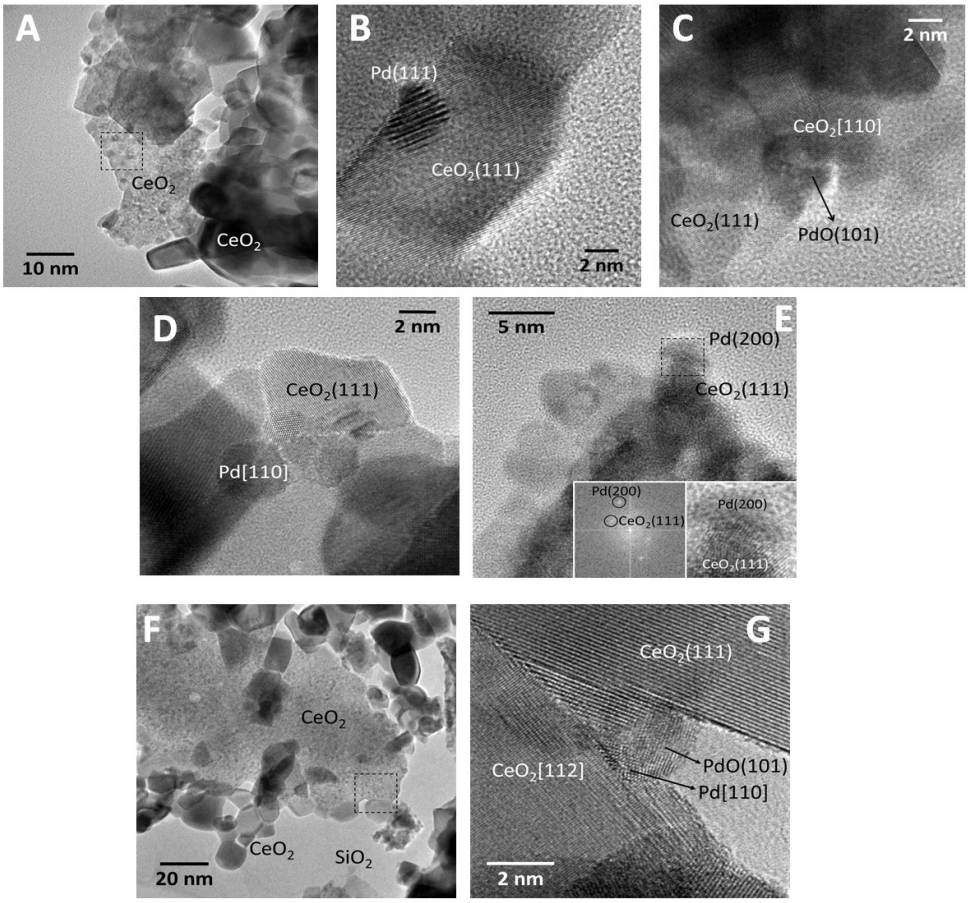

Figure 7.16: (A, B, C) HRTEM images of 1PdCeSi13 SCS collected during the second dry TPO cycle stopped@1123 (point 2); (D,E) HRTEM images of 1PdCeSi13 SCS collected during the second dry TPO cycle stopped@1180 (point 2'); (F,G) HRTEM images of 1PdCeSi13 SCS collected during the second wet TPO cycle stopped@1153 (point 3)

In the sample collected during the second TPO cycle in dry conditions stopped@1123K, there is a bimodal distribution of ceria crystallites (Figure 7.16 (A)). The area enclosed in the black rectangle is shown enlarged in Figure 7.16 (B). The inset corresponds to the FT of the image and shows rings corresponding to the different orientations of a large amount of ceria crystallites, ranging from 2 to 4 nm, approximately. However, a change in the state of palladium is clearly detected with respect to what reported for fresh 1PdceSi13 SCS (see Chapter 6, Figure 6.5). Figure 7.16 (B) evidences the presence of a metallic Pd particle showing the (111) crystallographic planes at 2.25 Å, which shows epitaxy with the (111) planes of the ceria crystallite support and originate a Moiré pattern. This means that palladium oxide in strong interaction with ceria has been reduced. In addition to the metal Pd nanoparticles, the sample still contains PdO (Figure 7.16 (C)). In Figure 7.16 (C) a PdO nanoparticle showing the characteristic (101) planes of PdO at 2.65 Å can be observed.

After heating up to 1180 K the sample only contains metallic Pd nanoparticles. Figures 7.16 (D) and Figure 7.16 (E) show several Pd nanoparticles in contact with the ceria support crystallites. In this case no particular epitaxial relationships are observed and all palladium occurs as Pd metal, irrespectively of the contact with the ceria support. As an example, Figure 7.16 (E) shows the detail of a Pd metal nanoparticle exhibiting the (200) crystallographic planes at 1.95 Å over a ceria crystallite showing the characteristic (111) planes at 3.12 Å, as measured in the corresponding FT image.

The sample subjected to a second TPO cycle in the presence of steam and quenched is virtually identical to the equivalent sample subjected to dry TPO and stopped at 1123 K. Again, a clear bimodal distribution of ceria crystallites is visible (Figure 7.16 (F)), with maxima at around 20 nm for the large particles and around 4 nm for the smaller ones, as well as minor amorphous silica phase. Figure 7.16 (G) clearly highlights the presence of palladium nanoparticles, and reveals the coexistence of both Pd metal and PdO. The presence of palladium nanoparticle containing both Pd and PdO is visible at the junction of two ceria crystallites (Figure 7.16 (G)), one showing (111) planes at 3.12 Å and the other one oriented along the [112] crystallographic direction and showing the (111) planes and the (220) planes at 1.91 Å. The palladium nanoparticle is highly disordered and shows two domains. One domain corresponds to Pd metal oriented along the [110] direction and shows the (111) and (200) crystallographic planes of Pd at 2.25 and 1.95 Å, respectively. The other domain shows lattice fringes at 2.65 Å, which corresponds to the (101) crystallographic planes of PdO.

From HRTEM analysis it seems that the samples after dry TPO cycle stopped@1123 and after wet TPO cycle stopped@1153 do not show significant differences from a morphological point of view. Nevertheless, the presence of two domain particles on the sample treated in presence of water might indicate that PdO decomposition takes place following a different route in this

case. It should also be observed that the presence of amorphous silica after TPO cycles prevents somehow the possibility to find a clear relationship between the different phases by HRTEM analysis, which is more accurate when crystal lattice fringes are present.

However, the adsorption of water molecules on the catalytic surface might change metal-support interaction [25], modifying the thermal stability of PdO interacting with the oxide carrier. Moreover, SiO_2 and H_2O can easily react leading to the formation of $Si(OH)_4$ species and this reaction is favoured above 973K [26, 27]. Alternatively, the presence of water at high temperature might promote a severe sintering of PdO particles [23]: larger PdO particles might require higher temperature to be decomposed.

The effect of water on the catalysts stability was evaluated by time-on-stream tests at 723 K with a constant concentration of water vapor (10 vol.% (v)). The evolution of methane concentration has been continuously monitored with time-on-stream. The results of time-on-stream experiments are reported in Figure 7.17.

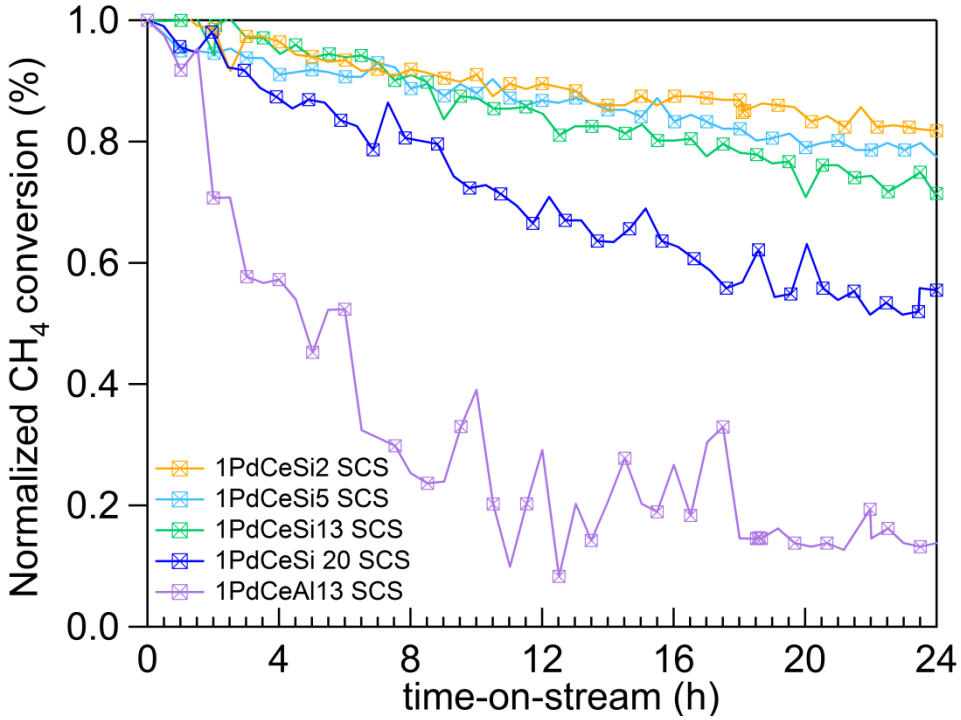

Figure 7.17: time-on-stream behavior of Si- and Al-doped catalysts at 723 K in the presence of water

The introduction of water accelerates the catalysts deactivation, especially in the early hours, according to the inhibition effect of water on methane oxidation [28, 29, 30]. The effect of SiO_2 loading on the stability is more remarkable than in dry conditions (Figure 7.6): the deactivation increases in the following order 1PdCeSi2 SCS < 1PdCeSi5 SCS < 1PdCeSi13 SCS < 1PdCeSi20 SCS with an activity loss after 24 hours of 18%, 20%, 28% and 40%, respectively. Lamber *et al.* indicated that, during hydrothermal treatment, SiO_2 can react with water

molecules leading to the formation of silanol species (Si-OH), which could cause the coalescence and migration of Pd particles [26].

For 1PdCeAl13 SCS, the effect of water poisoning becomes even more severe: the deactivation rate is faster compared to Si-doped samples, with an activity loss of about 60% during the first 4 hours. In the following hours, the conversion continues to decrease but more slowly, reaching an almost stable value after 18 hours. Stability data confirms what was observed during temperature programmed tests: when Al_2O_3 is added on the support, the catalysts are more susceptible to water poisoning. Even though no definitive explanation has been found yet, these results are in agreement with the ones obtained from other groups. Kikuchi *et al.* observed a poor stability of Pd-based catalysts when alumina is employed as support: they attributed this behavior to high coverage of active sites by OH groups, expressed by the more negative value of enthalpy of water adsorption [18]. Nomura *et al.* [21] and Araya *et al.* [31] attributed the higher deactivation degree of Pd/alumina to the greater affinity of the support for water . Moreover, the low oxygen mobility of alumina-based oxides has been proposed to cause the progressive deterioration of performance in the presence of water, in agreement with the previous results of Ciuparu's groups [10].

7.2.2 Catalytic activity in stoichiometric reaction conditions

The samples doped with 13 wt.% of metal oxide have been tested also under lower oxygen partial pressure and in the presence of water (0.5 % CH_4, 1.0 % O_2, 10% H_2O in He), with the aim to study the effect of oxygen concentration on the water poisoning. The second oxidation cycle performed in dry stoichiometric conditions is used as reference.

Figures 7.18 and 7.19 show the catalytic performance of the catalysts with and without water in the feed.

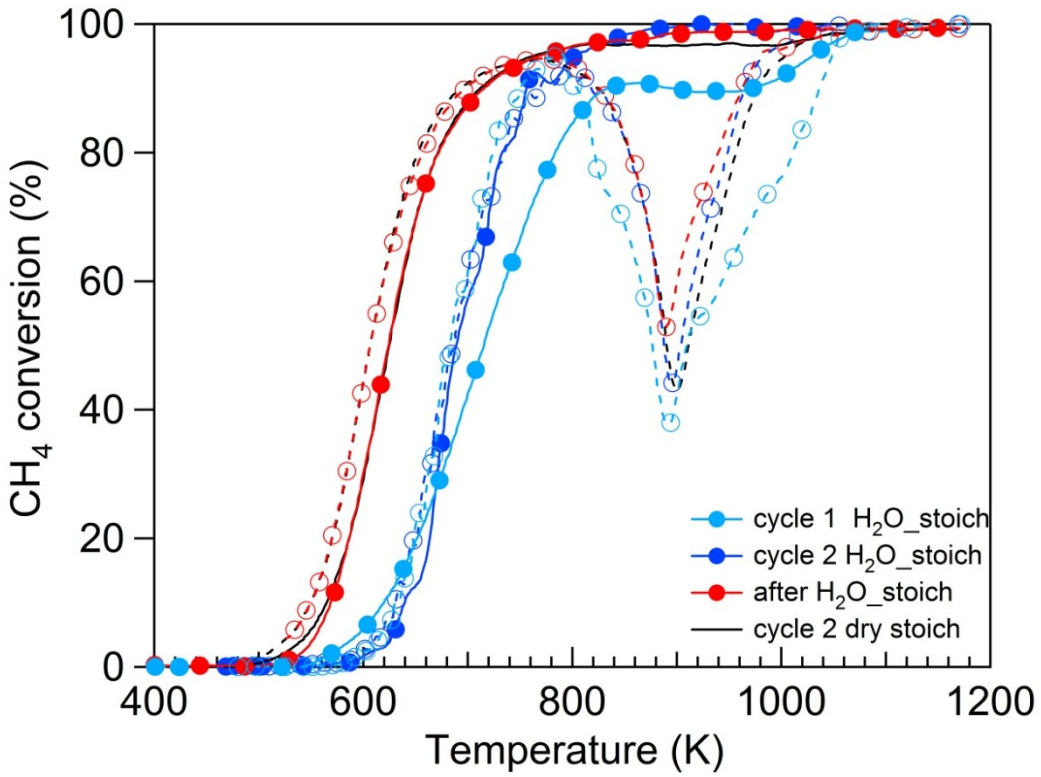

Figure 7.18: catalytic activity with and without water of 1PdCeSi13 SCS in stoichiometric conditions

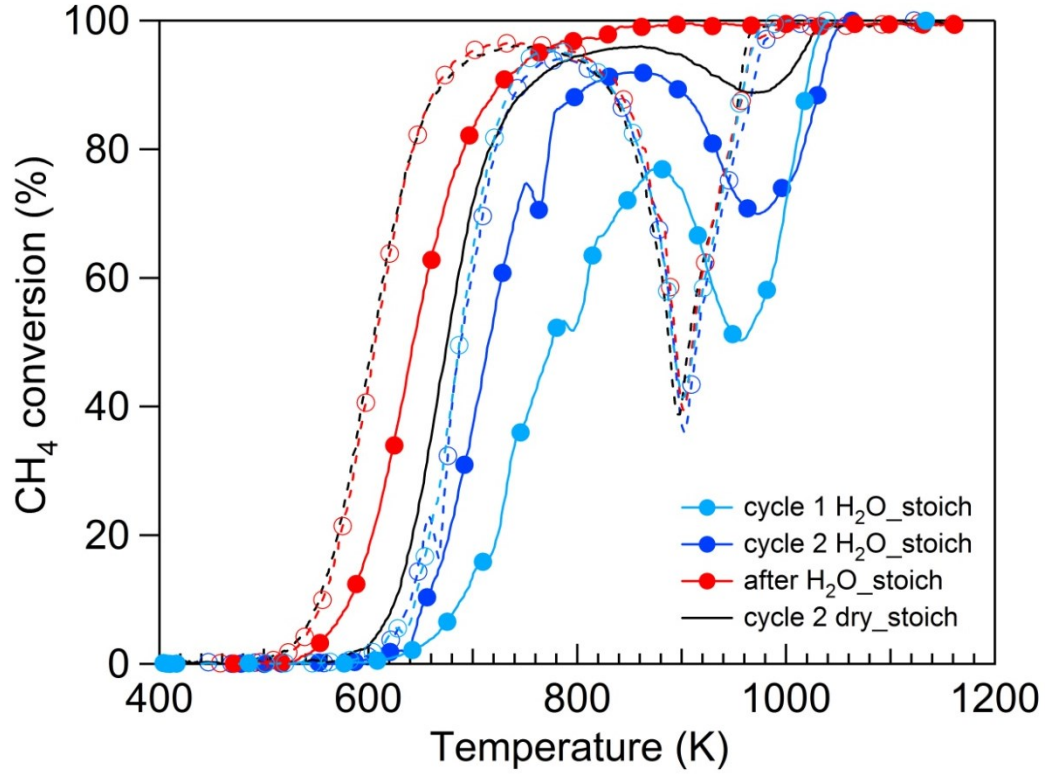

Figure 7.19: catalytic activity with and without water of 1PdCeAl13 SCS in stoichiometric conditions

Looking at the catalytic performance of 1PdCeSi13 SCS (Figure 7.18), during the second oxidation cycle in wet conditions, the onset of the methane oxidation increases from 563 K to 637 K and 50% of methane conversion is reached 54 K higher with respect to the dry

atmosphere. No effect operated by water, instead, is observed on the transient deactivation at high temperature after the first cycle in presence of water. Once water is switched off, the initial activity is quickly recovered and overlaps with the one recorded during cycle 2 dry. The deactivation due to PdO-Pd transformation during cooling is slightly improved, reaching a minimum of 51 % against 43 % in dry atmosphere.

By observing the results obtained for Al-doped catalyst (Figure 7.19) and focusing on the heating ramp of cycle 1 H_2O, a strong inhibition effect of water is detected, where T_{10} and T_{50} increase of 65 K and 100 K, respectively, reaching the full conversion only above 1000 K when there is likely also the contribution of homogeneous reaction. A dramatic loss in conversion due to PdO-Pd transition is observed in fact during heating, indicating a strong effect of water in stoichiometric conditions on the stability of the PdO phase in presence of water. Performing a new oxidation cycle, the activity is enhanced with respect to the previous cycle, with a shift of light off temperatures of only 29 K and 40 K, much lower than in fuel lean conditions (Figure 7.13). Nevertheless, again at temperatures above 840 K the activity dramatically decreases due to the decomposition of palladium oxide. When water is removed from the feed, the activity is strongly improved during the heating ramp with respect to cycle 2 dry.

Table 7.4 summarizes the temperature differences in terms of T_{10} and T_{50} between *cycle 2 dry* and *cycle 2 H_2O* in lean and stoichiometric conditions, calculated as follows:

$$\Delta T_{10} = T_{10,cycle2H2O} - T_{10,cycle2dry}$$
$$\Delta T_{50} = T_{50,cycle2H2O} - T_{50,cycle2dry}$$

Table 7.4: ΔT_{10} and ΔT_{50} values in lean and stoichiometric conditions

	ΔT_{10} (K)		**ΔT_{50} (K)**	
Catalyst	**lean**	**stoich**	**lean**	**stoich**
1PdCeSi13 SCS	66	74	71	54
1PdCeAl13 SCS	116	29	107	40

The effect of oxygen partial pressure on the deactivation caused by water is not straightforward to define and seems to be strictly correlated to the nature of the support, even if in both cases a reduction of the deactivation is observed, the effect being much more evident for 1PdCeAl13 SCS. This result seems to be in good agreement with the one obtained recently by Mihai *et al.* on Pd/Al_2O_3 catalyst [32]: at increasing oxygen partial pressure in the feed, the inhibition effect of water was much greater.

Conclusions

The catalytic performance of the series of Pd-supported on CeO_2-SiO_2 with different SiO_2 loadings and CeO_2-Al_2O_3 samples have been evaluated under different reaction conditions in the presence and in the absence of external water.

- **Methane oxidation in the absence of water**: Pd-based catalysts supported on different ceria-silica and ceria-alumina mixed oxides have been tested for methane oxidation. Catalytic measurements reveal that SiO_2 introduction affects positively the activity for methane oxidation for some SiO_2 loadings: the addition of 2, 5 and 20 wt.% of silica enhances the activity, reaching a maximum value for 1PdCeSi20 SCS. On the contrary, the catalytic performance of the sample containing 13 wt.% of SiO_2 is similar to the one of 1PdCe SCS. The addition of alumina into CeO_2 support further improves the activity for methane oxidation in temperature programmed tests, even more with respect to silica-containing samples. Nevertheless, the latter ones exhibit a good stability under long-time exposure to reaction mixture whereas alumina-doped sample deactivates more severely, losing ~ 12% of its initial conversion (against 3-5% for Si-doped catalysts).

  The effect of gas composition on the catalytic performance has been evaluated for the sample doped with 13 wt.% of silica or alumina. When O_2/CH_4 ratio is decreased from lean to stoichiometric, the activity of 1PdCeSi13 SCS is not substantially modified in the low temperature window. For the sample doped with alumina, instead, the activity is drastically reduced and the hysteresis behavior depends on the feed composition.

  Based on these results, it seems that even if the addition of alumina improves the light-off behavior of Pd-ceria catalysts, the addition of silica is more effective in stabilizing the performances under stoichiometric conditions and prolonged time-on-stream operation.
- **Methane oxidation in the presence of water**: when methane oxidation is carried out in lean reaction conditions, the addition of water causes an increase of the light-off temperature which does not markedly depend on the composition of the support, being equal to ~ 70-80 K for all samples. For some silica loadings (i.e 5 and 13 wt.%), the activity is not immediately recovered when water is removed from the gas feed, while for 1PdCeSi2 SCS and 1PdCeSi20 SCS, the activity is quickly restored. When Pd/CeO_2 is doped with alumina, the introduction of water induces a severe deactivation of the catalyst, shifting T_{10} and T_{50} of ~ 110 K to higher values. After water removal, the activity

remains lower than the one recorded in dry atmosphere, suggesting that water poisoning is not reversible on 1PdCeAl13 SCS.

The presence of water in the feed does not only affect the catalytic performance but also PdO-Pd-PdO phase transformation, as observed from TPO experiments. The decomposition of PdO to metallic Pd evolves differently in wet atmosphere: the onset of the third decomposition step, i.e PdO species in interaction with the support, increases of 54 K for Al_2O_3-containing sample and 55-70 K for SiO_2-based ones. Moreover, the presence of water markedly changes the distribution of PdO fraction decomposed in each step: for Si-doped samples, a higher amount of PdO decomposes at higher temperature, while for Al-doped one a minor fraction of PdO interacts with the support and this might explain the lower activity and stability of this catalyst under wet conditions. HRTEM analysis does not reveal a significant difference between the sample after oxidation in dry and wet atmosphere under a morphological point of view. The adsorption of water/hydroxyls on the catalytic surface or the formation of $Si(OH)_4$, at high temperature [26, 27] might change metal-support interaction and modify the onset of the decomposition of PdO species in contact with the oxide carrier. Moreover, the presence of water at high temperature is able to promote PdO sintering [23], which might need higher temperature to decompose.

Prolonged exposure to wet atmosphere accelerates the catalysts deactivation with time-on-stream and the degree of deactivation increases with SiO_2 amount on the support. For alumina-ceria-based sample, the presence of water speeds up the deactivation over time, much more than for Si-doped ones. High affinity of Al_2O_3 for water molecules or lower oxygen mobility of the support or the minor fraction of palladium which interacts strongly with the support, as inferred from TPO profile in wet atmosphere (Figure 7.15), can contribute to its severe deactivation [10, 19].

The deactivation degree induced by water vapor on Si-containing sample seems to be independent of oxygen partial pressure, as inferred from tests in stoichiometric conditions, whereas for 1PdCeAl13 SCS water poisoning is more severe than what observed in lean atmosphere, at least at high temperature. Water deactivation, however, is completely reversible for both samples and the activity recorded in dry conditions is easily recoverable.

References

[1] K. Fujimoto, F. Ribeiro, M. Borja and E. Iglesia , *Journal of Catalysis,* vol. 179, pp. 431-442, 1998.

[2] A.K. Datye, J. Bravo, T. Nelson, P. Atasanova, M. Lyubovsky and L. Pfefferle, *Applied Catalysis A: General,* vol. 198, n. Issues 1–2, p. 179–196, 2000.

[3] H. Gabasch, W. Unterberger, K. Hayek, B. Klotzer, E. Kleimenov, D. Teschner , S. Zefeiratos, M. Havecker, A. Knop-Gericke, R. Schlogl, J. Han, F. Ribeiro, B. Aszalos-Kiss, T. Curtin and D. Zemlyanov, *Surface Science,* vol. 600, pp. 2980-2989, 2006.

[4] P. Gelin and M. Primet, *Applied Catalysis B: Environmental,* vol. 39, pp. 1-37, 2002.

[5] G. Groppi, C. Cristiani, L. Lietti, and P. Forzatti, *Studies in Surface Science and Catalysis,* vol. 130, pp. 3801-3806, 2000.

[6] P. Forzatti, *Catalysis Today,* vol. 83, pp. 3-18, 2003.

[7] M. Hoffmann, S. Kreft, G. Georgi, G. Fulda, M. Pohl, D. Seeburg, C. Berger-Karin, E. Kondatenko, and S. Wohlrab, *Applied Catalyis B: Environmental,* vol. 179, pp. 313-320, 2015.

[8] D. Ciuparu, N. Katsikis and L.D. Pfefferle, *Applied Catalysis A: General,* vol. 216, pp. 20-215, 2001.

[9] K. Persson, A. Ersson, S. Colussi, A. Trovarelli and S. Jaras, *Applied Catalysis B: Environmental,* vol. 66, pp. 175-185, 2006.

[10] D. Ciuparu, E. Perkins, and L.D. Pfefferle , *Applied Catalysis A: General,* vol. 263, pp. 145-153, 2004.

[11] J-H. Park, J-H. Ahn, H-I Sim, G. Seo, H.S Han, and C-H Shin, *Catalysis Communications,* vol. 56, pp. 157-163, 2014.

[12] S. Colussi, A. Trovarelli, E. Vesselli, A. Baraldi, G. Comelli, G. Groppi, and J. Llorca, *Applied Catalysis A: General,* vol. 390, pp. 1-10, 2010.

[13] M. Monai, M. Montini , E. Fonda, R. Gorte and P. Fornasiero, *ChemCatChem,* vol. 6, pp. 1-14, 2014.

[14] F. Huang, J. Chen, W. Hu, G. Li, S. Yuan, L. Zhong and Y. Chen, *Applied Catalysis B: Environmental,* vol. 219, pp. 73-81, 2017.

[15] M. Lyubovsky, L. L. Smith, M. Castaldi, H. Karim, B. Nentwick, S. Etemad, R. LaPierre and W.C. Pfefferle, *Catalysis Today,* vol. 83, pp. 71-84, 2003.

[16] D. Bounechada, G. Groppi, P. Forzatti, K. Kallinen and T. Kinnunen, *Applied Catalysis B: Environmental,* Vols. 91-99, pp. 119-120, 2012.

[17] D. Ferri, M. Elsener and O. Krocher, *Applied Catalysis B: Environmental,* vol. 220, pp. 67-77, 2018.

[18] R. Kikuchi, S. Maeda, K. Sasaki, S. Wennerstrom, and K. Eguchi, *Applied Catalysis A: General,* vol. 232, pp. 23-28, 2002.

[19] W.R. Schwartz, D. Ciuparu, and L.D. Pfefferle, *J. Phys. Chem. C,* vol. 116, pp. 8587-8593, 2012.

[20] J.-H. Park, B. Kim, C.-H. Shin, G. Seo, S. H. Kim and S. B. Hong, *Top Catal ,* vol. 52, p. 27–34 , 2009.

[21] K. Nomura, K. Noro, Y. Nakamura, H. Yoshida, A. Satsuma and T. Hattori, *Catalysis Letters,* vol. 58, p. 127–130, 1999.

[22] B. Zhang, X. Wang, O. M' Ramadj, D. Li, H. Zhang and G. Lu, *Journal of Natural Gas Chemistry,* vol. 17, p. 87–92, 2008.

[23] R. Gholami, M. Alyani, and K. Smith, *Catalysts,* vol. 5, pp. 561-594, 2015.

[24] S. Colussi, A. Trovarelli and J. Llorca, *Catalysis Communications,* vol. 8, pp. 1263-1266, 2007.

[25] T.W. Hansen, A.T. DeLaRiva, S.R. Challa and A.K. Datye, *Acc. Chem. Res,* vol. 43, pp. 1720-1730, 2013.

[26] R. Lamber, N. Jaeger, and G. Schulz-Ekloff, *Journal of Catalysis*, vol. 123, pp. 285-297, 1990.

[27] R. Gholami and K. J. Smith, *Applied Catalysis B: Environmental,* vol. 168, pp. 153-163, 2015.

[28] G. Diannan, W. Sheng, Z. Chun, Y. Shongzhan and W. Shudong, *Chin J Catal,* vol. 29(12), p. 1221–1225, 2008.

[29] K. Persson, L. Pfefferle, L. Schwartz, A. Ersson and S. G. Jaras, *Applied Catalysis B: Environmental,* vol. 74, pp. 242-250, 2007.

[30] M. Alyani and K. J. Smith, *Ind. Eng. Chem. Res.,* vol. 55, no. 30, pp. 8309–8318, 2016.

[31] P. Araya, S. Guerrero, J. Robertson and F. Gracia, *Applied Catalysis A: General,* vol. 283, pp. 225-233, 2005.

[32] O. Mihai, G. Smedler, U. Nylen, M. Olofsson and L. Olsson, *Catalysis Science & Technology,* vol. 7, pp. 3084-3096, 2017.

Conclusions

The research work developed in this PhD thesis has been focused on the investigation of the catalytic methane oxidation over different Pd/CeO_2-based catalysts. The main focus has been directed to gain further insights on the effect of water poisoning, a key issue for Pd-based catalysts in NGVs application. Pd-based materials supported on various metal oxides ($Ce_xZr_{1-x}O_2$, Ce-Si and Ce-Al) have been prepared by *single-step solution combustion synthesis* (SCS), and their catalytic performance has been evaluated in lean and stoichiometric reaction conditions, in the absence and in the presence of water vapor.

When methane oxidation was carried out in lean conditions and in the absence of water, solution combustion synthesized catalysts supported on intrinsically active oxides like CeO_2 and $Ce_{0.75}Zr_{0.25}O_2$ displayed the best performance in terms of reaction rate. The presence of CeO_2 has been also demonstrated to be beneficial in terms of transient deactivation, which occurs at high temperatures due to PdO-Pd-PdO phase transformation: the use of reducible oxides enables to better stabilize PdO phase, yielding a faster PdO re-formation with an improvement of activity loss during the cooling part of the light-off. By comparing the catalytic behavior of SCS samples with that of the corresponding ones prepared by conventional IW method, SCS proved to be a more effective procedure to obtain Ce-based materials with an enhanced activity towards methane oxidation. This improvement was also observed during time-on-stream-test, where SCS catalysts showed a lower deactivation degree with time, maintaining a high conversion level during long-time exposure to reaction stream. The higher catalytic performance of 1PdCe SCS and 1PdCZ75 SCS in terms of lower light-off temperatures, transient deactivation and stability can be attributed to the presence of Pd-O sites stabilized by strong Pd/ceria and Pd/ceria-zirconia interaction, promoted by high temperature and redox conditions achieved during the combustion synthesis.

Experimental results have also pointed out that decreasing the ceria content, the preparation procedure plays a minor role in the improvement of catalytic performance: ZrO_2-supported catalysts, in fact, showed nearly identical light-off behavior and resistance to lean-aging treatment. However, the use of ZrO_2 remarkably enhances the stability of Pd catalysts, which showed a low deactivation extent after long-time exposure to reaction mixture.

The catalytic tests carried out in the presence of external water have highlighted the inhibition/deactivation role of water vapor on the activity and stability of Pd-based catalysts,

irrespective of the feed composition. Water deactivation has been found to be completely reversible for solution combustion synthesized $Pd/Ce_xZr_{1-x}O_2$, which demonstrated a remarkable light-off performance and an improved resistance to hydrothermal aging with respect to their IW counterparts, attaining a complete regeneration after prolonged exposure to water. Different kind of PdO species and/or heterogeneous Pd/PdO particle size distribution, smaller noble metal particles, higher oxygen mobility and strong Pd/Ce interaction via Pd-O-Ce sites formation effectively enhance the catalytic performance and resistance to aging treatment. The use of $Ce_{0.75}Zr_{0.25}O_2$ mixed oxide has been found to reduce catalyst deactivation: its higher oxygen mobility seems to prevent or minimize the deactivation induced by water vapor, making it a promising support for the application to NGVs.

Despite of a similar catalytic performance has been observed for ZrO_2-supported catalysts during transient and steady state tests, 1PdZr SCS displayed an enhanced resistance to hydrothermal treatment with respect to its IW counterpart, outperforming analogues $Pd/Ce_xZr_{1-x}O_2$ SCS. Polymorphic structure of zirconia, acid/base properties and/or Pd-zirconia interaction could be involved in the improvement of resistance to water deactivation.

The introduction of SiO_2 and Al_2O_3 into solution combustion synthesized Pd/CeO_2 strongly enhances the catalytic performance in the absence of water, especially when Al_2O_3 is used as dopant. Nevertheless, when the gas stream contains a large amount of water vapor, this improvement is not maintained and the addition of small amount of SiO_2 represents a better choice to stabilize the catalytic performance with respect to Al_2O_3. The introduction of SiO_2 or Al_2O_3 has a clear effect on the occurrence of PdO-Pd-PdO phase transformation in the presence of water: the dynamic behavior of PdO/Pd conversion is strongly modified in wet atmosphere, and the results of HRTEM characterization might suggest that the decomposition of PdO likely follows a different path with respect to the one observed in dry conditions.

When oxygen partial pressure is decreased from 2 vol.% to 1 vol.%, the light-off temperatures of 1PdCe SCS and 1PdCeSi13 SCS remained almost similar to the ones obtained in rich oxygen atmosphere, both in the absence and in the presence of water vapor. Contrarily, for 1PdCZ75 SCS and 1PdCeAl13 SCS the activity and deactivation degree in the presence of water were sensitive to the change of oxygen partial pressure. Side reactions such as methane reforming or WGS could take place at varying temperature and catalyst composition, suggesting that catalytic activity of Pd-supported catalysts and their deactivation is closely related to O_2/CH_4 ratio.

To conclude, solution combustion synthesis appears to be an interesting approach to prepare more efficient and stable $Pd/Ce_xZr_{1-x}O_2$ catalysts with a greater tolerance to water poisoning and high durability. Moreover, the results also highlighted that structural, physic-chemical properties of the support and oxygen partial pressure could effectively influence the

deactivation extent of catalysts, outlining a complex picture where several aspects are involved in the deactivation/inhibition effect of water.

For a deeper understanding of PdO-Pd decomposition process in wet atmosphere, HRTEM investigation of undoped and Al-doped catalysts, following the same procedure used for Si-containing catalyst, would be useful to gain further insights on the complex mechanism of PdO/Pd transformation.